Preprint of
R. Sevilla, S. Fernández-Méndez and A. Huerta
NURBS-Enhanced Finite Element Method (NEFEM): A seamless bridge between CAD and FEM
Archives of Computational Methods in Engineering, 18 (4); 441-484, 2011

NURBS-Enhanced Finite Element Method (NEFEM). A seamless bridge between CAD and FEM

Ruben Sevilla[1], Sonia Fernández-Méndez[2], Antonio Huerta[2]

[1] *Civil and Computational Engineering Centre (C^{2}EC), College of Engineering, Swansea University, Singleton Park, Swansea, SA2 8PP, Wales, UK.*

[2] *Laboratori de Càlcul Numèric (www-lacan.upc.edu), Departament de Matemàtica Aplicada III, E.T.S. de Ingenieros de Caminos, Canales y Puertos, Universitat Politècnica de Catalunya, Jordi Girona 1, E-08034 Barcelona, Spain.*

Abstract

The development of NURBS-Enhanced Finite Element Method (NEFEM) is revisited. This technique allows a seamless integration of the CAD boundary representation of the domain and the finite element method (FEM). The importance of the geometrical model in finite element simulations is addressed and the benefits and potential of NEFEM are discussed and compared with respect to other curved finite element techniques.

Keywords: NURBS, boundary representation, CAD, finite elements, discontinuous Galerkin, high-order isoparametric approximations

1. Introduction

This paper revisits the state of the art of an efficient methodology to integrate the NURBS boundary representation of the domain into a standard finite element framework: the so-called NURBS-enhanced finite element method (NEFEM).

Non-uniform rational B-splines (NURBS, see [72]) are nowadays widely used for geometric description in Computer Aided Design (CAD). Other popular options for geometric description in CAD are polynomial B-splines (a

Email addresses: R.Sevilla@swansea.ac.uk (Ruben Sevilla[1]), sonia.fernandez@upc.edu (Sonia Fernández-Méndez[2]), antonio.huerta@upc.edu (Antonio Huerta[2])

Preprint of
R. Sevilla, S. Fernández-Méndez and A. Huerta
NURBS-Enhanced Finite Element Method (NEFEM): A seamless bridge between CAD and FEM
Archives of Computational Methods in Engineering, 18 (4); 441-484, 2011

particular case of NURBS) and subdivision surfaces. This fact has motivated the development of novel numerical techniques considering CAD descriptions of the computational domain.

NURBS-Enhanced Finite Element Method uses NURBS to accurately describe the boundary of the computational domain and the solution is approximated using polynomials defined with Cartesian coordinates, directly in the physical space. From a practical point of view, NEFEM considers efficient strategies for numerical integration on elements affected by curved boundaries. It is worth remarking that at elements not intersecting the boundary classical finite elements (FEs) are used, preserving the efficiency of the finite element method (FEM).

NEFEM was first presented for 2D domains in [79], showing the advantages in front of classical isoparametric FEs using both continuous and discontinuous Galerkin formulations for the numerical solution of some test problems. It is important to remark that all the ideas presented in [79] are valid not only when the boundary of the domain is parametrized by NURBS, but for any piecewise boundary parametrization. The discussion is centered on NURBS boundary parametrization because they are the most extended technology in CAD. In [80] NEFEM was shown to be a porwerful tool for solving compressible flow problems governed by the Euler equations of gas dynamics.

Several high-order FE methodologies for the treatment of curved boundaries are discussed and compared in [82], including isoparametric FEM, Cartesian FEM, p-FEM and NEFEM. Numerical examples show that NEFEM is not only more accurate than FE methods with an approximate boundary representation, but also outperforms p-FEM with an exact boundary representation, showing the advantages of combining Cartesian approximation with exact boundary representation.

In [81] the extension of NEFEM to 3D domains is presented. Although conceptually easy, the extension of NEFEM to 3D requires attention to several geometric aspects. The advantages of NEFEM in front of other curved FE techniques are discussed and illustrated using numerical examples.

This paper is organized as follows. In Section 2 a review of FE techniques for curved boundaries with a historical perspective is presented. An introductory overview of Non-Uniform Rational B-Splines is given in Section 3. Section 4 is devoted to review NEFEM. The core concept is first described and technical details regarding the polynomial approximation and the numerical integration in curved elements is presented. Optimal a priori

Preprint of
R. Sevilla, S. Fernández-Méndez and A. Huerta
NURBS-Enhanced Finite Element Method (NEFEM): A seamless bridge between CAD and FEM
Archives of Computational Methods in Engineering, 18 (4); 441-484, 2011

error estimates for NEFEM are recalled and, finally, some implementation details are summarized in order to facilitate the adoption of NEFEM by the FE community. In Section 5 a critical comparison between FE techniques used in domains with curved boundaries is presented, with particular emphasis in two issues: the exact boundary representation of the domain and the consistency of the approximation. The numerical examples presented in Section 6 range from second-order elliptic problems to more complex problems involving the numerical solution of Euler and Maxwell's equations. The application of NEFEM in continuous and discontinuous Galerkin frameworks is illustrated. In the numerical examples NEFEM is shown as a powerful strategy to efficiently treat curved boundaries and to avoid excessive mesh refinement when complex geometric objects are considered. Finally, Section 7 summarizes the main conclusions and Section 8 discusses some areas of future research.

2. Historical perspective

The origin of the finite element method (FEM) is mainly attributed to pioneer works in the field of airplane structural analysis, see [104, 19] for an overview of the early history of the FEM. The need of curved elements to improve the quality of the shape discretization soon arose and the first approach introduced to efficiently deal with curved boundaries were the so-called *isoparametric elements*, see [35, 103]. In these works the authors pointed out that in a practical setting, mesh refinement is governed by the need to accurately represent curved geometric objects, and the use of curved elements was proposed in order to retain accurate boundary descriptions without performing excessive mesh refinement. The key idea of isoparametric elements was to employ the same polynomial functions to approximate the solution and to define the mapping between the reference element and the physical element, hence the term *isoparametric*. This approach was rapidly adopted for solid mechanics applications due to its straightforward implementation and its relatively good performance.

During the 1970s, there was an increasing interest in the development and analysis of curved finite elements, see [17, 77, 93, 107, 106, 108, 38, 39]. The technique presented in [106, 108] is recognized to be the first FEM considering an exact boundary representation. Triangular elements with one curved edge were introduced, and the isoparametric mapping was modified to map a reference element into the triangular element with an exact boundary de-

Preprint of
R. Sevilla, S. Fernández-Méndez and A. Huerta
NURBS-Enhanced Finite Element Method (NEFEM): A seamless bridge between CAD and FEM
Archives of Computational Methods in Engineering, 18 (4); 441-484, 2011

scription. A similar approach was developed in [77], also using triangular elements with one curved side corresponding to the exact boundary. Alternatives to the standard polynomial approximation of the solution were also proposed within the context of curved FEs with an exact boundary representation, see for instance the rational basis in [93, 94]. Nevertheless, all these FE techniques with exact boundary representation were not considered a practical tool, but a mathematical idealization, due to the impossibility to extend the ideas to 3D domains.

The necessity of accurate geometric descriptions in the automotive industry was the origin of the so-called *blending mappings* proposed in [38]. This mappings represented an inflection point in the development of general procedures to exactly treat curved boundaries as they were the core concept of a new and successful family of elements called *transfinite elements*, see [39]. The key idea was to introduce blending functions to define a mapping between a reference square and a subdomain with the boundary given by four parametric curves. The problem of geometric inaccuracies associated to the isoparametric transformation are removed by blending mappings, and higher degrees of interpolation can be successfully employed. Therefore, blending mappings were naturally adopted in the so-called p-version of the FEM (p-FEM), see [4] and a recent review in [86]. In this approach the mesh remain fixed (usually containing large elements) and the degree of the approximations is increased in order to properly capture the solution. Therefore, an accurate geometric description is crucial in this context.

During the 1980s a great effort was dedicated to the study of approximation spaces that guarantee optimal convergence of the finite element method in the presence of curved boundaries, see for instance [14, 95, 32, 61, 12].

Despite the early introduction of curved FE techniques for solid mechanics applications, in the 1980s and 1990s the geometric description was an important handicap for computational fluid dynamics (CFD). In particular, linear approximation of curved walls in numerical solutions of Euler equations of gas dynamics was identified as the origin of spurious entropy production near curved boundaries. In a finite volume (FV) context, see [7], the problem was identified in [27, 8]. In cite [98] a local approximation of the curvature is used in order to enhance the imposition of the wall boundary condition on curved boundaries, resulting in a dramatic reduction of the entropy production. More recently, in the so-called spectral volume method, see [99], the accurate treatment of curved boundaries has been identified as a critical issue. In [97] the spectral volume method is extended to the two-dimensional

Preprint of
R. Sevilla, S. Fernández-Méndez and A. Huerta
NURBS-Enhanced Finite Element Method (NEFEM): A seamless bridge between CAD and FEM
Archives of Computational Methods in Engineering, 18 (4); 441-484, 2011

Euler equations with curved boundaries and in [44] the authors implement the ideas of [55] to enhance the accuracy of the approximation in the presence of curved walls. In a discontinuous Galerkin (DG) context, see [20], the same problematic when solving Euler equations was identified in [9]. In [92] a detailed study of this problem is presented to conclude that accurate results can only be obtained taking into account the curvature of the boundary. More recently, in [55] a new methodology is presented for the computation of the fluxes across curved boundaries but, unfortunately, the proposed method is not conservative. In [34], the advantages of using high-order isoparametric elements for the numerical solution of inviscid compressible flow problems are also illustrated. Using ultra-coarse meshes and high-order approximations the authors show the benefits of curved elements. In fact, this work evidences the necessity of better than isoparametric boundary representation when coarse meshes are considered because the $\mathcal{C}^0$ continuity of the curved boundary between elements is shown to have an important impact in quantities of interest such as the pressure coefficient over an airfoil profile. More recently, in [37] a different mapping is proposed based on the boundary representation with Bézier curves. Imposing $\mathcal{C}^1$ continuity of the approximated boundary an important improvement is obtained compared to standard isoparametric mappings. It is worth recalling that the necessity of curved elements and a $\mathcal{C}^1$ continuity approximation of the boundary in fluid mechanics applications was very early pointed out as a key issue for obtaining accurate solution without excessive mesh refinement, see for instance [68].

Accurate geometric descriptions are also relevant in other areas of fluid mechanics such as the numerical solution of the Navier-Stokes equations, see for instance [62, 57], but the importance of the geometrical model is not exclusive of fluid mechanics. Maxwell's equations are also very sensitive to an accurate geometric description. In [102] the error induced by isoparametric approximations of curvilinear geometries is studied. By solving the 3D Maxwell's equations in a sphere, the authors show that an exact description of the geometry reduces the error in one order of magnitude compared to isoparametric elements. Similar conclusions are derived in [64] for linear elasticity problems. They conclude that sizable errors are present in the numerical solution when the order of the geometric approximation is lower than the order of the functional interpolation. The relevance of an accurate geometric model for some applications in solid mechanics is also illustrated in [69], where the use of B-splines is proposed for the geometric representation of the interface in frictionless contact problems.

Preprint of
R. Sevilla, S. Fernández-Méndez and A. Huerta
NURBS-Enhanced Finite Element Method (NEFEM): A seamless bridge between CAD and FEM
Archives of Computational Methods in Engineering, 18 (4); 441-484, 2011

Curved FE were developed during the 1970s and 1980s without regarding the emerging CAD industry. The great impact of CAD technology in the FE community arrived in the 1980s. In fact, researchers on the field of shape optimization were the first to promote the so-called *marriage of CAD and FE*. In a shape optimization process, the integration of CAD into the analysis stage is crucial to avoid the geometric approximation inherent in a mesh. In [75] transfinite elements were implemented using NURBS for the geometric description. Obviously, the rational nature of NURBS leads to rational function maps between the reference element and the element in the physical space. Note however that the solution is approximated using polynomials. Some inaccuracies associated to the lack of satisfaction of the isoparametric concept are mentioned in [75], but not further explained. To obtain an isoparametric approach, the exact boundary representation was abandoned, and a simplification of the geometry with polynomial B-Splines was proposed. Thus, some of the advantages of NURBS, such as exact representation of conics, were lost.

Over the 1990s, other authors focused their attention on integrating NURBS technology into FE codes. For instance, in [29] an element geometric mapping also based on blending functions with NURBS is proposed. More recently, in [67], p-FEM with NURBS for the boundary representation is applied to plane elasticity problems. The inaccuracies previously mentioned in [75] are also reported, and the lack of satisfaction of the isoparametric concept is alleviated by a rational enrichment of the polynomial basis used to approximate the solution.

The relevance of an accurate geometry description also motivated, in the late 1990s, a new family of FE-like techniques based on CAD, which is still today object of intensive research: *isogeometric methods*. The key idea is to use the same CAD representation for both geometrical design and analysis. Thus, contrary to classical FE methodologies, the whole domain is treated as a CAD entity, not only the boundary of the domain. Moreover, classical polynomial approximations of the solution are abandoned and the solution is approximated with the same basis used in the CAD environment. The first application is again encountered on shape optimization, using B-Splines for the geometrical description and for the mechanical analysis, see [53]. In the 2000s, more advanced CAD technology have been applied following the same rationale. In [18] *subdivision surfaces* are used for thin shell analysis and relevant advantages are found due to the sensitivity of shells to an inaccurate geometric representation. More recently, NURBS have been used to develop

Preprint of
R. Sevilla, S. Fernández-Méndez and A. Huerta
NURBS-Enhanced Finite Element Method (NEFEM): A seamless bridge between CAD and FEM
Archives of Computational Methods in Engineering, 18 (4); 441-484, 2011

isogeometric methods, see for instance [51, 49]. In [51] the application of a NURBS isogeometric method to shape optimization processes is presented. Finally, in [49] a more general framework known as *isogeometric analysis* is proposed. This approach is not only focused on the accurate representation of the geometry, but also in the possibilities of NURBS as a basis for the approximation. See more recent advances in [25].

3. Non-Uniform Rational B-Splines (NURBS)

This section provides a brief introduction to NURBS curves and surfaces. Core concepts used in the following sections are introduced and the reader is referred to [72, 74] for a complete presentation.

3.1. NURBS curves

A qth-degree NURBS curve is a piecewise rational function defined in parametric form as

$$\boldsymbol{C}(\lambda) = \left(\sum_{i=0}^{\mathtt{n_{cp}}} \nu_i \, \boldsymbol{B}_i \, C_i^q(\lambda)\right) \Big/ \left(\sum_{i=0}^{\mathtt{n_{cp}}} \nu_i \, C_i^q(\lambda)\right) \qquad 0 \leq \lambda \leq 1,$$

where $\{\boldsymbol{B}_i\}$ are the coordinates of the $\mathtt{n_{cp}}+1$ *control points* (forming the *control polygon*), $\{\nu_i\}$ are the control weights, and $\{C_i^q(\lambda)\}$ are the normalized B-spline basis functions of degree q, which are defined recursively by

$$C_i^0(\lambda) = \begin{cases} 1 & \text{if } \lambda \in [\lambda_i, \lambda_{i+1}[, \\ 0 & \text{elsewhere,} \end{cases}$$
$$C_i^k(\lambda) = \frac{\lambda - \lambda_i}{\lambda_{i+k} - \lambda_i} C_i^{k-1}(\lambda) + \frac{\lambda_{i+k+1} - \lambda}{\lambda_{i+k+1} - \lambda_{i+1}} C_{i+1}^{k-1}(\lambda),$$

for $k = 1 \dots q$, where λ_i, for $i = 0, \dots, \mathtt{n_k}$, are the *knots* or *breakpoints*, which are assumed ordered $0 \leq \lambda_i \leq \lambda_{i+1} \leq 1$. They form the so-called *knot vector*

$$\Lambda = \{\underbrace{0, \dots, 0}_{q+1}, \lambda_{q+1}, \dots, \lambda_{\mathtt{n_k}-q-1}, \underbrace{1, \dots, 1}_{q+1}\},$$

which uniquely describes the B-spline basis functions. The multiplicity of a knot, when it is larger than one, determines the decrease in the number of continuous derivatives. The number of control points, $\mathtt{n_{cp}}+1$, and knots,

Preprint of
R. Sevilla, S. Fernández-Méndez and A. Huerta
NURBS-Enhanced Finite Element Method (NEFEM): A seamless bridge between CAD and FEM
Archives of Computational Methods in Engineering, 18 (4); 441-484, 2011

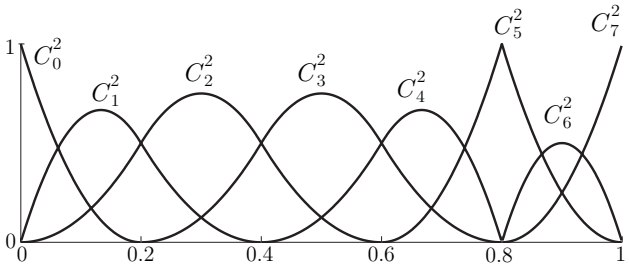

Figure 1: B-spline basis functions for the knot vector (1)

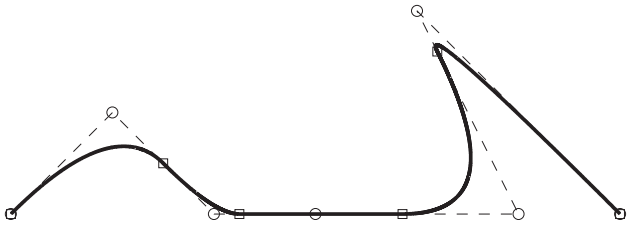

Figure 2: NURBS curve (solid line), control points (denoted by ∘), control polygon (dashed line) and breakpoints (denoted by □)

$\mathtt{n_k}+1$, are related to the degree of the parametrization, q, by the relation $\mathtt{n_k} = \mathtt{n_{cp}} + q + 1$, see [72] for more details. Figure 1 shows the B-spline basis functions for the knot vector

$$\Lambda = \{0, 0, 0, 0.2, 0.4, 0.6, 0.8, 0.8, 1, 1, 1\}. \tag{1}$$

Note that NURBS are piecewise rational functions, whose definition changes at knots. An example of a NURBS curve is represented in Figure 2 with the corresponding control polygon. The image of the breakpoints or knots by the NURBS are depicted in order to stress the discontinuous nature of the parametrization. In practice CAD manipulators work with *trimmed* NURBS, which are defined as the initial parametrization restricted to a subspace of the parametric space. Figure 3 shows the NURBS curve of Figure 2 trimmed to the subinterval $[0.05, 0.75]$.

Preprint of
R. Sevilla, S. Fernández-Méndez and A. Huerta
NURBS-Enhanced Finite Element Method (NEFEM): A seamless bridge between CAD and FEM
Archives of Computational Methods in Engineering, 18 (4); 441-484, 2011

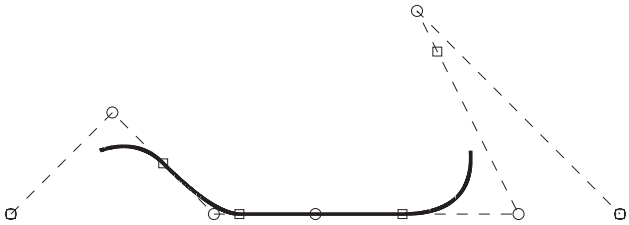

Figure 3: Trimmed NURBS curve with $\lambda \in [0.05, 0.75]$ (solid line), control points (denoted by $\circ$), control polygon (dashed line) and breakpoints (denoted by $\square$)

3.2. NURBS surfaces

A NURBS surface of degree q in λ and degree l in κ, is a piecewise rational function defined in parametric form as

$$\boldsymbol{S}(\lambda,\kappa) = \left(\sum_{i=0}^{\mathtt{n}_{\mathtt{cp}}^{\lambda}}\sum_{j=0}^{\mathtt{n}_{\mathtt{cp}}^{\kappa}} \nu_{ij}\,\boldsymbol{B}_{ij}\,S_{i,j}^{q,l}(\lambda,\kappa)\right) \Big/ \left(\sum_{i=0}^{\mathtt{n}_{\mathtt{cp}}^{\lambda}}\sum_{j=0}^{\mathtt{n}_{\mathtt{cp}}^{\kappa}} \nu_{ij}\,S_{i,j}^{q,l}(\lambda,\kappa)\right), \quad 0 \leq \lambda,\kappa \leq 1,$$

where $\{\boldsymbol{B}_{ij}\}$ are the coordinates of the $(\mathtt{n}_{\mathtt{cp}}^{\lambda}+1)(\mathtt{n}_{\mathtt{cp}}^{\kappa}+1)$ *control points* (defining the *control net*), $\{\nu_{ij}\}$ are the control weights, and $\{S_{i,j}^{q,l}(\lambda,\kappa)\}$ are the 2D B-spline basis functions of degree q in λ and l in κ. Each 2D B-Spline basis function is defined as a tensor product of 1D basis functions, that is

$$S_{i,j}^{q,l}(\lambda,\kappa) := C_i^q(\lambda)C_j^l(\kappa). \tag{2}$$

Figure 4 shows two 2D B-spline basis functions for knot vectors

$$\Lambda^{\lambda} = \{0,0,0,0.2,0.6,0.6,1,1,1\},$$

$$\Lambda^{\kappa} = \{0,0,0,0,0.4,1,1,1,1\}.$$

Complete 1D basis are represented for each direction to illustrate the construction of 2D basis functions as described in Equation (2).

Note that NURBS surfaces change their definition along *knot lines*, that is when $\lambda = \lambda_i$, for $i = 1,\ldots,\mathtt{n}_{\mathtt{k}}^{\lambda}$, or $\kappa = \kappa_i$, for $i = 1,\ldots,\mathtt{n}_{\mathtt{k}}^{\kappa}$. An example of a NURBS surface is represented in Figure 5 with the corresponding control net. Knot lines are represented on the NURBS surface in order to stress the discontinuous nature of the parametrization. An example of a trimmed NURBS surface is represented in Figure 6, showing the NURBS surface of

Preprint of
R. Sevilla, S. Fernández-Méndez and A. Huerta
NURBS-Enhanced Finite Element Method (NEFEM): A seamless bridge between CAD and FEM
Archives of Computational Methods in Engineering, 18 (4); 441-484, 2011

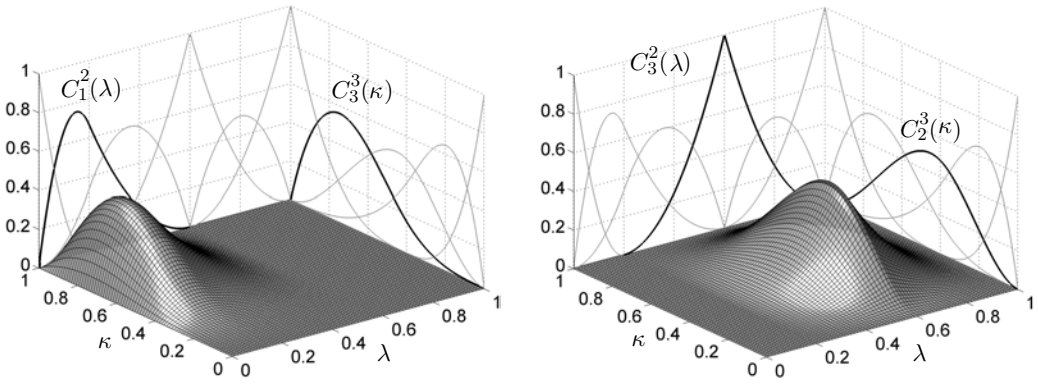

(a) $S_{1,3}^{2,3}(\lambda,\kappa) := C_1^2(\lambda)C_3^3(\kappa)$ (b) $S_{3,2}^{2,3}(\lambda,\kappa) := C_3^2(\lambda)C_2^3(\kappa)$

Figure 4: Example of 2D B-spline basis functions

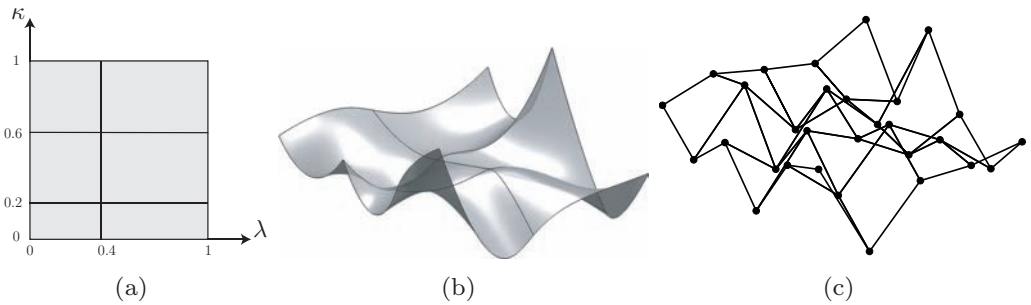

(a) (b) (c)

Figure 5: (a) Parametric space, (b) NURBS surface with knot lines, and (c) control net

Preprint of
R. Sevilla, S. Fernández-Méndez and A. Huerta
NURBS-Enhanced Finite Element Method (NEFEM): A seamless bridge between CAD and FEM
Archives of Computational Methods in Engineering, 18 (4); 441-484, 2011

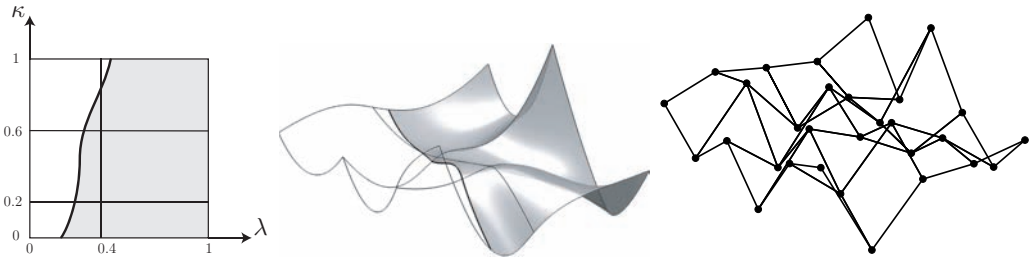

Figure 6: (a) Parametric space trimmed by the thick curve, (b) trimmed NURBS surface with knot lines and the thick curve used to trim the initial surface of Figure 5, and (c) control net

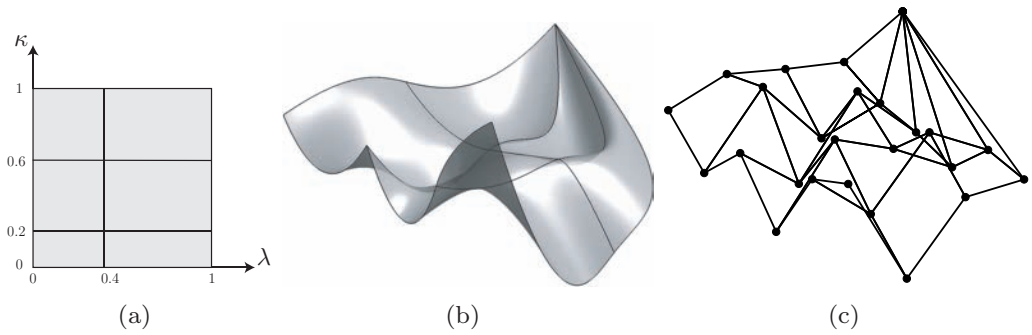

Figure 7: (a) Parametric space, (b) singular NURBS surface with knot lines, and (c) control net

Figure 5 trimmed with the thick curve. In practical applications, it is also common to deal with *singular* (or *singularly parametrized*) NURBS surfaces. Such surfaces contain at least one *singular point*, defined as a point where a directional derivative is zero. For these surfaces, knot lines typically converge to the singular point, see an example in Figure 7.

4. NURBS-Enhanced Finite Element Method (NEFEM)

This section introduces the fundamental ideas of NEFEM in 2D and 3D domains, see [79, 81] for further details. The core concept is first described and the strategy to define curved entities in NEFEM is detailed. Special attention is paid to the design of efficient strategies in order to define high-order approximations and to perform the numerical integration on curved NEFEM elements. Optimal a priori error estimates for h and p refinement

Preprint of
R. Sevilla, S. Fernández-Méndez and A. Huerta
NURBS-Enhanced Finite Element Method (NEFEM): A seamless bridge between CAD and FEM
Archives of Computational Methods in Engineering, 18 (4); 441-484, 2011

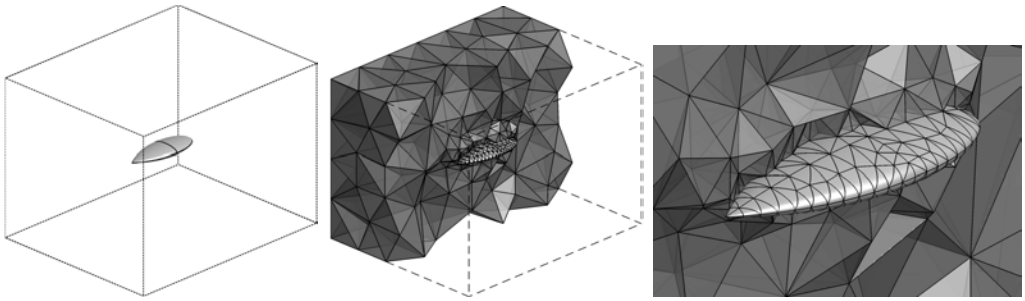

(a) (b) (c)

Figure 8: (a) Domain with part of the boundary defined by curved NURBS surfaces corresponding to the NASA almond, (b) cut through an unstructured tetrahedral mesh with the surface triangular mesh on the almond, and (c) detail of the mesh near the almond

are recalled, and implementation details are given in order to facilitate the adoption of NEFEM.

4.1. NEFEM concept

Consider an open bounded domain Ω whose boundary $\partial\Omega$, or a portion of it, is parametrized by NURBS curves in 2D or surfaces in 3D. In 2D every NURBS is assumed to be parametrized by

$$\boldsymbol{C} : [0,1] \longrightarrow \boldsymbol{C}([0,1]) \subseteq \partial\Omega \subset \mathbb{R}^2.$$

Analogously, in 3D every NURBS is assumed to be parametrized by

$$\boldsymbol{S} : [0,1]^2 \longrightarrow \boldsymbol{S}([0,1]^2) \subseteq \partial\Omega \subset \mathbb{R}^3.$$

A regular partition of the domain $\overline{\Omega} = \bigcup_e \overline{\Omega}_e$ in simplices is assumed, such that $\Omega_i \bigcap \Omega_j = \emptyset$, for $i \neq j$. For instance, Figure 8 shows a 3D computational domain with part of the boundary defined by NURBS surfaces corresponding to the NASA almond [30], a useful geometry for benchmarking electromagnetic scattering codes. A cut through an unstructured tetrahedral mesh is also represented in Figure 8, including the surface triangular mesh on the almond.

As usual in FE mesh generation codes, it is assumed that every curved boundary face belongs to a unique NURBS. That is, one element face can not be defined by portions of two, or more, different NURBS. Note however

Preprint of
R. Sevilla, S. Fernández-Méndez and A. Huerta
NURBS-Enhanced Finite Element Method (NEFEM): A seamless bridge between CAD and FEM
Archives of Computational Methods in Engineering, 18 (4); 441-484, 2011

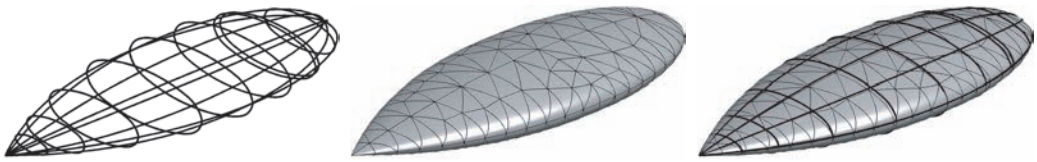

(a) (b) (c)

Figure 9: (a) Knot lines of the NURBS surfaces defining the NASA almond, (b) surface triangulation, and (c) surface triangulation and knot lines

that the piecewise definition of each NURBS is independent on the mesh discretization. Thus, NURBS parametrization can change its definition within one face, that is, FE edges do not need to coincide with knot lines. Figure 9 shows the image of the knot lines of the NASA almond surfaces and the surface triangulation corresponding to the mesh represented in Figure 8. It can be observed that spatial discretization is independent of the piecewise NURBS surface parametrization. It is worth remarking that allowing changes of NURBS parametrization to be independent on the spatial discretization means that special attention must to be paid to the numerical integration over elements affected by the NURBS boundary representation, see Section 4.4.2.

An element without any edge or face in contact with NURBS boundaries has planar faces and it is defined and treated as a standard FE. Therefore, in the vast majority of the domain, interpolation and numerical integration are standard, preserving the computational efficiency of classical FEM. Specifical numerical strategies for interpolation and numerical integration are needed only for those elements affected by NURBS boundaries.

4.2. Curved elements

In NEFEM, curved elements are defined in terms of the NURBS boundary representation of the domain. The formal definition of curved faces and elements in a NEFEM mesh is given in this section.

4.2.1. 2D elements

Let Γ_e be an edge on the NURBS boundary parametrized by $\boldsymbol{C}$, and $\boldsymbol{x}_1, \boldsymbol{x}_2 \in \partial\Omega$ the two vertices on the NURBS boundary, see Figure 10. The edge is defined by

$$\Gamma_e := \boldsymbol{C}([\lambda_1^e, \lambda_2^e]),$$

Preprint of
R. Sevilla, S. Fernández-Méndez and A. Huerta
NURBS-Enhanced Finite Element Method (NEFEM): A seamless bridge between CAD and FEM
Archives of Computational Methods in Engineering, 18 (4); 441-484, 2011

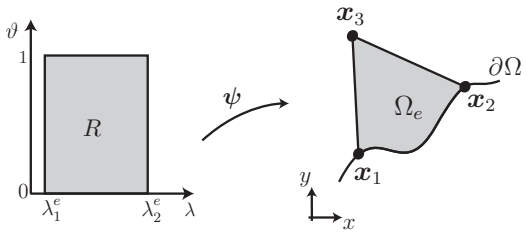

Figure 10: Parametrization of a curved triangular element with a edge on the NURBS boundary

where λ_1^e and λ_2^e are the parametric coordinates (in the parametric space of the NURBS) of the end points of Γ_e.

A curved triangular element with an edge on the NURBS boundary is defined as a convex linear combination of the curved NURBS edge and the interior vertex. For instance, element represented in Figure 10 is parametrized by

$$\begin{aligned} \boldsymbol{\psi} \ &: R \longrightarrow \Omega_e \\ (\lambda, \vartheta) &\longmapsto \boldsymbol{\psi}(\lambda, \vartheta) := (1-\vartheta)\boldsymbol{C}(\lambda) + \vartheta \boldsymbol{x}_3, \end{aligned} \tag{3}$$

where $R = [\lambda_1^e, \lambda_2^e] \times [0, 1]$ and $\boldsymbol{x}_3$ is the internal vertex of Ω_e, see Figure 10.

4.2.2. 3D elements

Let Υ_e be a tetrahedral face on the NURBS boundary parametrized by $\boldsymbol{S}$, and $\boldsymbol{x}_1, \boldsymbol{x}_2, \boldsymbol{x}_3 \in \partial\Omega$ the three vertices on the NURBS boundary, see Figure 11. Assuming that the vertices $\boldsymbol{x}_1, \boldsymbol{x}_2, \boldsymbol{x}_3$ do not correspond to singular points of the NURBS parametrization, a straight-sided triangle Λ_e in the parametric space of the NURBS is uniquely defined by the parametric coordinates of the vertices, $\boldsymbol{S}^{-1}(\boldsymbol{x}_1)$, $\boldsymbol{S}^{-1}(\boldsymbol{x}_2)$ and $\boldsymbol{S}^{-1}(\boldsymbol{x}_3)$. The curved face with a NURBS boundary representation, Υ_e, is defined as the image of the straight-sided triangle Λ_e by the NURBS parametrization $\boldsymbol{S}$,

$$\Upsilon_e := \boldsymbol{S}(\Lambda_e), \tag{4}$$

as illustrated in Figure 11.

Note that when the surface $\boldsymbol{S}$ is trimmed by a curve $\boldsymbol{C}$ in the parametric space of the NURBS, the edges of the triangle Λ_e must be replaced by trimmed NURBS curves. In such cases Λ_e is a curved triangle in the parametric space of the NURBS and curved edges of Λ_e are NURBS curves (used to trim the original surface), see an example in Figure 12. Finally, assuming

Preprint of
R. Sevilla, S. Fernández-Méndez and A. Huerta
NURBS-Enhanced Finite Element Method (NEFEM): A seamless bridge between CAD and FEM
Archives of Computational Methods in Engineering, 18 (4); 441-484, 2011

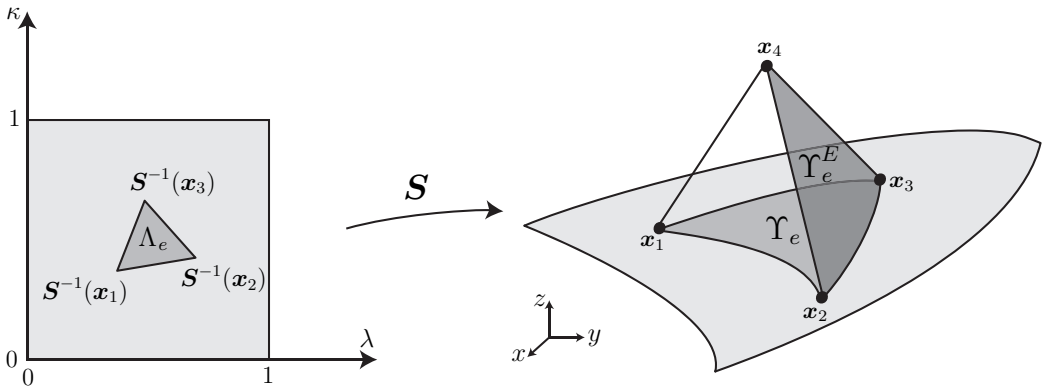

Figure 11: Parametrization of a curved tetrahedral element with a face on the NURBS boundary, showing a face Υ_e on the NURBS boundary, and a face Υ_e^E with an edge on the NURBS boundary, Υ_e^E

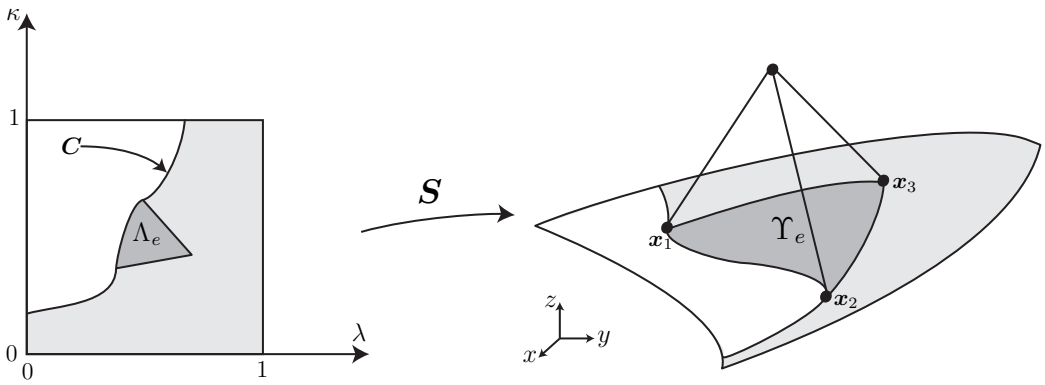

Figure 12: Curved tetrahedral face on a trimmed NURBS boundary. NURBS surface $\boldsymbol{S}$ is trimmed by NURBS curve $\boldsymbol{C}$, leading to a curved triangle Λ_e in the parametric space

Preprint of
R. Sevilla, S. Fernández-Méndez and A. Huerta
NURBS-Enhanced Finite Element Method (NEFEM): A seamless bridge between CAD and FEM
Archives of Computational Methods in Engineering, 18 (4); 441-484, 2011

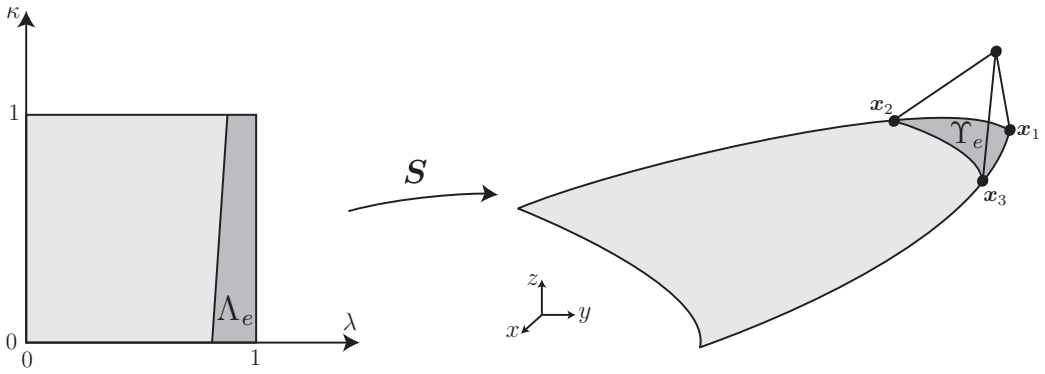

Figure 13: Curved tetrahedral face on a singular NURBS boundary with a singular point, leading to a quadrilateral Λ_e in the parametric space

that one of the vertices of the tetrahedral face corresponds to a singular point of the NURBS parametrization, Λ_e must be defined as a quadrilateral in the parametric space of the NURBS, see an example in Figure 13.

Interior curved faces with an edge on the NURBS boundary are defined as a convex linear combination of the curved edge and the interior face node. For instance, curved face Υ_e^E represented in Figure 11 is parametrized by

$$\begin{aligned} \boldsymbol{\Theta}_{\boldsymbol{x_4}} \ : [\varrho_1, \varrho_2] \times [0,1] &\longrightarrow \Upsilon_e^E \\ (\varrho, \sigma) &\longmapsto \boldsymbol{\Theta}_{\boldsymbol{x_4}}(\varrho, \sigma) := (1-\sigma)\boldsymbol{\theta}(\varrho) + \sigma \boldsymbol{x}_4, \end{aligned} \tag{5}$$

where $\boldsymbol{\theta}([\varrho_1, \varrho_2])$ parametrizes the curved edge from vertex $\boldsymbol{x}_2$ to vertex $\boldsymbol{x}_3$. Note that this approach to define interior curved faces ensures the same definition of an interior curved face as seen from the two elements sharing this face. Note also that other types of curved faces are present in real meshes, such as faces with several edges over the NURBS boundary. A systematic way of defining all possible curved faces is presented in Section 4.4.2.

With this definition of curved faces, a curved tetrahedral element with a face on the NURBS boundary is defined by a convex linear combination of the curved NURBS face and the interior vertex. For instance, element represented in Figure 11 is parametrized by

$$\begin{aligned} \boldsymbol{\Psi} \ : \Lambda_e \times [0,1] &\longrightarrow \Omega_e \\ (\lambda, \kappa, \vartheta) &\longmapsto \boldsymbol{\Psi}(\lambda, \kappa, \vartheta) := (1-\vartheta)\boldsymbol{S}(\lambda, \kappa) + \vartheta \boldsymbol{x}_4, \end{aligned} \tag{6}$$

where $\boldsymbol{x}_4$ denotes the interior vertex of Ω_e. Similarly, an element with an edge on the NURBS boundary corresponds to a convex linear combination

Preprint of
R. Sevilla, S. Fernández-Méndez and A. Huerta
NURBS-Enhanced Finite Element Method (NEFEM): A seamless bridge between CAD and FEM
Archives of Computational Methods in Engineering, 18 (4); 441-484, 2011

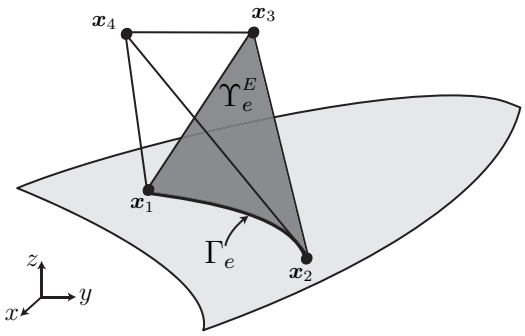

Figure 14: Curved tetrahedral elements with an edge on the NURBS boundary

of one of its curved faces an the opposite node, and can be parametrized by

$$\begin{aligned} \boldsymbol{\Phi} \ : [\varrho_1, \varrho_2] \times [0,1]^2 &\longrightarrow \Omega_e \\ (\varrho, \sigma, \tau) &\longmapsto \boldsymbol{\Phi}(\varrho, \sigma, \tau) := (1-\tau)\boldsymbol{\Theta}_{\boldsymbol{x_3}}(\varrho, \sigma) + \tau \boldsymbol{x}_4, \end{aligned} \tag{7}$$

where $\boldsymbol{x}_3$ and $\boldsymbol{x}_4$ are the interior vertices of Ω_e, see Figure 14. Note that the definition of $\boldsymbol{\Phi}$ in Equation (7) is independent on the order of the interior vertices $\boldsymbol{x}_3$ and $\boldsymbol{x}_4$. That is, element Ω_e can be equivalently parametrized by

$$\boldsymbol{\Phi}(\varrho, \sigma, \tau) := (1-\tau)\boldsymbol{\Theta}_{\boldsymbol{x_4}}(\varrho, \sigma) + \tau \boldsymbol{x}_3.$$

It is worth remarking that interior edges, (i.e, edges with no more than one node over the NURBS boundary) are considered as straight edges. Note that this assumption allows to ensure that the elements affected by the NURBS boundary representation of the domain are only elements with at least one face or one edge over the NURBS boundary, and therefore, the overhead introduced by NEFEM is restricted to a very small portion of the total number of elements.

4.3. High-order approximation in curved elements

NEFEM considers nodal polynomial interpolation in each element. To ensure reproducibility of polynomials in the physical space, NEFEM defines the approximation directly with Cartesian coordinates, $\boldsymbol{x}$, that is

$$u(\boldsymbol{x}) \simeq u^h(\boldsymbol{x}) = \sum_{i=1}^{\mathtt{n_{en}}} u_i N_i(\boldsymbol{x}), \tag{8}$$

Preprint of
R. Sevilla, S. Fernández-Méndez and A. Huerta
NURBS-Enhanced Finite Element Method (NEFEM): A seamless bridge between CAD and FEM
Archives of Computational Methods in Engineering, 18 (4); 441-484, 2011

where u_i are nodal values, N_i are polynomial shape functions (Lagrange polynomials) of order p in $\boldsymbol{x}$, and $\mathtt{n_{en}}$ is the number of element nodes. Recall that in isoparametric FEM or p-FEM the approximation is defined in a reference element. However, contrary to NEFEM, the definition of the polynomial basis for high-order curved elements does not ensure reproducibility of polynomials in the physical space.

To make the computation of Lagrange polynomial basis more systematic, for any degree and for any distribution of nodes, the implementation proposed in [83, 46] is adapted to define the approximation in Cartesian coordinates.

Given a nodal set with coordinates $\{\boldsymbol{x}_i\}_{i=1}^{\mathtt{n_{en}}}$, the Lagrange polynomial basis $\{N_i(\boldsymbol{x})\}_{i=1}^{\mathtt{n_{en}}}$ can be expressed in terms of the polynomial basis $\{P_i(\boldsymbol{x})\}_{i=1}^{\mathtt{n_{en}}}$ as

$$N_i(\boldsymbol{x}) = \sum_{j=1}^{\mathtt{n_{en}}} \left[\boldsymbol{V}^{-1}\right]_{ji} P_j(\boldsymbol{x}), \tag{9}$$

where the multidimensional Vandermonde matrix is defined as $V_{ij} := P_j(\boldsymbol{x}_i)$, for $i, j = 1, \ldots, \mathtt{n_{en}}$. Note that Equation (9) holds for any polynomial basis $\{P_i(\boldsymbol{x})\}_{i=1}^{\mathtt{n_{en}}}$. Here a polynomial basis $\{P_i(\boldsymbol{x})\}_{i=1}^{\mathtt{n_{en}}}$ with the required degree and whose definition is independent of the nodal coordinates is considered. In fact, the polynomial basis considered here is derived from the Jacobi polynomials, see [87, 33], to ensure moderate condition number for the Vandermonde matrix $\boldsymbol{V}$, see also [54].

Different options can be considered to define a nodal distribution in Ω_e. Any nodal distribution, such as equally-spaced nodal distributions, can be defined on the (imaginary) element with planar edges/faces given by the vertices of Ω_e, or adapted to the NURBS geometry, see Figures 15 and 16. It is worth remarking that, even if the nodes are placed over an imaginary element with planar faces, the approximation is only defined on the interior of the curved element Ω_e with the NURBS boundary representation.

The definition of a nodal distribution on the element with planar faces, see Figures 15 (a) and 16 (a), induces a marginal extra efficiency, avoiding to define a specific nodal distribution for each curved element. Adapting a nodal distribution to the NURBS geometry, see Figures 15 (b) and 16 (b), allows a seamless imposition of boundary conditions in strong form, directly imposing the value of the solution at nodes on the boundary. But, nodal distributions adapted to curved boundaries do not represent any implementation advantage if boundary conditions are imposed in weak form, as usual in DG formulations. Note however the evolution of the condition number,

Preprint of
R. Sevilla, S. Fernández-Méndez and A. Huerta
NURBS-Enhanced Finite Element Method (NEFEM): A seamless bridge between CAD and FEM
Archives of Computational Methods in Engineering, 18 (4); 441-484, 2011

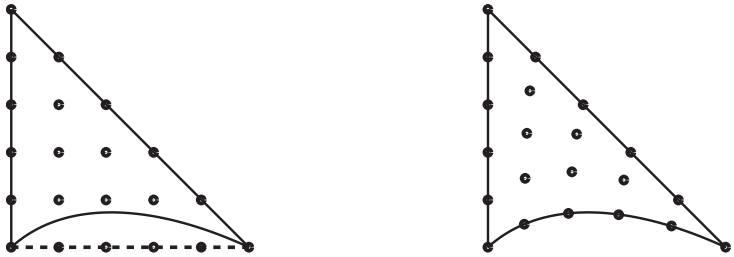

(a) (b)

Figure 15: Equally-spaced nodal distribution for $p = 5$ (a) defined using the (imaginary) triangle with planar faces, and (b) adapted to the curved geometry

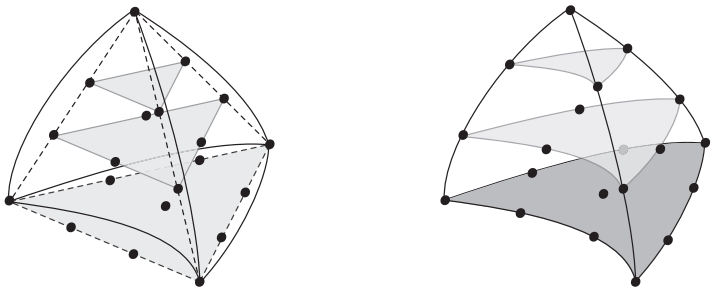

(a) (b)

Figure 16: Equally-spaced nodal distribution for $p = 3$ (a) defined using the (imaginary) tetrahedral with planar faces, and (b) adapted to the curved geometry

Preprint of
R. Sevilla, S. Fernández-Méndez and A. Huerta
NURBS-Enhanced Finite Element Method (NEFEM): A seamless bridge between CAD and FEM
Archives of Computational Methods in Engineering, 18 (4); 441-484, 2011

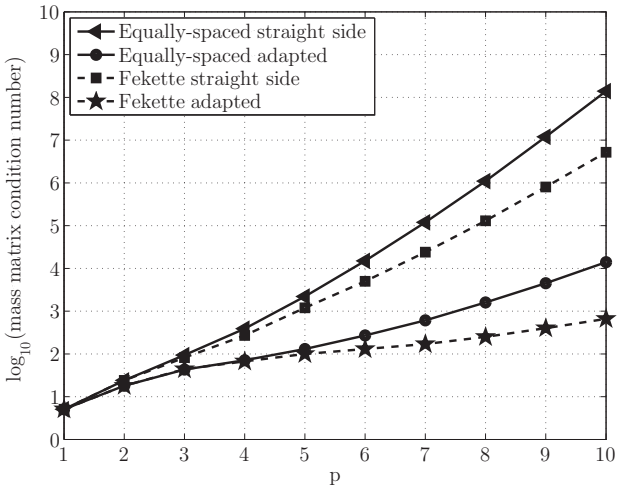

Figure 17: Condition number of the mass matrix as a function of the interpolation degree (p)

shown in Figure 17, for the element mass matrix as a function of the polynomial degree of approximation, p. Adapted distributions of nodes induce an important reduction on condition number.

For very high-order approximations, let say $p > 5$, equally-spaced nodal distributions may lead to ill-conditioned elemental matrices, even if adapted distributions are considered. In this case, it is more convenient to use special distributions of nodes in order to reduce the condition number of the resulting element matrices, see for instance the distributions proposed in [15, 16, 89, 45, 63, 100]. Figures 18 and 19 show Fekette nodal distribution in a triangle and the distribution proposed in [45] in a tetrahedral element. Adaptation of such distributions to the curved geometry lead to an extra reduction in condition number of the elemental matrices, see Figure 17.

In the examples of Figures 15, 16, 18 and 19, the use of nodal distributions non-adapted to the NURBS boundary implies that some nodes lie outside the region of interest (i.e., the area/volume that defines the curved element). Shape functions associated to those nodes contribute very little to the elemental mass matrix deteriorating its condition number, see for instance the shape functions associated to a triangular with a degree of interpolation $p = 3$ for adapted and non-adapted Fekette nodal distributions in Figure 20. The problem is far more evident as the degree of the approximation is increased because more nodes lie outside the region of interest. Obviously, the

Preprint of
R. Sevilla, S. Fernández-Méndez and A. Huerta
NURBS-Enhanced Finite Element Method (NEFEM): A seamless bridge between CAD and FEM
Archives of Computational Methods in Engineering, 18 (4); 441-484, 2011

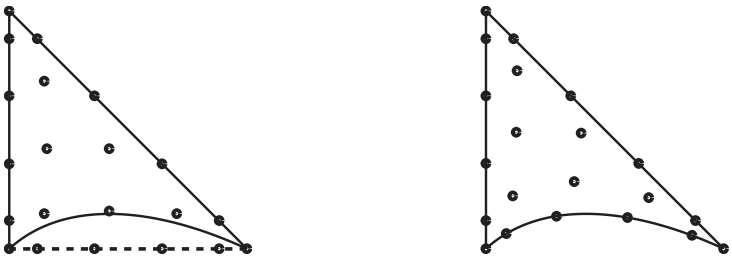

(a) (b)

Figure 18: Fekette nodal distribution for $p = 5$ (a) defined using the (imaginary) triangle with planar faces, and (b) adapted to the curved geometry

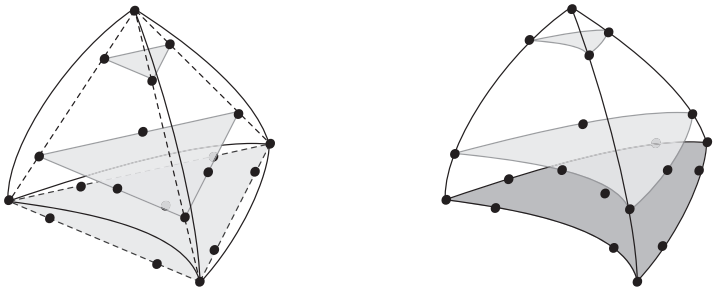

(a) (b)

Figure 19: Fekette nodal distribution for $p = 3$ (a) defined using the (imaginary) tetrahedral with planar faces, and (b) adapted to the curved geometry

Preprint of
R. Sevilla, S. Fernández-Méndez and A. Huerta
NURBS-Enhanced Finite Element Method (NEFEM): A seamless bridge between CAD and FEM
Archives of Computational Methods in Engineering, 18 (4); 441-484, 2011

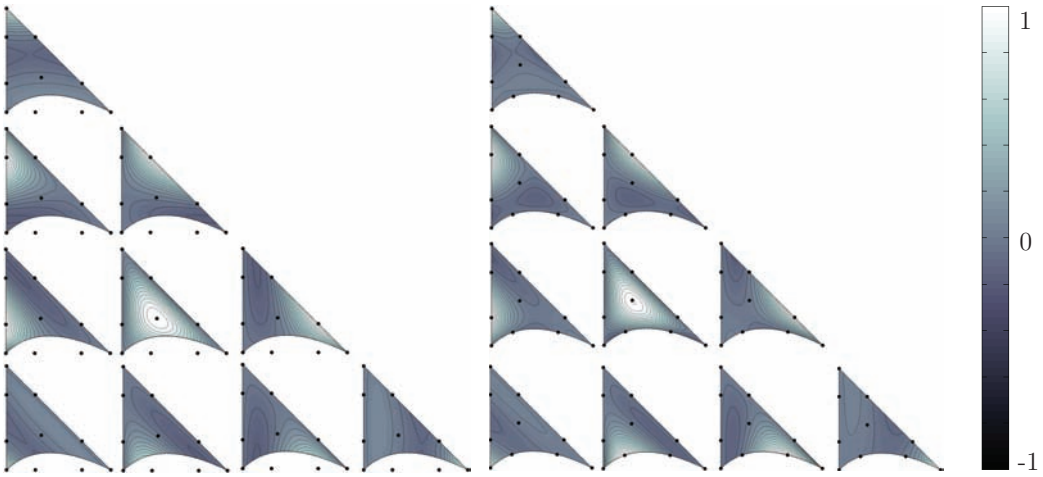

Figure 20: Polynomial basis functions for a NEFEM curved element with Fekette nodal distributions and $p = 3$: (a) on the straight-sided triangle given by its vertices, and (b) adapted to the exact geometry

condition number of elemental matrices for non-adapted nodal distributions is highly dependent on the geometry of the curved element. To illustrate that dependence, Figure 21 shows the evolution of the condition number of the elemental mass matrix as a function of d/h where h is the characteristic element size and d is the maximum distance between the curved boundary and the straight line connecting the two vertex on the boundary. It is worth remarking that the condition number for adapted distributions does not deteriorate as the element is distorted.

4.4. Numerical integration in curved elements

Weak form of the problem requires both integrations over element edges/faces and in element interiors. Integrals in elements not having an edge or face in contact with NURBS boundaries are computed using standard procedures. For an element Ω_e affected by the NURBS boundary representation, design of specific quadratures is necessary. Special attention must be paid to the definition of suitable quadratures accounting for changes of NURBS parametrization within an element face or edge.

This section present numerical integration on curved edges/faces (line/surface integrals, usually related to the implementation of natural boundary conditions or to flux evaluation over the face in a DG context) and in curved

Preprint of
R. Sevilla, S. Fernández-Méndez and A. Huerta
NURBS-Enhanced Finite Element Method (NEFEM): A seamless bridge between CAD and FEM
Archives of Computational Methods in Engineering, 18 (4); 441-484, 2011

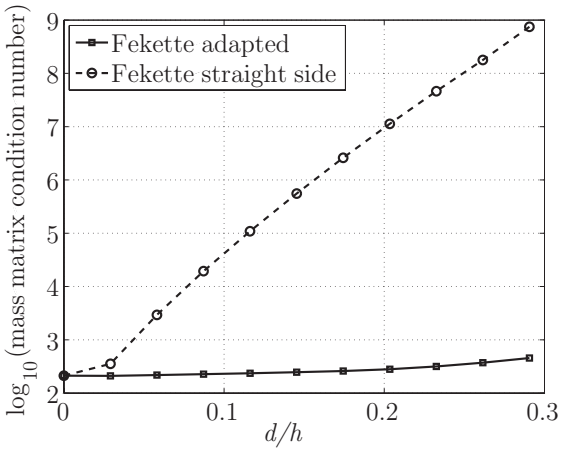

Figure 21: Condition number of the elemental mass matrix as a function of d/h

elements (volume integrals).

4.4.1. 2D case

A line integral to be computed along a curved boundary edge given by a trimmed NURBS, $\Gamma_e = \boldsymbol{C}([\lambda_1^e, \lambda_2^e])$, can be written as

$$\int_{\Gamma_e} f \, d\ell = \int_{\lambda_1^e}^{\lambda_2^e} f\big(\boldsymbol{C}(\lambda)\big) \, \|J_{\boldsymbol{C}}(\lambda)\| \, d\lambda,$$

where f is a generic function (usually polynomial), and $\|J_{\boldsymbol{C}}\|$ denotes the norm of the differential of the NURBS parametrization $\boldsymbol{C}$ (which, in general, is not a polynomial). As usual, a 1D numerical quadrature is used for the numerical computation of the integral, namely

$$\int_{\Gamma_e} f \, d\ell \approx \sum_{i=1}^{\mathtt{n_{ip}}} f\big(\boldsymbol{C}(\lambda_i)\big) \, \|J_{\boldsymbol{C}}(\lambda_i)\| \, \omega_i, \tag{10}$$

where λ_i and ω_i are the coordinates and weights of the $\mathtt{n_{ip}}$ integration points in $[\lambda_1^e, \lambda_2^e]$.

Recall that a NURBS parametrization, $\boldsymbol{C}$, is a piecewise rational function whose definition changes at the breakpoints. Thus, an independent numerical quadrature must be considered for each one of the intervals between breakpoints in order to take into account the discontinuous nature of the parametrization.

Preprint of
R. Sevilla, S. Fernández-Méndez and A. Huerta
NURBS-Enhanced Finite Element Method (NEFEM): A seamless bridge between CAD and FEM
Archives of Computational Methods in Engineering, 18 (4); 441-484, 2011

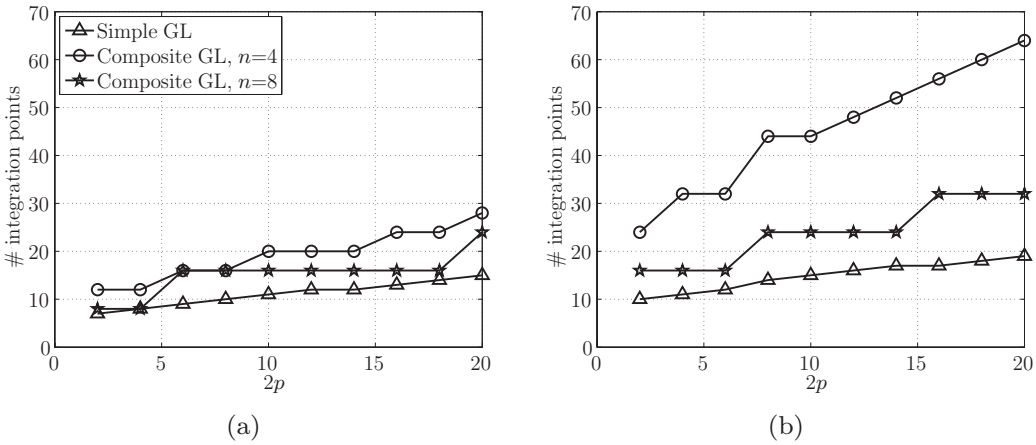

Figure 22: Number of integration points required to integrate all the polynomials of degree of equal to $2p$ with an accuracy of (a) 10^{-6} and (b) 10^{-10} along the trimmed NURBS describing a quarter of a circle

When a polynomial interpolation of degree p is considered in the NEFEM context, it is interesting to know the minimum number of integration points needed to integrate all the polynomials of degree less or equal to $2p$ with a desired accuracy. Figure 22 shows the number of integration points needed to integrate all the polynomials of a degree less or equal to $2p$ with an accuracy of 10^{-6} and 10^{-10} respectively along the trimmed NURBS describing a quarter of a circle. The results using simple and composite Gauss-Legendre quadratures are displayed. For a NEFEM computation with polynomials of degree $p = 5$, simple Gauss-Legendre quadratures provide an accuracy of 10^{-6} in the boundary integrals using 10 integration points. Gauss-Legendre composite quadratures with $\mathtt{n} = 4$ require 5 subintervals, i.e. 20 integration points, to obtain the same accuracy, and Gauss-Legendre composite quadratures with $\mathtt{n} = 8$ require 2 subintervals, i.e. 16 points. For a NEFEM computation with polynomials of degree 10, an accuracy of 10^{-6} is attained with simple Gauss-Legendre quadratures with 15 integration points whereas composite Gauss-Legendre quadratures with $\mathtt{n} = 4$ require 28 integration points and composite Gauss-Legendre quadratures with $\mathtt{n} = 8$ require 24 integration points. If the desired accuracy is 10^{-10} the number of integration points is only slightly increased for simple quadratures whereas composite quadrature suffer from a higher increase in computation cost. For instance,

Preprint of
R. Sevilla, S. Fernández-Méndez and A. Huerta
NURBS-Enhanced Finite Element Method (NEFEM): A seamless bridge between CAD and FEM
Archives of Computational Methods in Engineering, 18 (4); 441-484, 2011

for a NEFEM computation with polynomials of degree 10, simple Gauss-Legendre quadrature require 19 points, composite quadratures with $\mathtt{n} = 4$ require 16 subintervals, i.e. 64 points, and composite quadratures with $\mathtt{n} = 8$ require 4 subintervals, i.e. 32 points. Same conclusions are obtained for the integration along other trimmed NURBS, see [].

Although the faster convergence is obtained for high-order simple quadratures, the use of composite rules is very attractive, allowing to control the error in a straightforward manner, see for instance [28]. Numerical experiments reveal that other popular quadrature rules such as trapezoidal and Simpson composite rules or Romberg's integration are not competitive compared to Gauss-Legendre quadrature rules.

NEFEM also requires to compute integrals in an element Ω_e with one edge Γ_e on the NURBS boundary, see Figure 10. Using the transformation in Equation (3), element integrals are computed as

$$\int_{\Omega_e} f \, d\Omega = \int_R f\big(\boldsymbol{\psi}(\lambda,\vartheta)\big) \, |J_{\boldsymbol{\psi}}(\lambda,\vartheta)| \, d\lambda \, d\vartheta,$$

where $|J_{\boldsymbol{\Psi}}|$ is the determinant of the Jacobian of the transformation $\boldsymbol{\psi}$. The integral can be evaluated using 1D Gauss-Legendre quadratures in each direction as

$$\int_{\Omega_e} f \, d\Omega \simeq \sum_{i=1}^{\mathtt{n_{ip}}} \sum_{j=1}^{\mathtt{m_{ip}}} f(\boldsymbol{\xi}_{ij}) |J_{\boldsymbol{\psi}}(\lambda_i,\vartheta_j)| \, \omega_i \varpi_j. \tag{11}$$

where $\mathtt{n_{ip}}$ and $\mathtt{m_{ip}}$ are the number of integration points in λ and ϑ directions, respectively, $\boldsymbol{\xi}_{ij} := \boldsymbol{\psi}(\lambda_i,\vartheta_j)$, and $\{\lambda_i,\omega_i\}_{i=1}^{\mathtt{n_{ip}}}$ and $\{\vartheta_j,\varpi_j\}_{j=1}^{\mathtt{m_{ip}}}$ are the 1D quadrature points and weights for $[\lambda_1^e,\lambda_2^e]$ and $[0,1]$ respectively.

Remark 1. *When the transformation from the rectangle $\boldsymbol{\psi}$ is considered, the integrals involved in the elemental matrices, for a NEFEM solution with interpolation of degree p, can be exactly computed for one of the parameters, ϑ, using a Gauss-Legendre quadrature with $p+1$ integration points. The other dimension, λ, can be integrated using the same quadrature considered for line integrals over NURBS.*

Note that the rational definition of application $\boldsymbol{\psi}$ is only due to the rational definition of the boundary. Thus, in the particular case of a geometry given by a q-th degree B-spline, i.e. a piecewise polynomial parametrization, the elemental matrices can be exactly computed with Gauss-Legendre quadratures with $p+1$ integration points for the ϑ parameter, and $q(p+1)$ integration points for the NURBS parameter λ.

Preprint of
R. Sevilla, S. Fernández-Méndez and A. Huerta
NURBS-Enhanced Finite Element Method (NEFEM): A seamless bridge between CAD and FEM
Archives of Computational Methods in Engineering, 18 (4); 441-484, 2011

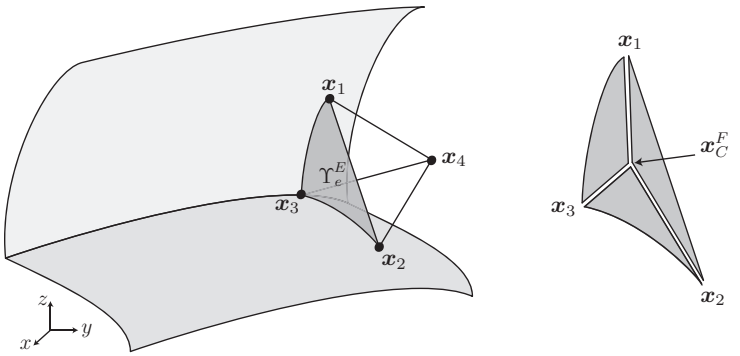

Figure 23: Tetrahedral element with two edges on different NURBS boundaries, and face splitting used for numerical integration (no new degrees of freedom are introduced)

4.4.2. 3D case

Curved faces on a NEFEM tetrahedral mesh can be classified in boundary faces or curved faces with at least one edge on a NURBS boundary. To reduce casuistics in the implementation (i.e., to avoid implementing a different parametrization for each curved face), faces with several edges on different NURBS boundaries are split in *subfaces* with only one edge on a NURBS boundary. It is worth remarking that subdivisions are only applied to design a numerical quadrature without a special treatment of each face typology, no new degrees of freedom are introduced.

To illustrate the proposed strategy, let us consider a face with two edges on different NURBS boundaries, see Figure 23. Curved face Υ_e^E is split in three *subfaces*, which are defined as a linear convex combination of the edges of Υ_e^E and its center of mass $\boldsymbol{x}_C^F$, see Figure 23. After subdivision each *subface* has at most one edge on a NURBS boundary. In the example of Figure 23, two *subfaces* have one edge on a NURBS boundary (they are parametrized using application $\boldsymbol{\Theta}$ in Equation (5)), and the third face, given by $\boldsymbol{x}_2$, $\boldsymbol{x}_1$ and $\boldsymbol{x}_C^F$, is planar.

With this splitting technique, it is only necessary to describe the strategy to perform the numerical integration on curved boundary faces and curved faces with only one edge on a NURBS boundary.

A surface integral on a curved boundary face $\Upsilon_e = \boldsymbol{S}(\Lambda_e)$, see Figure 11, can be written as

$$\int_{\Upsilon_e} f \, dA = \int_{\Lambda_e} f\big(\boldsymbol{S}(\lambda,\kappa)\big) \, \|J_{\boldsymbol{S}}(\lambda,\kappa)\| \, dA, \tag{12}$$

Preprint of
R. Sevilla, S. Fernández-Méndez and A. Huerta
NURBS-Enhanced Finite Element Method (NEFEM): A seamless bridge between CAD and FEM
Archives of Computational Methods in Engineering, 18 (4); 441-484, 2011

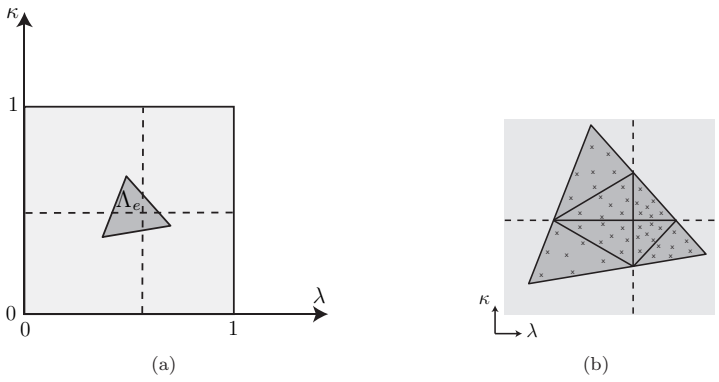

Figure 24: Definition of a numerical quadrature on Λ_e for the numerical integration on a curved tetrahedral face with changes of NURBS parametrization along discontinuous lines (knot lines): (a) triangle in the parametric space and (b) detailed view of the composite quadrature

where f is a generic function (here a polynomial) and $\|J_{\boldsymbol{S}}(\lambda,\kappa)\|$ denotes the norm of the differential of the NURBS parametrization $\boldsymbol{S}$ (which, in general, is not a polynomial). An efficient option to evaluate integral (12) is to use a triangle quadrature [65, 96, 84] in Λ_e. Recall that the spatial discretization is independent on the NURBS boundary representation. Therefore, a boundary face can be intersected by knot lines of the NURBS surface, see Figure 9. If changes of NURBS parametrization are present within the parametric triangle Λ_e, a numerical quadrature must be designed to account for the piecewise NURBS parametrization. For instance, a triangulation of Λ_e such that each *subtriangle* has no changes of NURBS parametrization can be considered, with the associated composite quadrature (triangle quadrature in each *subtriangle*), see Figure 24.

An integral on a curved face Υ_e^E with an edge on the NURBS boundary, see Figure 11, can be written as

$$\int_{\Upsilon_e^E} f\, dA = \int_{\varrho_1}^{\varrho_2} \int_0^1 f\big(\boldsymbol{\Theta}(\varrho,\sigma)\big)\, \|J_{\boldsymbol{\Theta}}(\varrho,\sigma)\|\, dA, \tag{13}$$

where f is a generic function and $\|J_{\boldsymbol{\Theta}}(\varrho,\sigma)\|$ denotes the norm of the differential of mapping $\boldsymbol{\Theta}$, defined in Equation (5), which in general is not a polynomial. Numerical integration can be performed using 1D Gauss-Legendre quadratures in each direction. In fact, application $\boldsymbol{\Theta}$ is linear in the second parameter, σ, and exact integration is feasible in this direction. For a NE-

Preprint of
R. Sevilla, S. Fernández-Méndez and A. Huerta
NURBS-Enhanced Finite Element Method (NEFEM): A seamless bridge between CAD and FEM
Archives of Computational Methods in Engineering, 18 (4); 441-484, 2011

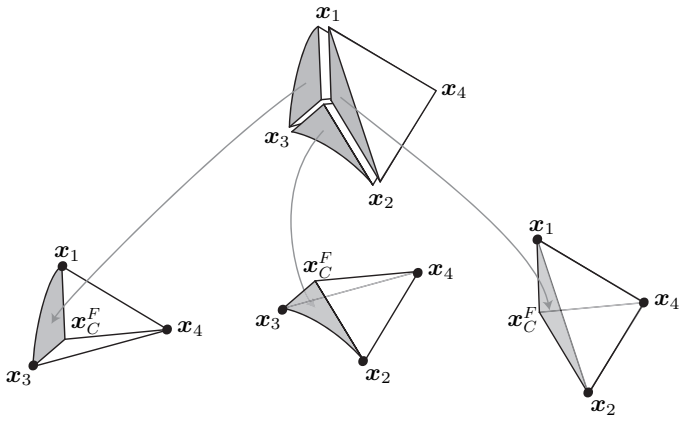

Figure 25: Splitting used for numerical integration in an element with two edges defined by different NURBS (no new degrees of freedom are introduced)

FEM solution with a degree of approximation p, integral in Equation (13) can be exactly computed for this direction, using a Gauss-Legendre quadrature with $p+1$ integration points. Numerical integration for the first direction, given by NURBS parameter ϱ, presents the same difficulty as integration over a NURBS curve.

As usual, the evaluation of integral in Equation (13) requires taking into account the piecewise nature of the NURBS parametrization, considering composite quadratures for ϱ direction.

The strategy to perform the element integrals follows the same rationale. Elements with several faces and/or edges on different NURBS boundaries are split in *subelements* with only one face or one edge on a NURBS boundary. Again, it is worth remarking that subdivisions are only applied to design a numerical quadrature without a special treatment of each element typology, no new degrees of freedom are introduced.

Two examples are presented to illustrate the proposed strategy. First example considers a tetrahedral element with two edges on different NURBS boundaries, see Figure 23. To design a numerical quadrature on Ω_e, three *subelements* are defined as a linear convex combination of the *subfaces* and interior vertex of the element, $\boldsymbol{x}_4$, see Figure 25. In this example, two *subelements* have one edge on a NURBS boundary and the third one has planar faces. Second example considers an element Ω_e with two faces on different NURBS boundaries, as represented in Figure 26. To perform numerical integration in Ω_e, the element is split in four *subelements* using its center of

Preprint of
R. Sevilla, S. Fernández-Méndez and A. Huerta
NURBS-Enhanced Finite Element Method (NEFEM): A seamless bridge between CAD and FEM
Archives of Computational Methods in Engineering, 18 (4); 441-484, 2011

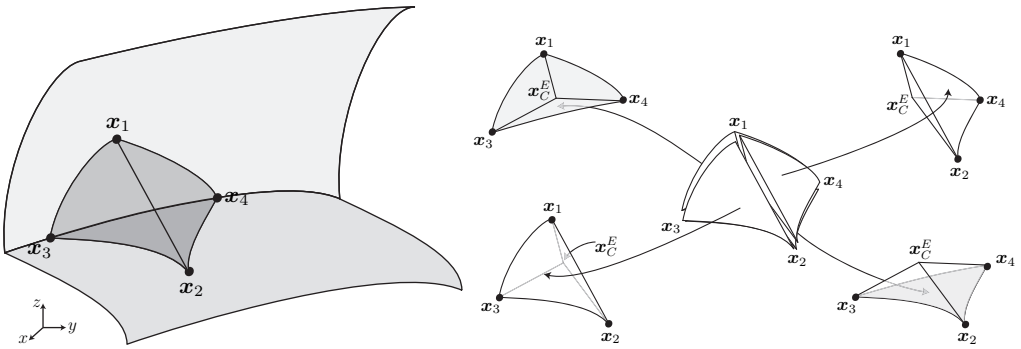

Figure 26: Splitting used for numerical integration in an element with two faces defined by different NURBS (no new degrees of freedom are introduced)

mass, $\boldsymbol{x}_C^E$. *Subelements* are defined as a linear convex combination of $\boldsymbol{x}_C^E$ and original faces of Ω_e, having at most one face on a NURBS boundary.

By combination of these two subdivision strategies, any element with several faces and/or edges on the NURBS boundary can be split into elements with only one face or one edge on the NURBS boundary. Thus, it is only necessary to describe the strategy to perform the numerical integration on these two element typologies.

Volume integrals for an element with one face on a NURBS boundary are performed using parametrization in Equation (6) as

$$\int_{\Omega_e} f \, dV = \int_{\Lambda_e} \int_0^1 f\big(\boldsymbol{\Psi}(\lambda, \kappa, \vartheta)\big) \, |J_{\boldsymbol{\Psi}}(\lambda, \kappa, \vartheta)| \, dV,$$

where f is a generic function (here a polynomial), and $|J_{\boldsymbol{\Psi}}|$ denotes the determinant of the Jacobian of transformation $\boldsymbol{\Psi}$. A numerical quadrature on $\Lambda_e \times [0, 1]$ is easily defined as a tensor product of a triangle quadrature in Λ_e and a 1D Gauss-Legendre quadrature in $[0, 1]$, see Figure 27. In fact, exact integration is feasible in third parameter due to the linearity of $\boldsymbol{\Psi}$ with respect to ϑ. For a NEFEM solution with a degree of approximation p, exact integration in this direction is provided by a Gauss-Legendre quadrature with $p+2$ integration points. To account for changes of NURBS parametrization, only the quadrature in Λ_e is modified, see Figure 24.

Similarly, for an element with one edge on a NURBS boundary, volume

Preprint of
R. Sevilla, S. Fernández-Méndez and A. Huerta
NURBS-Enhanced Finite Element Method (NEFEM): A seamless bridge between CAD and FEM
Archives of Computational Methods in Engineering, 18 (4); 441-484, 2011

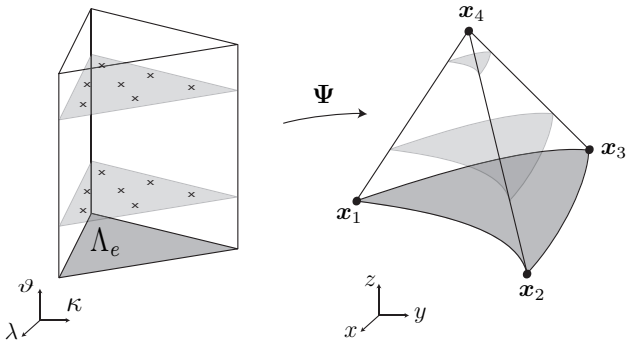

Figure 27: Transformation from $\Lambda_e \times [0,1]$ to Ω_e to perform numerical integration on an element with a face on the NURBS boundary

integrals are performed using parametrization in Equation (7) as

$$\int_{\Omega_e} f \, dV = \int_{\varrho_1}^{\varrho_2} \int_0^1 \int_0^1 f\big(\boldsymbol{\Phi}(\varrho,\sigma,\tau)\big) \, |J_{\boldsymbol{\Phi}}(\varrho,\sigma,\tau)| \, dV,$$

where $|J_{\boldsymbol{\Phi}}|$ is the determinant of the Jacobian of transformation $\boldsymbol{\Phi}$. Note that application $\boldsymbol{\Phi}$ is linear in second and third parameters, σ and τ. Therefore, integrals involved in the elemental matrices, for a NEFEM solution with interpolation of degree p, can be exactly computed for these directions using a Gauss-Legendre quadrature with $p+2$ integration points. No exact integration is feasible in NURBS parameter ϱ, and composite quadratures must be considered if changes of NURBS parametrization are present.

4.5. A priori *error estimates*

Since NEFEM considers standard FE polynomial interpolation, see Section 4.3, a priori error estimates have similar expressions to those of classical FE. For instance, the result for the solution of second-order elliptic problems is recalled in the following theorem.

Theorem 1. *Let $\mathcal{T}_h$ be a non-degenerate discretization in elements (i.e. there is a positive constant β such that $\varrho_e/h_e \geq \beta$, for all $\Omega_e \in \mathcal{T}_h$, where h_e and ϱ_e are the diameters of Ω_e and of the sphere inscribed in Ω_e, respectively). Assuming that all boundary conditions along curved boundaries are imposed in weak form and no interior curved faces/edges are present in the mesh, the following a priori estimate holds*

$$\|u - u_h\|_{E(\Omega)} \leq K h^p |u|_{\mathcal{H}^p(\Omega)}, \tag{14}$$

Preprint of
R. Sevilla, S. Fernández-Méndez and A. Huerta
NURBS-Enhanced Finite Element Method (NEFEM): A seamless bridge between CAD and FEM
Archives of Computational Methods in Engineering, 18 (4); 441-484, 2011

where $\|\cdot\|_{E(\Omega)}$ *is the energy norm,* $u \in \mathcal{H}^{p+1}(\Omega)$ *and* u_h *are the exact and the NEFEM solutions respectively,* K *is a constant depending on* β*,* h *is the mesh size, and* p *is the polynomial degree of interpolation.*

Moreover, for p-refinement convergence the following estimate also holds,

$$\|u - u_h\|_{E(\Omega)} \leq C \exp(-kN^r), \tag{15}$$

where C *and* k *are positive constants,* N *is the number of degrees of freedom, and* $r \gtrsim 1/n_{sd}$*, with* n_{sd} *the number of spatial dimensions.*

With NEFEM (as well as for FE in a domain with polygonal boundaries) the spatial discretization does not introduce geometric errors. Moreover, NEFEM uses polynomials to approximate the solution in Cartesian coordinates, see section 4.3. Consequently, all a priori error estimates demonstrated for FE in domains with polygonal boundaries can be reproduced exactly for NEFEM, even in the presence of elements far from having straight edges. The results for standard FE in domains with polygonal boundaries can be found in [13, 73, 52] for h-refinement and in [3, 85, 41] for p-refinement.

It is worth noting that contrary to NEFEM, the proof of a priori error estimates for isoparametric FE in the presence of curved boundaries requires special attention. This issue is discussed in detail in Section 5.3.

Theorem 1 assumes that essential boundary conditions are imposed in weak form, for instance with numerical fluxes in a DG context, or with Nitsche's method in a continuous formulation, see for instance [70, 36]. If Dirichlet boundary conditions are imposed in strong form, an additional condition is required to keep optimal convergence rates: optimal nodal distributions on every curved element have to be considered, see Figure 19 (b). Theorem 1 also assumes that no interior curved faces/edges are present in the mesh. Again, this extra hypothesis is only needed if a continuous Galerkin approximation is considered and optimal nodal distributions are required to keep optimal convergence rates. This is formally stated in the next result.

Theorem 2. *Under the assumptions of Theorem 1, the error bounds* (14) *and* (15) *hold for NEFEM in a continuous Galerkin framework, if optimal nodal distributions on every curved element along the Dirichlet boundary or with interior curved faces/edges are considered.*

The requirement of Fekette nodal distributions is necessary for an accurate interpolation of Dirichlet boundary conditions on curved boundaries.

Preprint of
R. Sevilla, S. Fernández-Méndez and A. Huerta
NURBS-Enhanced Finite Element Method (NEFEM): A seamless bridge between CAD and FEM
Archives of Computational Methods in Engineering, 18 (4); 441-484, 2011

Due to the use of polynomial nodal basis in Cartesian coordinates, the errors in the approximation of the prescribed value along the boundary may deteriorate the convergence of the solution. This is the case for NEFEM as well as for other approaches considering Cartesian polynomial approximations. For instance, in [78] optimal convergence rates are proven when nodes on the boundary correspond to Lobatto points (i.e Fekette points in 1D).

4.6. Implementation

Introducing the NEFEM concept into an existing FE code requires little effort. Note that the main difference of a NEFEM code with a standard FE code is at the level of the computation of elemental matrices and vectors for curved elements and faces (3D) or edges (2D). In fact, fortunately, the usual routines for the computation of elemental matrices and vectors for straight-sided elements can be directly used, without any modification. The usual input of these routines are the integration points and the shape functions evaluated at these points. In the case of curved elements intersecting the NURBS boundary, these inputs are computed as described in previous sections. Thus, most of the routines usual in a standard FE code (routines for assembly, computation of elemental matrices and vectors, etc) can be directly used.

The most crucial point in the implementation may be the inclusion of the NURBS boundary information. The information of all NURBS describing the boundary and the associated NURBS information for each curved element have to be stored.

In 2D, for every NURBS boundary the associated knot vector and the control polygon are necessary. For each curved edge on a NURBS boundary Γ^e, the parametric coordinates of the boundary nodes λ_1^e and λ_2^e, and a pointer to the corresponding NURBS curve $\boldsymbol{C}$ has to be stored, see Figure 10. In order to compute the parameters λ_1^e and λ_2^e, a NURBS projection algorithm can be easily implemented, see for instance [72, 66]. It is worth noting that the efficiency of the projection algorithm is not crucial because it is performed once at the preprocessing stage.

In 3D, for every NURBS boundary the associated knot vectors and the control net are necessary. For each curved face on the NURBS boundary Υ_e, the parametric coordinates of the boundary nodes $(\lambda_1^e, \kappa_1^e)$, $(\lambda_2^e, \kappa_2^e)$ and $(\lambda_3^e, \kappa_3^e)$, and a pointer to the corresponding NURBS surface $\boldsymbol{S}$ are stored, see Figure 11.

Preprint of
R. Sevilla, S. Fernández-Méndez and A. Huerta
NURBS-Enhanced Finite Element Method (NEFEM): A seamless bridge between CAD and FEM
Archives of Computational Methods in Engineering, 18 (4); 441-484, 2011

It is worth noting that for trimmed and singular surfaces extra information must be stored. First, for each edge on the NURBS boundary corresponding to a trimming curve, see Figure 12, the parametric coordinates of the edge vertices associated to the trimming curve and a pointer to that curve has to be stored. Second, for each vertex corresponding to a singular point of a NURBS surface two parametric coordinates must be stored, see Figure 13.

Obviously, routines for the evaluation of NURBS and their derivatives at a given parametric coordinates are necessary. This routines can be easily obtained or implemented, see [72] and reference therein.

5. Why NEFEM?

This section is devoted to recall and compare several methodologies for the treatment of curved boundaries: isoparametric FEM and Cartesian FEM, with an approximate description of the geometry, and p-FEM with an exact boundary representation. To simplify the presentation, triangular elements with one curved side are considered.

Let $\Omega \subset \mathbb{R}^2$ be an open bounded domain whose boundary $\partial\Omega$, or a portion of it, is curved. A regular partition of the domain $\overline{\Omega} = \bigcup_e \overline{\Omega}_e$ in triangular elements is assumed, such that $\Omega_i \bigcap \Omega_j = \emptyset$, for $i \neq j$. It is important to remark that, in the following, Ω_e denotes the element with an exact description of the curved boundary, also referred as *physical subdomain*. This is not the case of classical isoparametric FE, where the *computational element*, Ω_e^h, corresponds to a polynomial approximation of the curved boundary.

5.1. Approximated boundary representation

The standard FE technique used in the presence of curved boundaries is isoparametric FEM, see [35, 103]. A nodal interpolation of the solution, u, is considered in the reference element I with local coordinates $\boldsymbol{\xi} = (\xi, \eta)$, see Figure 28,

$$u(\boldsymbol{\xi}) \simeq u^h(\boldsymbol{\xi}) = \sum_{i=1}^{\mathtt{n_{en}}} u_i N_i(\boldsymbol{\xi}), \tag{16}$$

where u_i are nodal values, N_i are polynomial shape functions of order p in $\boldsymbol{\xi}$, and $\mathtt{n_{en}}$ is the number of element nodes. The isoparametric transformation

Preprint of
R. Sevilla, S. Fernández-Méndez and A. Huerta
NURBS-Enhanced Finite Element Method (NEFEM): A seamless bridge between CAD and FEM
Archives of Computational Methods in Engineering, 18 (4); 441-484, 2011

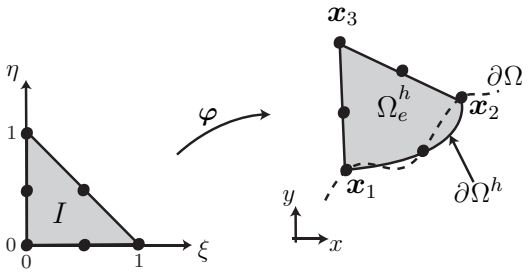

Figure 28: Isoparametric mapping between the reference element I, with local coordinates $\boldsymbol{\xi}$, and an approximation of the physical subdomain in Cartesian coordinates $\boldsymbol{x}$, namely $\Omega_e^h = \boldsymbol{\varphi}(I)$

is used to relate local and Cartesian coordinates

$$\begin{aligned} \boldsymbol{\varphi} \ &: I \longrightarrow \Omega_e^h \\ \boldsymbol{\xi} &\longmapsto \boldsymbol{\varphi}(\boldsymbol{\xi}) := \sum_{i=1}^{\mathtt{n_{en}}} \boldsymbol{x}_i N_i(\boldsymbol{\xi}), \end{aligned} \tag{17}$$

where $\boldsymbol{x}_i$ are the nodal coordinates of the computational element Ω_e^h. Note that Ω_e^h is a polynomial approximation of the physical subdomain Ω_e, in particular, of its boundary, see Figure 28. In fact, the term *isoparametric* stands for the use of the same polynomial shape functions to define the functional approximation u^h, and to describe the geometry of the computational element in Cartesian coordinates, see Equation (17).

Numerical integration in the computational element Ω_e^h (approximation of Ω_e) is performed using the isoparametric transformation given in Equation (17), with a numerical quadrature in the reference element I. For instance, a stiffness elemental matrix coefficient is computed as

$$K_{ij}^e = \int_{\Omega_e^h} \boldsymbol{\nabla}_{\boldsymbol{x}} N_i\big(\boldsymbol{\xi}(\boldsymbol{x})\big) \cdot \boldsymbol{\nabla}_{\boldsymbol{x}} N_i\big(\boldsymbol{\xi}(\boldsymbol{x})\big)\ d\Omega = \int_I \Big(\boldsymbol{J}_{\boldsymbol{\varphi}}^{-1} \boldsymbol{\nabla}_{\boldsymbol{\xi}} N_i(\boldsymbol{\xi})\Big) \cdot \Big(\boldsymbol{J}_{\boldsymbol{\varphi}}^{-1} \boldsymbol{\nabla}_{\boldsymbol{\xi}} N_j(\boldsymbol{\xi})\Big) |\boldsymbol{J}_{\boldsymbol{\varphi}}|\ d\boldsymbol{\xi}, \tag{18}$$

where $\boldsymbol{J}_{\boldsymbol{\varphi}}$ is the Jacobian of the isoparametric transformation, see Equation (17). For curved elements the isoparametric mapping is non-linear. Therefore, the inverse of the Jacobian, $\boldsymbol{J}_{\boldsymbol{\varphi}}^{-1}$, is not a polynomial function, and no exact integration is feasible with standard quadrature rules. In practice, a symmetric triangle quadrature [96] on I, with a sufficiently large number of

Preprint of
R. Sevilla, S. Fernández-Méndez and A. Huerta
NURBS-Enhanced Finite Element Method (NEFEM): A seamless bridge between CAD and FEM
Archives of Computational Methods in Engineering, 18 (4); 441-484, 2011

integration points, is usually employed to compute (18). In fact, a quadrature of order $2p-1$ provides optimal convergence of the isoparametric FEM, see [105].

There are two sources of error in isoparametric FEM. First, the isoparametric mapping in Equation (17) introduces geometric errors, due to the approximation of the physical subdomain Ω_e by the computational element Ω_e^h. In fact, the boundary of the computational domain $\partial\Omega_h$ is a piecewise polynomial approximation of the exact boundary $\partial\Omega$, see Figure 28. Second, for high-order approximations on curved elements, the definition of the polynomial interpolation in Equation (16) in local coordinates, $\boldsymbol{\xi}$, implies a loss of consistency: a polynomial interpolation of degree $p>1$ in $\boldsymbol{\xi}$ does not correspond to a polynomial interpolation of degree p in $\boldsymbol{x}$. This implies that the approximation is able to reproduce linear functions but it is not able to reproduce higher order polynomials in Cartesian coordinates. In other words, curved isoparametric FEs pass the patch test but they fail to pass the so-called *higher order patch tests*, see [105] for further details.

Remark 2. *Optimal convergence of isoparametric FEs is obtained under some smoothness assumptions on the isoparametric mapping. In practice, a specific node placement of interior nodes in curved elements of order $p>2$ is mandatory to guarantee optimal rates of h and p convergence, see [17, 61].*

An alternative to ensure consistency of the approximation, and optimal convergence for any nodal distribution, is the so-called Cartesian FEM. This approach defines the polynomial basis for the approximation of the solution directly in the physical space, with Cartesian coordinates $\boldsymbol{x}$. Nevertheless, the isoparametric transformation in Equation (28) and the computational element Ω_e^h, are still considered for integration purposes. For instance, a stiffness elemental matrix coefficient is computed as

$$K_{ij}^e = \int_{\Omega_e^h} \boldsymbol{\nabla}_{\boldsymbol{x}} N_i(\boldsymbol{x}) \cdot \boldsymbol{\nabla}_{\boldsymbol{x}} N_j(\boldsymbol{x})\, d\Omega = \int_I \boldsymbol{\nabla}_{\boldsymbol{x}} N_i\big(\boldsymbol{x}(\boldsymbol{\xi})\big) \cdot \boldsymbol{\nabla}_{\boldsymbol{x}} N_j\big(\boldsymbol{x}(\boldsymbol{\xi})\big) |\boldsymbol{J}_{\boldsymbol{\varphi}}|\, d\boldsymbol{\xi}. \tag{19}$$

The definition of the approximation with Cartesian coordinates, $\boldsymbol{x}$, ensures reproducibility of polynomials (i.e., consistency of order p). Moreover, exact integration is feasible because shape functions and their derivatives are polynomials, not only with Cartesian coordinates $\boldsymbol{x}$, but also with local coordinates $\boldsymbol{\xi}$. More precisely, for a degree of interpolation p, $N_i\big(\boldsymbol{x}(\boldsymbol{\xi})\big)$ and

Preprint of
R. Sevilla, S. Fernández-Méndez and A. Huerta
NURBS-Enhanced Finite Element Method (NEFEM): A seamless bridge between CAD and FEM
Archives of Computational Methods in Engineering, 18 (4); 441-484, 2011

$\boldsymbol{\nabla}_{\boldsymbol{x}} N_i\big(\boldsymbol{x}(\boldsymbol{\xi})\big)$ are polynomials of degree p and $p-1$, respectively. Therefore, the function to be integrated, $f(\boldsymbol{\xi}) = \boldsymbol{\nabla}_{\boldsymbol{x}} N_i\big(\boldsymbol{x}(\boldsymbol{\xi})\big) \cdot \boldsymbol{\nabla}_{\boldsymbol{x}} N_j\big(\boldsymbol{x}(\boldsymbol{\xi})\big)|\boldsymbol{J}_{\boldsymbol{\varphi}}|$, is a polynomial of degree $p(4p-3)$ in $\boldsymbol{\xi}$. The evaluation of integral in Equation (19) can be exact with a triangle quadrature of order $p(4p-3)$ on the reference element I.

It is worth noting that Cartesian approximation can be considered with Lagrangian, Eulerian, arbitrary Lagrangian-Eulerian or updated Lagrangian formulations. Obviously, Cartesian approximation introduces an overhead with respect to isoparametric FEs because it requires a specific definition of the approximation for each curved element. When the mesh is fixed, this overhead is restricted to elements affected by the curved boundary description, usually a very small portion of the total number of elements. For meshes evolving with the simulation this overhead is repeated each time step, and internal curved edges must be considered. It is worth remarking that the extra cost introduced by Cartesian FEM is justified by the improved accuracy with respect to isoparametric FEs. In addition, Cartesian approximation allows to ensure optimal convergence with no dependence on the node placement for curved elements, see Remark 2 and Section 5.3.

Although Cartesian FEM ensures reproducibility of polynomials in the physical space, the numerical integration in Cartesian FEM is still done in the (approximated) computational element Ω_e^h. Thus, Cartesian FEM precludes the lack consistency of isoparametric FEM, but it still suffers from geometric error. This is not the case for p-FEM and NEFEM formulations.

5.2. NURBS boundary representation

This section recalls the basics of p-FEM formulation considering an exact boundary representation, see [85, 86].

Nodal interpolation in p-FEM is defined in the reference element using local coordinates $\boldsymbol{\xi}$, see Equation (16), but an exact mapping is employed between the reference element I and the physical subdomain Ω_e. For instance, assuming a NURBS parametrization $\boldsymbol{C}(\xi)$ of the curved edge of Ω_e, a simple p-FEM mapping may be

$$\begin{aligned} \boldsymbol{\phi} \; &: I \longrightarrow \Omega_e \\ \boldsymbol{\xi} \longmapsto \boldsymbol{\phi}(\boldsymbol{\xi}) &:= \frac{1-\xi-\eta}{1-\xi}\boldsymbol{C}(\xi) + \frac{\xi\eta}{1-\xi}\boldsymbol{x}_2 + \eta\boldsymbol{x}_3, \end{aligned} \tag{20}$$

where $\boldsymbol{x}_1 = \boldsymbol{C}(0)$ and $\boldsymbol{x}_2 = \boldsymbol{C}(1)$ are the vertices of Ω_e on the curved boundary, and $\boldsymbol{x}_3$ is the internal vertex, see Figure 29. Other options are

Preprint of
R. Sevilla, S. Fernández-Méndez and A. Huerta
NURBS-Enhanced Finite Element Method (NEFEM): A seamless bridge between CAD and FEM
Archives of Computational Methods in Engineering, 18 (4); 441-484, 2011

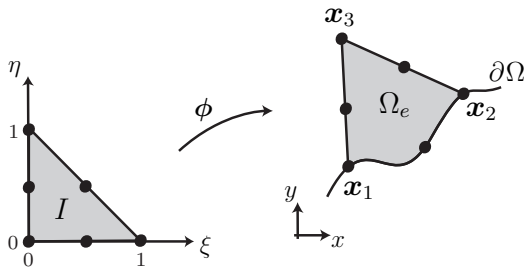

Figure 29: Exact mapping between the reference element I with local coordinates $\boldsymbol{\xi}$, and the physical subdomain Ω_e with Cartesian coordinates $\boldsymbol{x}$

possible in order to define an exact mapping from I to Ω_e, see for instance [71]. However, no relevant differences, depending on the particular mapping $\boldsymbol{\phi}$, are observed in the numerical tests discussed in Section 6.

In p-FEM, a stiffness elemental matrix coefficient is computed as

$$K_{ij}^e = \int_{\Omega_e} \boldsymbol{\nabla}_{\boldsymbol{x}} N_i\big(\boldsymbol{\xi}(\boldsymbol{x})\big) \cdot \boldsymbol{\nabla}_{\boldsymbol{x}} N_i\big(\boldsymbol{\xi}(\boldsymbol{x})\big)\, d\Omega = \int_I \Big(\boldsymbol{J}_{\boldsymbol{\phi}}^{-1} \boldsymbol{\nabla}_{\boldsymbol{\xi}} N_i(\boldsymbol{\xi})\Big) \cdot \Big(\boldsymbol{J}_{\boldsymbol{\phi}}^{-1} \boldsymbol{\nabla}_{\boldsymbol{\xi}} N_j(\boldsymbol{\xi})\Big) |\boldsymbol{J}_{\boldsymbol{\phi}}|\, d\boldsymbol{\xi},$$

integrating over the physical subdomain Ω_e, with an exact description of the geometry. Note that, the inverse of the Jacobian, $\boldsymbol{J}_{\boldsymbol{\phi}}^{-1}$, is not a polynomial function and, as for the isoparametric FEM, no exact integration is feasible with standard quadrature rules. Nevertheless, under some smoothness requirements on the parametrization $\boldsymbol{C}(\xi)$, the same quadrature order used in the isoparametric FEM, that is $2p-1$, guarantees optimal convergence for p-FEM, see [6].

Note that p-FEM presents a major advantage, compared to isoparametric or Cartesian FEM, which is the exact boundary representation. Nevertheless, p-FEM still suffers the same lack of consistency as isoparametric FEM, due to the definition of the polynomial shape functions in the reference element I, with local coordinates $\boldsymbol{\xi}$. This is not the case for NEFEM, see Section 4.3.

NEFEM considers the polynomial approximation with Cartesian coordinates $\boldsymbol{x}$, ensuring reproducibility of polynomials in the physical space for any order of approximation p. The exact description of the boundary is used to perform the numerical integration on the physical subdomain Ω_e. In NEFEM, a stiffness elemental matrix coefficient is computed as

$$K_{ij}^e = \int_{\Omega_e} \boldsymbol{\nabla}_{\boldsymbol{x}} N_i(\boldsymbol{x}) \cdot \boldsymbol{\nabla}_{\boldsymbol{x}} N_j(\boldsymbol{x})\, d\Omega = \int_R \boldsymbol{\nabla}_{\boldsymbol{x}} N_i(\boldsymbol{x}(\boldsymbol{\lambda})) \cdot \boldsymbol{\nabla}_{\boldsymbol{x}} N_j(\boldsymbol{x}(\boldsymbol{\lambda}))|\boldsymbol{J}_{\boldsymbol{\psi}}|\, d\boldsymbol{\lambda},$$

Preprint of
R. Sevilla, S. Fernández-Méndez and A. Huerta
NURBS-Enhanced Finite Element Method (NEFEM): A seamless bridge between CAD and FEM
Archives of Computational Methods in Engineering, 18 (4); 441-484, 2011

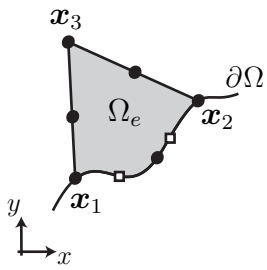

Figure 30: Triangle with a curved edge containing changes of NURBS parametrization (marked with □)

using the transformation in Equation (3).

It is worth recalling that NURBS are piecewise rational functions defined in parametric form, see Section 3. Therefore, numerical integration for p-FEM and NEFEM must be designed to account for changes of NURBS definition along the curved edge of the physical subdomain Ω_e. This issue is addressed in the next section.

5.2.1. Numerical integration for p-FEM and NEFEM

This section discusses the numerical integration for p-FEM and NEFEM when changes of NURBS parametrization are considered inside the curved boundary edge of a physical subdomain Ω_e.

For illustration purposes the triangle with a curved edge represented in Figure 30 is considered first. The curved edge is described with a piecewise parametrization $\boldsymbol{C}$, whose definition changes in two points on the curved edge, marked with □. The parametric coordinates of these points are called the *breakpoints* or *knots* of the NURBS parametrization, see Section 3.

In p-FEM, the piecewise definition of the boundary induces a piecewise definition of the mapping $\boldsymbol{\phi}$, see Equation (20). Therefore, a specifically designed numerical quadrature should be defined in the reference element I. For the triangle represented in Figure 30, with two changes of NURBS definition, the reference element should be partitioned as represented in Figure 31, where the discontinuous lines show the changes of definition of the mapping $\boldsymbol{\phi}$. Note that these lines originate at the breakpoints of the NURBS parametrization in the ξ axis, and are extended inside the reference element. A composite numerical quadrature on I should be defined by using different numerical quadratures in each region.

Preprint of
R. Sevilla, S. Fernández-Méndez and A. Huerta
NURBS-Enhanced Finite Element Method (NEFEM): A seamless bridge between CAD and FEM
Archives of Computational Methods in Engineering, 18 (4); 441-484, 2011

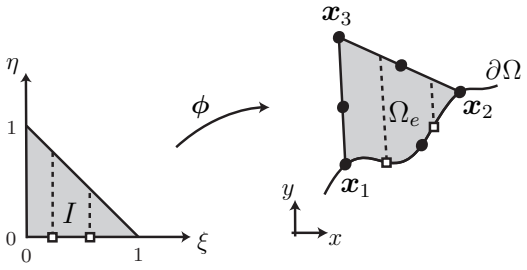

Figure 31: Numerical integration for 2D p-FEM: subdivision of the reference element I to design a numerical quadrature taking into account changes of NURBS parametrization $\boldsymbol{C}(\xi)$ at points marked with $\square$

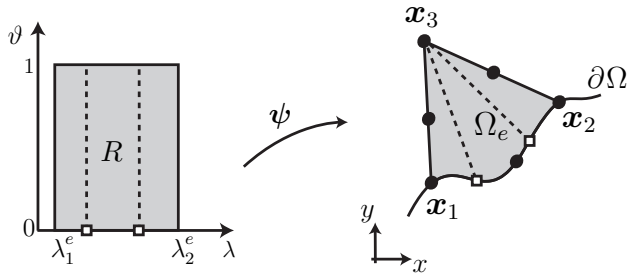

Figure 32: Numerical integration for 2D NEFEM: subdivision of the rectangle $R = [\lambda_1^e, \lambda_2^e] \times [0, 1]$ to design a numerical quadrature taking into account changes of NURBS parametrization $\boldsymbol{C}(\lambda)$ at points marked with $\square$

In NEFEM, changes of NURBS definition are easily accommodated using application $\boldsymbol{\psi}$, defined in Equation (3). The piecewise definition of the boundary also induces a piecewise definition of the element mapping $\boldsymbol{\psi}$. The rectangle R is subdivided using the breakpoints, as represented in Figure 32, and a numerical quadrature in R is defined only in terms of 1D quadratures. A composite 1D Gauss-Legendre quadrature is used in parameter λ to take into account the discontinuous nature of the NURBS parametrization. In the other parameter, ϑ, exact integration is feasible, as discussed in Section 4.4.1.

Changes of NURBS parametrization inside a curved face are easily treated in 3D NEFEM, see Section 4.4.2. The parametric triangle Λ_e is subdivided according to the changes of NURBS parametrization, and numerical quadra-

Preprint of
R. Sevilla, S. Fernández-Méndez and A. Huerta
NURBS-Enhanced Finite Element Method (NEFEM): A seamless bridge between CAD and FEM
Archives of Computational Methods in Engineering, 18 (4); 441-484, 2011

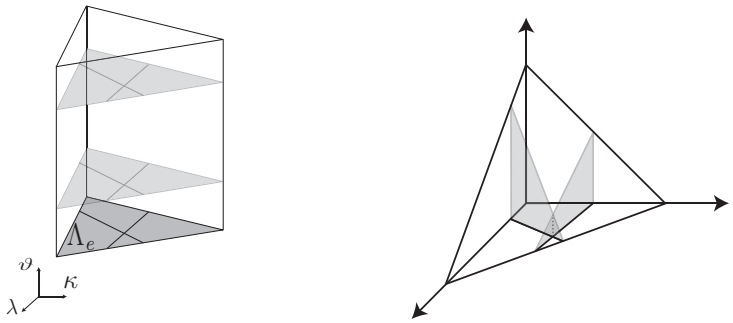

(a) (b)

Figure 33: Subdivisions to design a numerical quadrature taking into account changes of NURBS definition. (a) On the prism $\Lambda_e \times [0,1]$ for 3D NEFEM and (b) on the reference tetrahedral for 3D p-FEM

tures are defined in each subregion, see an example in the left plot of Figure 33.

In the 3D p-FEM context, the definition of a numerical quadrature on the reference tetrahedral accounting changes of NURBS parametrization is more complicated. The generalization of the 2D strategy requires subdivision of the reference tetrahedral element to account for changes of NURBS surface parametrization, see an example in the right plot of Figure 33. In general, different subregions are possible after subdivision. Thus, a simple option to define a quadrature on the reference element is to use further subdivision to obtain only tetrahedral subregions. Then, a composite quadrature may be defined on the reference element based on standard tetrahedral quadratures. In fact, a usual practice to facilitate the implementation of the 3D p-FEM is to consider a polynomial approximation of the boundary. For instance, in [26] a least-squares approximation of the exact boundary is considered in a p-FEM context. Although the polynomial approximation of the boundary can be selected to satisfy continuity requirements across element interfaces [64]. The exact boundary representation is therefore lost in order to simplify the computational implementation.

To conclude, the design of a numerical quadrature accounting for changes of NURBS definition requires specific strategies. For NEFEM, the complexity of the numerical integration in 3D domains is reduced to the design of a 2D numerical quadrature on the parametric triangle Λ_e, and exact integration is feasible in the third direction, see left plot in Figure 33. In contrast, the design of a numerical quadrature in the 3D p-FEM requires careful attention.

Preprint of
R. Sevilla, S. Fernández-Méndez and A. Huerta
NURBS-Enhanced Finite Element Method (NEFEM): A seamless bridge between CAD and FEM
Archives of Computational Methods in Engineering, 18 (4); 441-484, 2011

	Exact geometry	Consistency
Isoparametric FEM	NO	NO
Cartesian FEM	NO	YES
p-FEM	YES	NO
NEFEM	YES	YES

Table 1: Comparison of FE techniques used in domains with curved boundaries

The reference element must be partitioned and 3D composite quadratures must be considered to define a suitable quadrature in the reference element accounting for changes of NURBS definition, see right plot in Figure 33.

5.3. Critical comparison

The main differences between all the FE techniques considered in this work are summarized in Table 1. On one hand, the use of a non-linear mapping relating local and Cartesian coordinates (mapping of Equation (17) in the isoparametric FEM and the exact mapping of Equation (20) in the p-FEM) induces a loss of consistency. That is, a polynomial interpolation of degree $p > 1$ in local coordinates $\boldsymbol{\xi}$, does not correspond to a polynomial interpolation of degree p in Cartesian coordinates $\boldsymbol{x}$. On the other hand, the use of the isoparametric mapping to perform the numerical integration (as done in the isoparametric FEM and in the Cartesian FEM) introduces geometric errors, i.e., the boundary of the computational domain, $\partial\Omega_h$, is a piecewise polynomial approximation of the exact boundary, $\partial\Omega$. The only method ensuring both consistency of the approximation (for any p) and an exact boundary representation of the domain is NEFEM, see Table 1.

It is worth mentioning that, from a computational point of view, the definition of the polynomial basis in local coordinates $\boldsymbol{\xi}$, as done in the isoparametric FEM and in p-FEM, induces a marginal extra efficiency. In this case the polynomial basis is defined once in the reference element and used to define the approximation in each curved element, whereas a Cartesian approximation requires a specific definition of the polynomial basis for each curved element. The use of the isoparametric transformation to perform the numerical integration, as done in the isoparametric FEM and in the Cartesian FEM, also induces another marginal extra efficiency. A numerical quadrature is defined in the reference element I and used for each curved element. Whereas methods with an exact boundary representation require specific strategies for curved elements. Nevertheless, it is important to recall

Preprint of
R. Sevilla, S. Fernández-Méndez and A. Huerta
NURBS-Enhanced Finite Element Method (NEFEM): A seamless bridge between CAD and FEM
Archives of Computational Methods in Engineering, 18 (4); 441-484, 2011

that this extra cost is restricted to elements affected by the NURBS boundary representation, in most applications a very small portion of the total number of elements, those in contact with non polynomial boundaries.

A priori error estimates for the FE methodologies considered in this work have similar expressions, with optimal convergence in all cases. However, the hypotheses to obtain these estimates are different, depending on the definition of the approximation, in local or Cartesian coordinates, and on the boundary representation, that is, approximated or exact.

The influence of the definition of the polynomial basis in local or Cartesian coordinates is discussed first. When the polynomial basis is defined with local coordinates $\boldsymbol{\xi}$, the mapping relating local and Cartesian coordinates must be smooth enough to guarantee optimal convergence. In practice, for the isoparametric FEM specific nodal distributions on curved elements are necessary to obtain optimal convergence rates with $p > 2$, see Remark 2 and [17, 61]. For p-FEM, the NURBS parametrization of the curved boundary must be smooth enough to guarantee the necessary smoothness of the p-FEM mapping relating local and Cartesian coordinates, see [3]. In contrast, when the polynomial basis is defined with Cartesian coordinates $\boldsymbol{x}$, the derivation of *a priori* error estimates is very close to FE *a priori* error estimates in polygonal domains, which can be found in [52, 13]. For Cartesian FEM and NEFEM, no specific nodal distributions in curved elements are necessary to achieve optimal convergence. Moreover, smooth variations of the NURBS parametrization are not required to obtain the optimal convergence rates with NEFEM, see Section 4.5. Nevertheless, optimal *a priori* error estimates for FE methods with a Cartesian approximation require extra attention if a standard (continuous) Galerkin formulation is considered. If a strong imposition of Dirichlet boundary conditions is considered, or if curved internal edges/faces are present in the mesh, optimal nodal distributions in curved elements are necessary in order to guarantee optimal rates of convergence, see Theorems 1 and 2 in Section 4.5. The key issue is that test functions do not vanish over the curved boundary, even if the test function is associated to a node that is not located on the boundary. With specific nodal distributions, such as Fekette points, the error induced by this lack of consistency is lower than the approximation error and the optimal convergence is guaranteed. Obviously, this is not the case for weakly imposed Dirichlet boundary conditions, where optimal convergence is obtained irrespectively of the node placement. Recall that in a DG framework boundary conditions are usually imposed in a weak sense, and recent studies also suggest advantages

Preprint of
R. Sevilla, S. Fernández-Méndez and A. Huerta
NURBS-Enhanced Finite Element Method (NEFEM): A seamless bridge between CAD and FEM
Archives of Computational Methods in Engineering, 18 (4); 441-484, 2011

of imposing boundary conditions weakly in a standard continuous Galerkin framework, see [10].

The influence of the boundary representation in the convergence properties of the approximation is discussed next. For FE methods with an approximate boundary representation (isoparametric FEM and Cartesian FEM), optimal convergence is provided under the assumption that geometric errors are lower than the discretization error. The difference between the computational element Ω_e^h and the physical subdomain Ω_e must be bounded by γh^p, where γ is a constant, h is the characteristic mesh size and p is the interpolation degree. Moreover, bounds of the Jacobian of the isoparametric transformation and its first p derivatives are also necessary, see [17].

Thus, a curved element with an approximated boundary representation must verify two contradictory requirements. On one hand, the computational (polynomial) boundary $\partial\Omega^h$ has to be close enough to the exact boundary $\partial\Omega$. And, on the other hand, the discrepancy between the computational element and the straight-sided element given by its vertices must vanish fast enough, see [61].

6. Numerical examples

In this section the application and performance of NEFEM in the context of continuous and discontinuous Galerkin formulations are illustrated using several 2D and 3D examples.

First, the solution of second-order elliptic problems using a standard continuous Galerkin (CG) formulation is presented. A priori error estimates recalled in Section 4.5 are verified for both h and p refinement. NEFEM is compared to the methodologies for the treatment of curved boundaries discussed in Section 5, namely isoparametric and Cartesian FEM with an approximated boundary representation and p-FEM with a NURBS boundary representation. Finally, the issues associated to Cartesian approximations in the context of CG formulations are discussed.

Secondly, the solution of inviscid compressible flow problems is considered using a discontinuous Galerkin (DG) formulation. The importance of the geometrical model in this context is explored and the benefits of NEFEM are shown.

Finally, NEFEM is applied to the numerical solution of electromagnetic scattering problems using a DG formulation. The advantages of NEFEM in

Preprint of
R. Sevilla, S. Fernández-Méndez and A. Huerta
NURBS-Enhanced Finite Element Method (NEFEM): A seamless bridge between CAD and FEM
Archives of Computational Methods in Engineering, 18 (4); 441-484, 2011

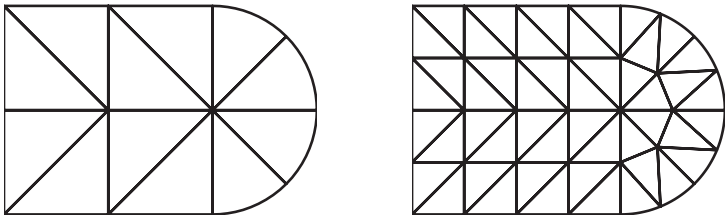

(a) Mesh 1 (b) Mesh 2

Figure 34: Coarse meshes for the second-order elliptic problem. Nested remeshing is used for refinement

this context are presented comparing the results to other curved FE techniques and to other methodologies used by the computational electromagnetics (CEM) community. In addition, the possibilities of NEFEM when the size of the geometrical model is subsidiary to the geometric complexity are shown.

6.1. Second-order elliptic problems

In this section the following model problem is considered

$$\left\{\begin{array}{rcll} -\Delta u + u & = & f & \text{in } \Omega \\ u & = & u_d & \text{on } \Gamma_d \\ \boldsymbol{\nabla} u \cdot \boldsymbol{n} & = & g_n & \text{on } \Gamma_n \end{array}\right.$$

where Ω is the domain, $\overline{\Gamma}_d \cup \overline{\Gamma}_n = \partial\Omega$ and $\boldsymbol{n}$ is the outward unit normal vector on $\partial\Omega$.

First, a 2D domain Ω is considered (see two computational meshes with curved elements in Figure 34). A Dirichlet boundary condition, corresponding to the analytical solution, is imposed in strong form in the polygonal part of the boundary Γ_d, and a Neumann boundary condition, also corresponding to the analytical normal flux, is imposed in the curved part of the boundary Γ_n. If desired, Dirichlet boundary conditions could be imposed in a strong sense over the curved boundary by considering Fekette nodal distributions on curved boundary edges, see Theorem 2 in Section 4.5 and the discussion in Section 5.3. The curved part of the boundary is given by the usual quadratic NURBS that describes a circle, see [72], trimmed to represent half a circle.

In order to illustrate both the relevance of an accurate boundary representation of the domain and the issue of consistency, a polynomial source

Preprint of
R. Sevilla, S. Fernández-Méndez and A. Huerta
NURBS-Enhanced Finite Element Method (NEFEM): A seamless bridge between CAD and FEM
Archives of Computational Methods in Engineering, 18 (4); 441-484, 2011

term is considered first, such that the analytical solution of the problem is a polynomial function of degree 7, namely

$$u(x,y) = x^5y^2 + x^3y^4 + y^7.$$

Figure 35 shows a p-convergence comparison in the coarse mesh of Figure 34. The energy error is represented as a function of the square root of the number of degrees of freedom ($\mathtt{n}_{\mathtt{dof}}$) when the polynomial order of the approximation is uniformly increased, starting with $p = 1$. In NEFEM, the boundary of the domain is exactly represented and the polynomial basis for the approximation is defined in Cartesian coordinates. Therefore, with a polynomial approximation of degree $p = 7$ the solution provided by NEFEM is the exact solution (except from rounding errors). With Cartesian FEs, the basis is also defined in Cartesian coordinates, but the computational boundary is a piecewise polynomial approximation of the circle. Thus, the difference between NEFEM and Cartesian FEM is only due to geometric errors. Although isoparametric FE and the p-FEM show the expected (exponential) convergence, the effect of a non-consistent approximation is clearly observed. The function to be approximated is a polynomial in Cartesian coordinates $u(\boldsymbol{x})$, but it is far from being a polynomial function in local coordinates $u\big(\boldsymbol{\xi}(\boldsymbol{x})\big)$. In this example, errors introduced by a non-consistent approximation are higher than geometric errors. Thus, isoparametric FEM and p-FEM provide the same performance.

Next, the same second-order elliptic problem is solved with a non-polynomial source term, such that the analytical solution of the problem is

$$u(x,y) = x\cos(y) + y\sin(x).$$

Convergence under h-refinement is first explored. Figure 34 shows the first two computational meshes; nested remeshing is used for refinement. The number of integration points is sufficiently large in order to ensure that no errors due to numerical integration are present. Energy error is depicted in Figure 36 for a polynomial approximation of degree $p = 5$ and $p = 6$. The optimal rate of h-convergence is exhibited by every FE technique considered, but some differences in accuracy are observed. In this example the use of a Cartesian approximation (Cartesian FEs and NEFEM) provides more accurate results than defining the approximation with local coordinates. NEFEM always provides the most accurate results due to the combined effect of the Cartesian approximation and exact boundary representation. With

Preprint of
R. Sevilla, S. Fernández-Méndez and A. Huerta
NURBS-Enhanced Finite Element Method (NEFEM): A seamless bridge between CAD and FEM
Archives of Computational Methods in Engineering, 18 (4); 441-484, 2011

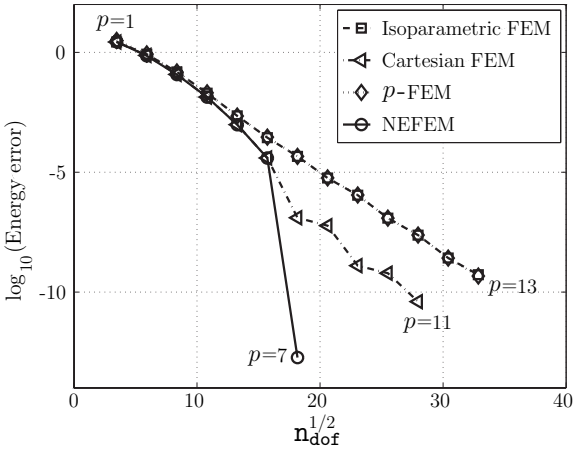

Figure 35: Poisson problem with polynomial analytical solution: p-convergence in the energy norm in the coarse mesh of Figure 34

$p = 6$, NEFEM is one order of magnitude more accurate than Cartesian FEs and two orders of magnitude more accurate than isoparametric FEs and p-FEM. In this example, p-FEM does not represent an advantage with respect to isoparametric FEs. The error induced by the geometric approximation of the boundary is lower than the error introduced by the definition of the polynomial basis in local coordinates.

Figure 37 shows a similar analysis but related to the Neumann boundary: h-convergence in the $\mathcal{L}^2(\Gamma_n)$ norm is compared for isoparametric FEM, Cartesian FEM, p-FEM and NEFEM with a polynomial interpolation up to degree $p = 4$. Optimal convergence rates, i.e $p + 1$, are obtained with isoparametric FEM, Cartesian FEM and p-FEM, but it is very important to note that NEFEM exhibits a superior rate of convergence, namely $p + 2$. In fact, almost identical results are obtained using NEFEM with a degree of approximation p and isoparametric FEM with a degree of approximation $p+1$, with a saving in the number of nodes between 25% and 50% Moreover, for the same mesh and order of interpolation, NEFEM is between two and three orders of magnitude more precise than the corresponding isoparametric FE solution. Thus, this numerical example illustrates the efficiency of NEFEM, in front of other FE techniques, for the computation of quantities of interest at (or near) curved boundaries. It is worth emphasizing that even if the exact boundary representation is considered by means of p-FEM the

Preprint of
R. Sevilla, S. Fernández-Méndez and A. Huerta
NURBS-Enhanced Finite Element Method (NEFEM): A seamless bridge between CAD and FEM
Archives of Computational Methods in Engineering, 18 (4); 441-484, 2011

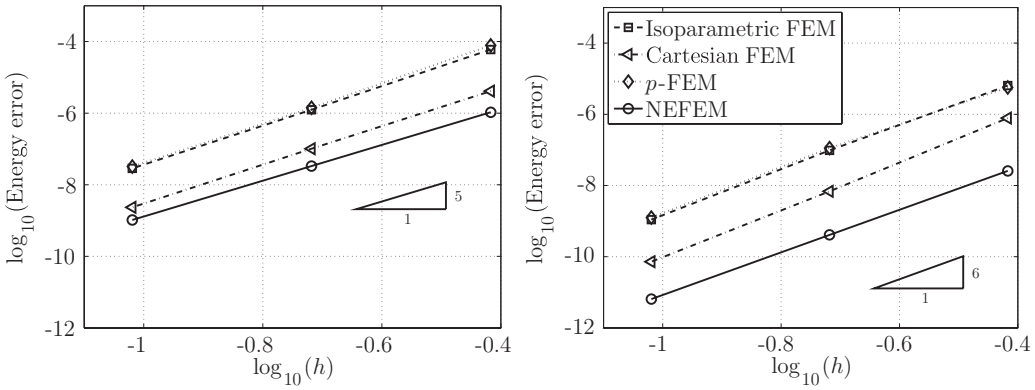

(a) p=5 (b) p=6

Figure 36: Second-order elliptic problem: h-convergence in the energy norm

results are much less accurate than using NEFEM evidencing, once more, the importance of the geometrical model in conjunction with the definition of the polynomial basis in Cartesian coordinates.

As shown in the h-convergence study, NEFEM is advantageous for low and high-order approximations. Next, convergence under p-refinement is explored and compared. Figure 38 represents the evolution of the energy error as a function of the square root of $\mathtt{n_{dof}}$. The polynomial degree of the approximation is uniformly increased starting with $p = 1$ and for the discretizations shown in Figure 34. As the order of the polynomial approximation is increased, NEFEM offers the best performance. In fact, the desired error is attained with the minimum $\mathtt{n_{dof}}$. Figure 38 shows that, for a given accuracy and the coarsest mesh in Figure 34, NEFEM allows to reduce drastically the $\mathtt{n_{dof}}$. In particular, a reduction of 40% compared to Cartesian FEM and up to 50% compared to isoparametric FEM or p-FEM.

The influence of the number of integration points $\mathtt{n_{ip}}$ on the accuracy is studied next. The coarsest mesh in Figure 34 with a polynomial approximation of degree $p = 6$ and $p = 8$ is used. To study quadrature accuracy, Figure 39 shows the evolution of the energy error versus the number of Gauss integration points for every curved boundary edge. When the polynomial basis is defined in Cartesian coordinates (Cartesian FEM and NEFEM), numerical integration requires more integration points to reach its maximum accuracy, compared to the other methods. For a given degree of interpolation, NEFEM is able to reach the same accuracy of isoparametric FEs with only one extra

Preprint of
R. Sevilla, S. Fernández-Méndez and A. Huerta
NURBS-Enhanced Finite Element Method (NEFEM): A seamless bridge between CAD and FEM
Archives of Computational Methods in Engineering, 18 (4); 441-484, 2011

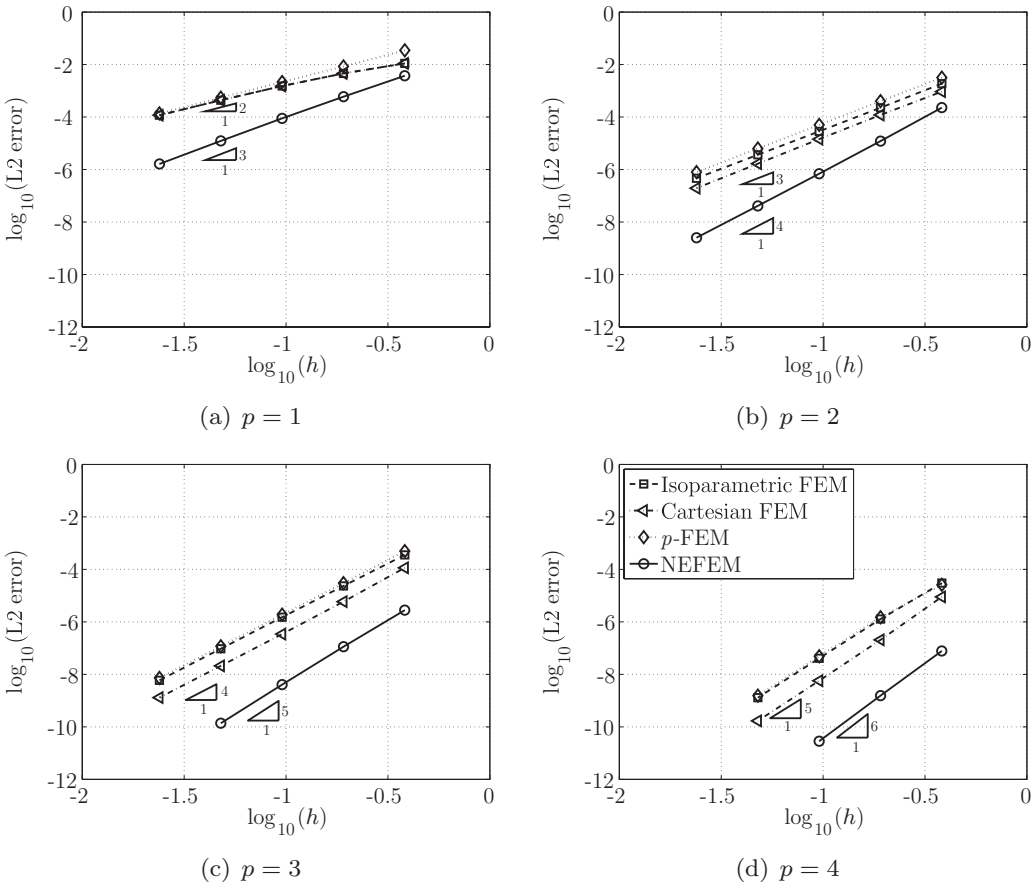

(a) $p = 1$ (b) $p = 2$

(c) $p = 3$ (d) $p = 4$

Figure 37: Second-order elliptic problem: h-convergence in the $\mathcal{L}^2(\Gamma_n)$ norm

Preprint of
R. Sevilla, S. Fernández-Méndez and A. Huerta
NURBS-Enhanced Finite Element Method (NEFEM): A seamless bridge between CAD and FEM
Archives of Computational Methods in Engineering, 18 (4); 441-484, 2011

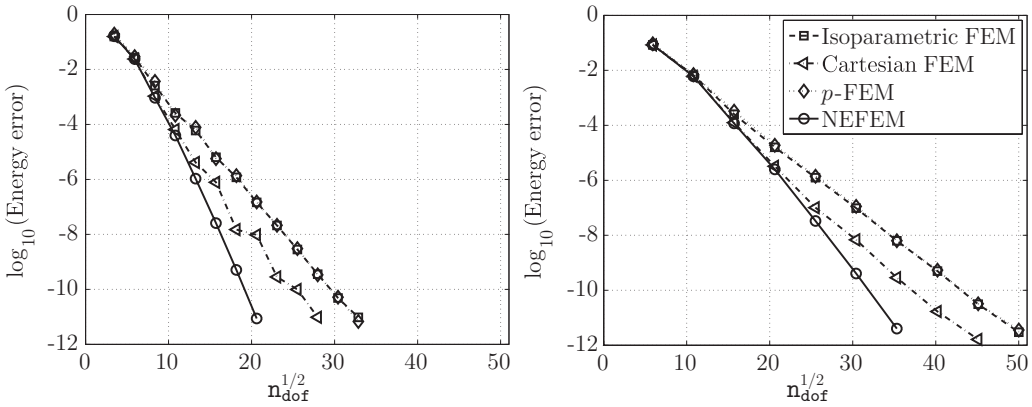

(a) Mesh 1 (b) Mesh 2

Figure 38: Second-order elliptic problem: p-convergence in the energy norm for the computational meshes represented in Figure 34

integration point. Moreover, with three or four integration points more than isoparametric FEM, NEFEM reaches its maximum accuracy. For a degree of interpolation $p = 8$, NEFEM is four orders of magnitude more precise than isoparametric FEM and p-FEM, and three orders of magnitude more precise than Cartesian FEM.

Comparing left and right plots in Figure 39 it is important to note that NEFEM with $p = 6$ and 9 Gauss integration points along curved boundary edges achieves comparable accuracy to isoparametric FEM with $p = 8$ and 9 Gauss integration points. That means, that NEFEM is able to reach the same accuracy than isoparametric FEs using the same number of integration points for boundary integrals but with a lower degree of approximation. Figure 40 shows the evolution of the energy error versus the total number of integration points for interior integrals as the degree of approximation p is increased.For each point of this figure the minimum number of integration points to achieve maximum accuracy for a given p is used. Due to the lower degree of approximation required by NEFEM, it achieves the same accuracy than isoparametric FEM with an important reduction in the total number of integration points. Therefore, although NEFEM requires more computational effort per integration point due to the Cartesian approximation and the NURBS boundary representation, this comparison shows that NEFEM is competitive because the required number of integration points

Preprint of
R. Sevilla, S. Fernández-Méndez and A. Huerta
NURBS-Enhanced Finite Element Method (NEFEM): A seamless bridge between CAD and FEM
Archives of Computational Methods in Engineering, 18 (4); 441-484, 2011

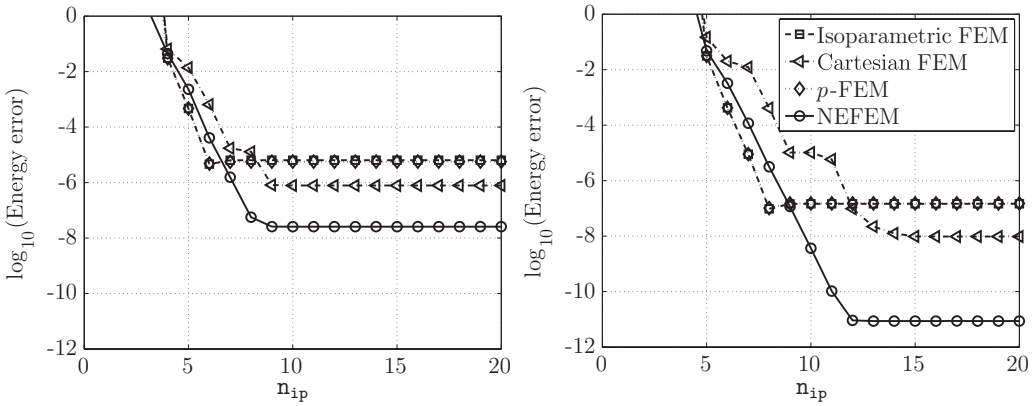

(a) p=6 (b) p=8

Figure 39: Second-order elliptic problem: Energy norm of the error as the number of integration points ($\mathtt{n_{ip}}$) along the curved boundary edge is increased. Coarse mesh of Figure 34

is substantially reduced to achieve a desired accuracy. Figure 40 also shows that Cartesian FEs are not competitive because the necessary number of integration points to achieve a comparable accuracy is much greater than using NEFEM or isoparametric FEM. Finally, note that the results using p-FEM are not displayed because in this problem it behaves as isoparametric FEM, see Figure 39.

Next the behavior of NEFEM in 3D for the solution of the second-order elliptic problem (6.1) is studied, where Ω is a sphere of unit radius. The analytical solution is $u(x, y) = x\cos(y) + y\sin(z) + z\cos(x)$, and the source term s is determined by analytical differentiation of u. Neumann boundary conditions corresponding to the analytical normal flux are imposed in $\partial\Omega$. A coarse mesh with only eight curved tetrahedral elements is considered, see Figure 41, and high-order approximations are introduced to properly capture the solution.

Figure 42 shows Cartesian FEM and NEFEM solutions with quadratic and cubic approximation. The piecewise polynomial approximation of the curved boundary introduced by isoparametric mapping is clearly observed. With quadratic FEs, the maximum difference between exact and approximated boundaries is 0.1037. For cubic approximation, geometric error is still important, 0.0268. Moreover, the piecewise polynomial approximation of the

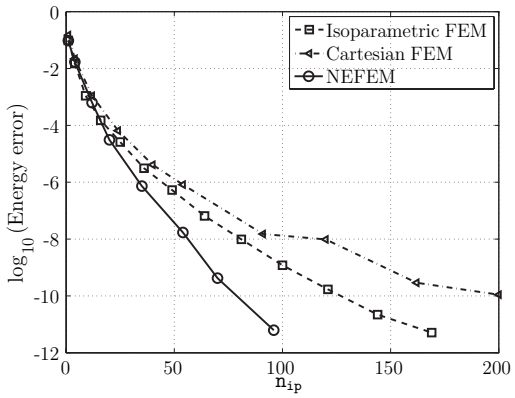

Figure 40: Second-order elliptic problem: Energy norm of the error vs number of integration points ($\mathtt{n_{ip}}$) for interior integrals as p increases using the coarsest mesh in Figure 34

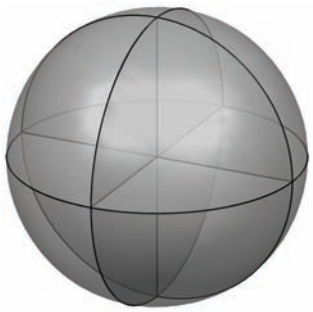

Figure 41: Coarse mesh of the sphere with eight curved tetrahedrons

Preprint of
R. Sevilla, S. Fernández-Méndez and A. Huerta
NURBS-Enhanced Finite Element Method (NEFEM): A seamless bridge between CAD and FEM
Archives of Computational Methods in Engineering, 18 (4); 441-484, 2011

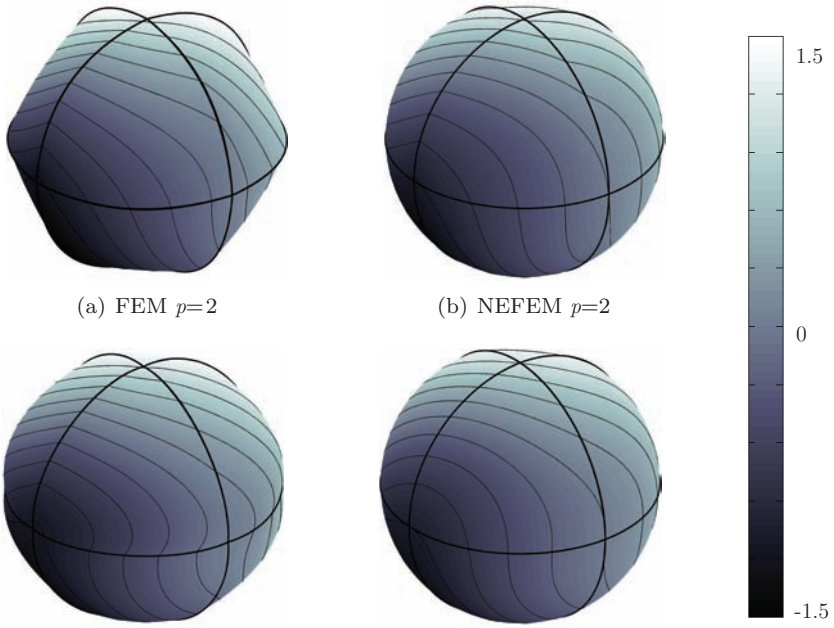

(a) FEM p=2 (b) NEFEM p=2

(c) FEM p=3 (d) NEFEM p=3

Figure 42: Second-order elliptic problem: surface plot of Cartesian FEM and NEFEM solutions using quadratic and cubic approximations

boundary induces a loss of regularity. Recall that the exact boundary $\partial\Omega$ is a $\mathcal{C}^\infty$ surface, whereas its piecewise isoparametric approximation $\partial\Omega^h$ is only $\mathcal{C}^0$ across boundary edges, see Figures 42 (a) and (c). NEFEM exactly describes the sphere boundary with one quadratic singular NURBS, independently of the spatial discretization (i.e. the polynomial degree of approximation), as represented in Figures 42 (b) and (d).

Figure 43 shows a p-convergence comparison when the polynomial order of approximation is uniformly increased starting with $p = 2$ and for the discretization shown in Figure 41. Errors in maximum and energy norms are represented as a function of the cube root of $\mathtt{n}_{\mathtt{dof}}$. For NEFEM, the expected (exponential) convergence for a problem with a smooth solution is obtained, whereas a much slower convergence is obtained for methods with an approximate boundary representation. Note that Cartesian and isoparametric FEs offer the same performance if error is measured in maximum norm. However, when error is measured in energy norm, Cartesian FEs perform slightly better. The definition of the polynomial basis in Cartesian coordinates offers a

Preprint of
R. Sevilla, S. Fernández-Méndez and A. Huerta
NURBS-Enhanced Finite Element Method (NEFEM): A seamless bridge between CAD and FEM
Archives of Computational Methods in Engineering, 18 (4); 441-484, 2011

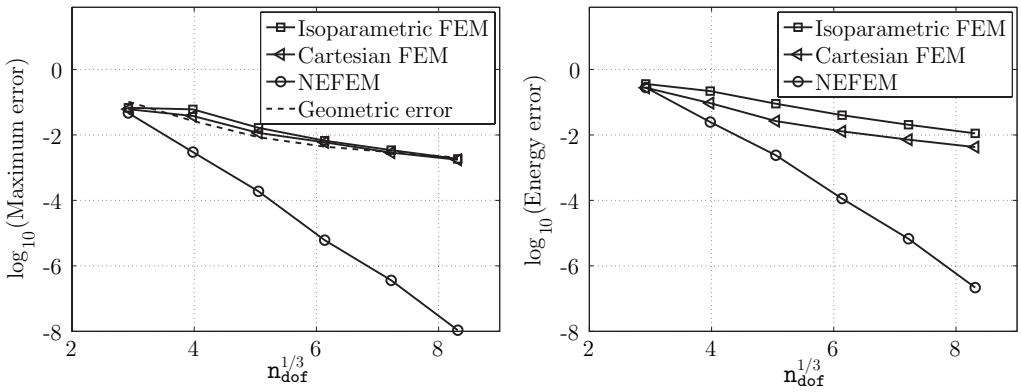

Figure 43: p-convergence comparison for the second-order elliptic problem. The polynomial degree of the approximation is uniformly increased from $p = 2$ and the error is measured (a) in the maximum norm and (b) in the energy norm

better approximation of derivatives compared to isoparametric FEs. Figure 43 (a) also depicts maximum geometric error (measured as the maximum distance between true boundary $\partial\Omega$ and its approximation $\partial\Omega^h$), revealing that geometric error controls solution error if an approximated boundary representation is considered (isoparametric FEM or Cartesian FEM).

This example stress the importance of geometrical model in FE simulations and critical conclusions are derived. In [85], p-FEM with an exact boundary description is compared to high-order subparametric elements (with a quadratic approximation of the boundary). Two dimensional examples confirm the expected exponential convergence of p-FEM, whereas subparametric approach leads to a suboptimal convergence rate. The 3D example shown in this section shows a more dramatic situation because NEFEM is compared to high-order isoparametric and Cartesian elements. Therefore, this example demonstrate that a high-order approximation of the geometry is not always sufficient to achieve maximum performance for a given spatial discretization.

In most situations, internal edges can be straight, but there are a number of situations in which internal curved edges are present in a computational mesh. For instance, curved internal edges must be considered in a boundary layer or in the presence of a curved material interface. Moreover, in 3D internal faces with an edge on the NURBS boundary are curved even when

Preprint of
R. Sevilla, S. Fernández-Méndez and A. Huerta
NURBS-Enhanced Finite Element Method (NEFEM): A seamless bridge between CAD and FEM
Archives of Computational Methods in Engineering, 18 (4); 441-484, 2011

Figure 44: Mesh of a sphere showing some internal curved faces

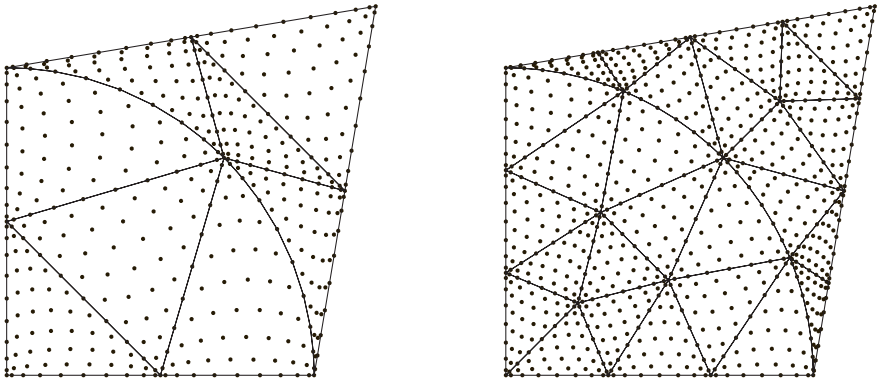

(a) Mesh 1 (b) Mesh 2

Figure 45: Two triangular meshes with interior curved edges and Fekette nodal distributions for a degree of approximation $p = 8$

internal edges are straight, see an example in Figure 44. The use of Cartesian approximations in that situation requires special attention, see Theorem 2 in Section 4.5 and the discussion in Section 5.3. In order to illustrate this issue the second-order elliptic problem (6.1) is solved in a 2D domain using elements with internal curved edges, see two computational meshes in Figure 45. Note that specific nodal distributions, such as Fekette nodes, must be used in order to achieve optimal performance of the Cartesian approximation. Figure 46 shows a p-convergence comparison by using different nodal distributions in the discretizations shown in Figure 45. The error in energy norm is represented as a function of the square root of $\mathtt{n}_{\mathtt{dof}}$. When equally-spaced nodal distributions are employed, exponential convergence is not achieved. The accuracy is substantially improved with Fekette nodal distributions adapted

Preprint of
R. Sevilla, S. Fernández-Méndez and A. Huerta
NURBS-Enhanced Finite Element Method (NEFEM): A seamless bridge between CAD and FEM
Archives of Computational Methods in Engineering, 18 (4); 441-484, 2011

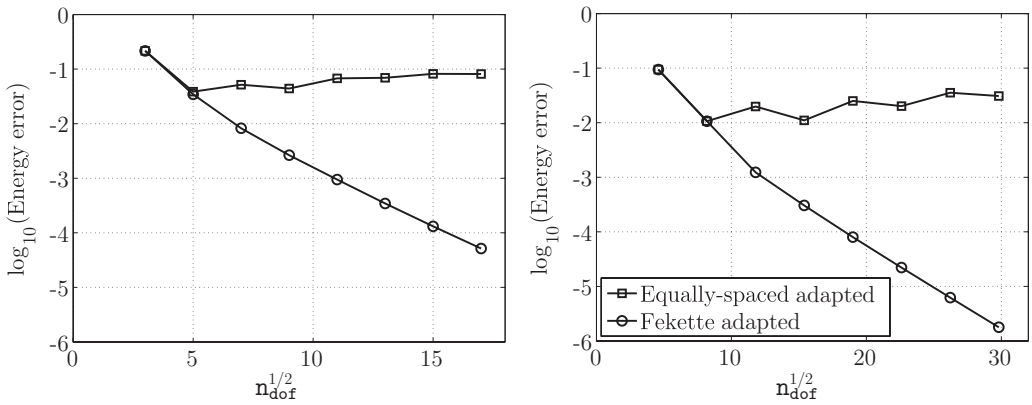

(a) Mesh 1 (b) Mesh 2

Figure 46: p-convergence of the error in the energy norm for different nodal distributions on the meshes of Figure 45

to the exact geometry, showing the expected (exponential) convergence.

A similar performance is observed in 3D simulations, see an example in Figure 47. The second-order elliptic problem (6.1) is solved in a sphere with the computational mesh represented in Figure 44. A detailed view of the numerical solution reveals a small discontinuity of the solution across curved boundary edges.

Remark 3. *As usual, for any formulation using Cartesian approximation, the reader should be aware that the continuity of the solution across internal curved faces is not guaranteed by imposing the continuity of the solution at face nodes. Optimal nodal distributions on curved internal faces can be used in order to guarantee optimal convergence or extra constraints must be imposed in order to guarantee continuity of the solution across internal faces. This difficulty does not appear if a DG framework because the continuity of the solution is weakly imposed, with numerical fluxes.*

6.2. Inviscid compressible flow

Euler equations of gas dynamics express the conservation of mass, momentum and energy for a compressible, inviscid and non-conducting fluid. The strong form of these conservation laws, in the absence of external volume forces, can be written in conservative form as

$$\frac{d\boldsymbol{U}}{dt} + \frac{\partial \boldsymbol{F}_k(\boldsymbol{U})}{\partial x_k} = \boldsymbol{0}, \tag{21}$$

Preprint of
R. Sevilla, S. Fernández-Méndez and A. Huerta
NURBS-Enhanced Finite Element Method (NEFEM): A seamless bridge between CAD and FEM
Archives of Computational Methods in Engineering, 18 (4); 441-484, 2011

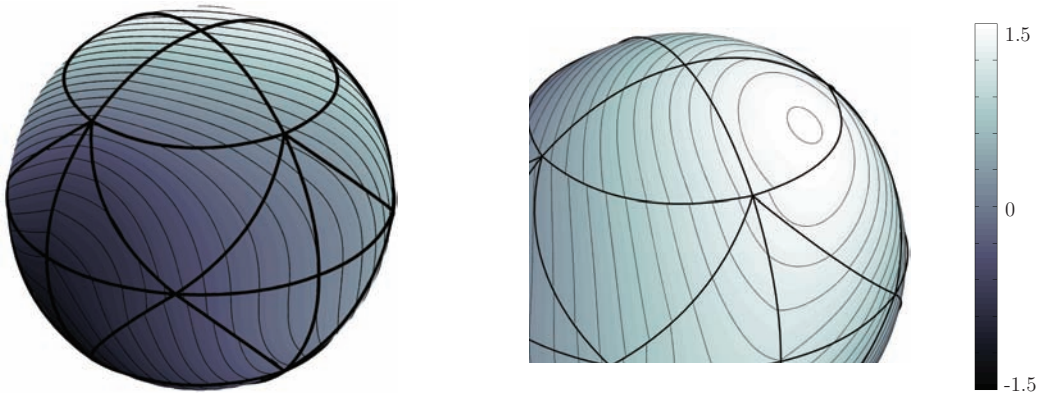

Figure 47: Solution of the Poisson problem in a sphere and detail of the solution showing a small discontinuity across curved boundary edges

where Einstein notation is assumed (that is repeated indices are implicity summed over), $\boldsymbol{U}$ is the vector of conservation variables and $\boldsymbol{F}_k(\boldsymbol{U})$ are the flux vectors for each spatial dimension x_k, that is

$$\boldsymbol{U} = \begin{pmatrix} \rho \\ \rho \boldsymbol{v} \\ \rho E \end{pmatrix}, \qquad \boldsymbol{F}_k(\boldsymbol{U}) = \begin{pmatrix} \rho v_k \\ \rho \boldsymbol{v} v_k + \boldsymbol{e}_k \mathrm{p} \\ (\rho E + \mathrm{p}) v_k \end{pmatrix},$$

where ρ is the density, $\rho \boldsymbol{v}$ is the momentum, ρE is the total energy per unit volume, $\boldsymbol{e}_k$ is the unitary vector in the x_k direction, and p is the pressure, see [31] for more details.

An equation of state, relating the internal energy to pressure and density, completes this system of nonlinear hyperbolic equations. For a perfect polytropic gas the equation of state is

$$\mathrm{p} = (\gamma - 1)\rho\Big(E - \frac{1}{2}\|\boldsymbol{v}\|^2\Big),$$

where γ is the ratio of the specific heat coefficients (specific heat at constant pressure over specific heat at constant volume), with value $\gamma = 1.4$ for air.

A usual quantity for postprocess of inviscid flow computations is the Mach number, defined as

$$M = \frac{\|\boldsymbol{v}\|}{c},$$

where $c = \sqrt{\gamma \mathrm{p}/\rho}$ is the speed of sound. For a more detailed presentation of the Euler equations see for instance [2, 47, 58].

Preprint of
R. Sevilla, S. Fernández-Méndez and A. Huerta
NURBS-Enhanced Finite Element Method (NEFEM): A seamless bridge between CAD and FEM
Archives of Computational Methods in Engineering, 18 (4); 441-484, 2011

The importance of the geometrical model in the numerical solution of Euler equations is crucial, see for instance [27, 9, 8, 22, 92, 98, 97, 55, 34, 37] to name a few. In this section NEFEM is presented as a powerful method for solving the Euler equations of gas dynamics in the presence of curved boundaries.

All computations in this section are advanced in time until the density residual is reduced to 10^{-10} in the $\mathcal{L}_2(\Omega)$ norm by using a third-order TVD Runge-Kutta scheme, see [23, 40]. The approximate Roe solver is considered for the evaluation of the numerical flux, see for instance [90]. In fact, the Roe flux provides more accurate results than the Lax-Friederichs one for low order approximations, but no significant differences are observed for high-order approximations. However, it is very important to remark that the conclusions of the work derived from the comparison of NEFEM and FEM are exactly the same with a Lax-Friederichs flux.

The first example considers the subsonic flow around a circle at free-stream Mach number $M_\infty = 0.3$. This example is a classical test case for inviscid flow solvers because it allows to quantify the numerical dissipation of a given scheme in the presence of curved boundaries. As shown first in [9] using a linear approximation for the geometry it is not possible to converge to the steady state solution, even if the mesh is drastically refined near the circle. As it is commented in [21], the singularities of the polygonal approximation of the boundary generate entropy and the solution develops a non-physical wake that makes impossible the convergence to the correct solution.

To illustrate that problem and to show the possibilities of NEFEM in this scenario, four O-meshes with 16×4, 32×8, 64×16, and 128×32 nodes (i.e. 128, 512, 2048 and 8192 elements respectively) are considered for low-order computations. A detailed view of these meshes near the circle is represented in Figure 48.

Figure 49 shows Mach number isolines for isoparametric FE with linear approximation. The results corroborate the conclusions first published by Bassi and Rebay: even if the mesh is highly refined near the circle, for instance using the fine mesh of Figure 48 with 128 curved elements along the circular boundary, a non-physical entropy production is observed behind the wall.

Figure 50 shows Mach number isolines computed with NEFEM using linear approximation. The results reveal a very good symmetry of the Mach number patterns, even if coarse meshes are used. More important, NEFEM allows convergence to the correct physical solution using the fine mesh with

Preprint of
R. Sevilla, S. Fernández-Méndez and A. Huerta
NURBS-Enhanced Finite Element Method (NEFEM): A seamless bridge between CAD and FEM
Archives of Computational Methods in Engineering, 18 (4); 441-484, 2011

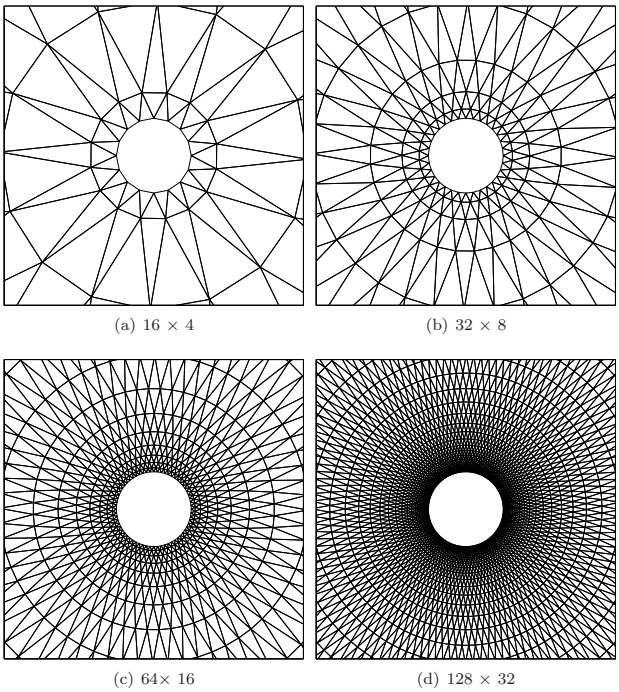

(a) 16 × 4 (b) 32 × 8

(c) 64× 16 (d) 128 × 32

Figure 48: Inviscid subsonic flow around a circle: detail of O-meshes for low-order computations

1

Preprint of
R. Sevilla, S. Fernández-Méndez and A. Huerta
NURBS-Enhanced Finite Element Method (NEFEM): A seamless bridge between CAD and FEM
Archives of Computational Methods in Engineering, 18 (4); 441-484, 2011

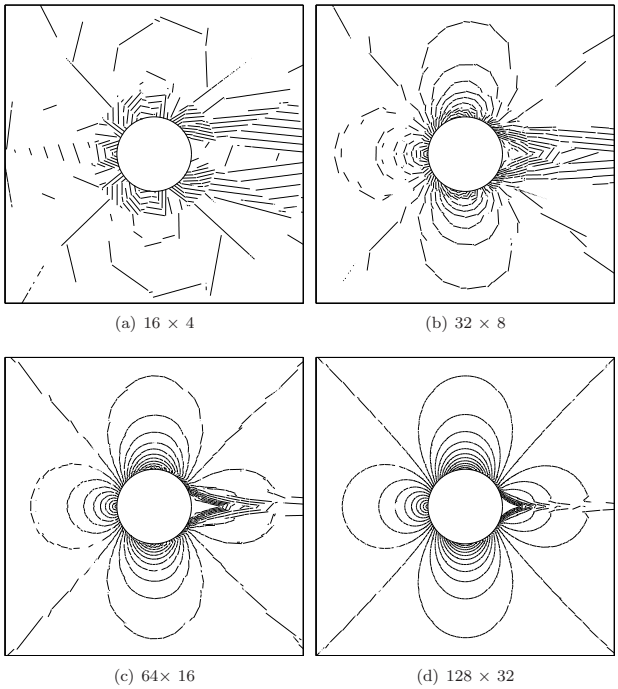

(a) 16 × 4 (b) 32 × 8

(c) 64× 16 (d) 128 × 32

Figure 49: Inviscid subsonic flow around a circle: Mach number isolines with isoparametric FE and p=1

1

Preprint of
R. Sevilla, S. Fernández-Méndez and A. Huerta
NURBS-Enhanced Finite Element Method (NEFEM): A seamless bridge between CAD and FEM
Archives of Computational Methods in Engineering, 18 (4); 441-484, 2011

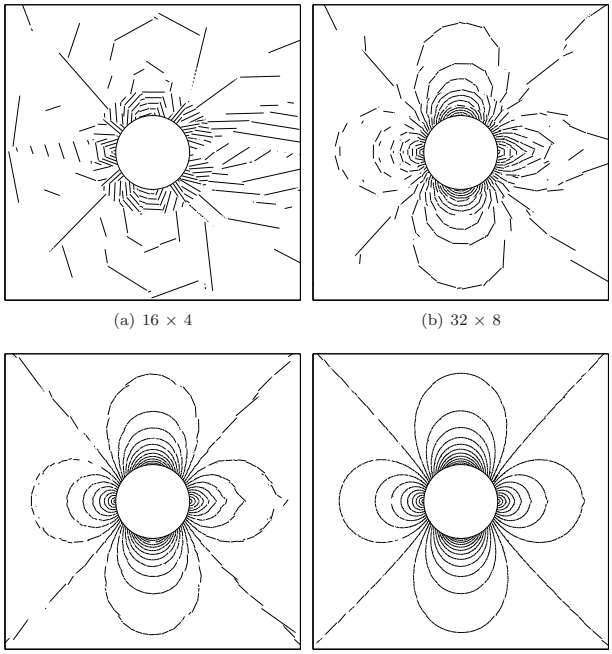

(a) 16 × 4 (b) 32 × 8

(c) 64× 16 (d) 128 × 32

Figure 50: Inviscid subsonic flow around a circle: Mach number isolines with NEFEM and p=1

a piecewise linear approximation of the solution. The exact computation of the outward unit normal improves the imposition of the solid wall boundary condition. This issue and the exact representation of the boundary drastically reduce the entropy production compared to isoparametric FE.

In order to provide a more quantitative analysis, other aerodynamic quantities for the evaluation of the accuracy are used, namely the entropy error

$$\epsilon_{\mathtt{ent}} = \frac{\mathrm{p}}{\mathrm{p}_\infty}\left(\frac{\rho_\infty}{\rho}\right)^\gamma - 1,$$

the pressure loss

$$\mathrm{p}_{\mathtt{loss}} = \frac{\mathrm{p}}{\mathrm{p}_\infty}\left(\frac{1+0.5(\gamma-1)M^2}{1+0.5(\gamma-1)M_\infty^2}\right)^{\frac{\gamma}{\gamma-1}},$$

Preprint of
R. Sevilla, S. Fernández-Méndez and A. Huerta
NURBS-Enhanced Finite Element Method (NEFEM): A seamless bridge between CAD and FEM
Archives of Computational Methods in Engineering, 18 (4); 441-484, 2011

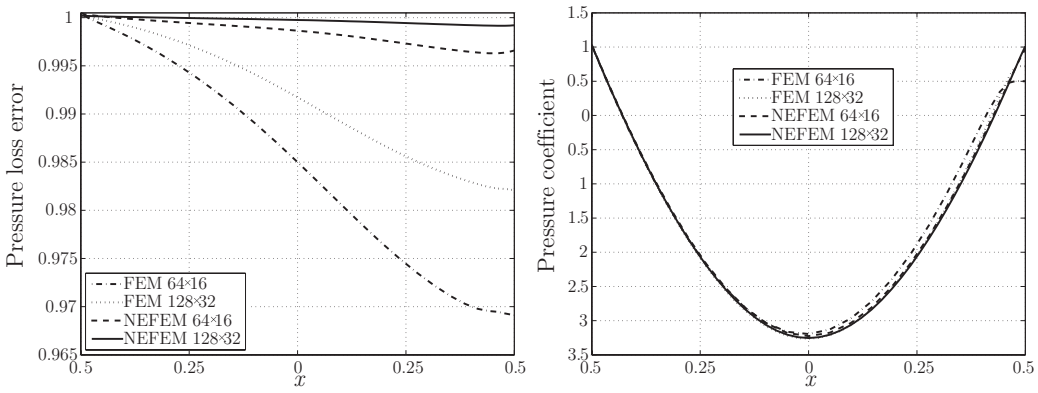

(a) (b)

Figure 51: Inviscid subsonic flow around a circle: (a) Pressure loss distribution and (b) pressure coefficient distribution, at the upper mid of the circle for p=1

and the pressure coefficient

$$C_{\mathrm{p}} = \frac{\mathrm{p} - \mathrm{p}_\infty}{0.5\rho_\infty v_\infty^2},$$

where the subscript ∞ indicates free-stream values.

Figure 51 shows pressure loss and pressure coefficient distributions on the upper mid of the circle. At the most critical point, the stagnation point behind the circle, the maximum pressure loss error with isoparametric FE in the fine mesh is 1.8×10^{-2}, whereas NEFEM maximum error is reduced more than one order of magnitude, namely 8.4×10^{-4}. Moreover, in the fine mesh, the pressure coefficient error at the stagnation point is 2.8×10^{-1} for standard FE and 4×10^{-3} for NEFEM, almost two orders of magnitude more precise for the same number of degrees of freedom.

Figure 52 represents h-convergence of the entropy error on the upper part of the circle. Entropy production observable in Figure 49 deteriorates the h-convergence of standard isoparametric FEs. In contrast, NEFEM exhibits the optimal convergence rate for linear approximation.

The next example involves the subsonic flow over a NACA0012 airfoil at free stream Mach number $M_\infty = 0.3$ and angle of attack $\alpha = 0^o$. Four O-meshes with 16×4, 32×8, 64×16, and 128×32 nodes (i.e. 128, 512, 2048 and 8192 elements respectively) are considered for low-order computations. A detailed view of these meshes near the airfoil is represented in Figure 53.

Preprint of
R. Sevilla, S. Fernández-Méndez and A. Huerta
NURBS-Enhanced Finite Element Method (NEFEM): A seamless bridge between CAD and FEM
Archives of Computational Methods in Engineering, 18 (4); 441-484, 2011

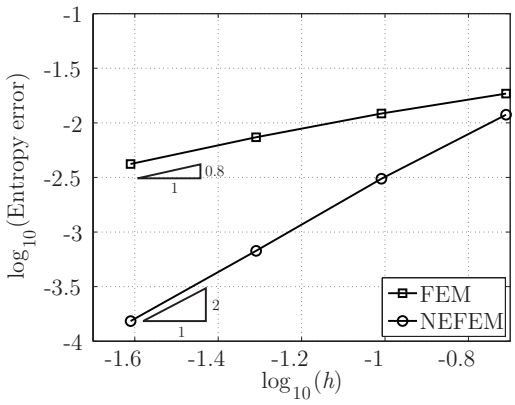

Figure 52: Inviscid subsonic flow around a circle: h-convergence of the entropy error for isoparametric FEs and NEFEM ($p = 1$)

To design such meshes, a conformal mapping is applied to previous meshes used for the flow around a circle.

Figure 54 shows Mach number isolines for isoparametric FE with linear approximation. Again, the results illustrate the spurious entropy production caused by the polygonal approximation of curved boundaries. Figure 55 shows Mach number isolines computed with NEFEM using linear approximation. The results show, once more, a remarkable improvement due to the exact boundary representation. To quantify accuracy, Figure 56 compare the entropy production and pressure loss in the upper part of the airfoil for isoparametric FE and NEFEM in the finest mesh if Figure 53. With isoparametric FE the $\mathcal{L}^2$ norm of the entropy error on the airfoil profile is 1.3×10^{-3} in the finest mesh. The exact boundary representation considered in NEFEM reduces the $\mathcal{L}^2$ norm of the entropy error on the airfoil profile to 4×10^{-4}, almost three times more accurate than isoparametric FEs. As usual in subsonic inviscid flow simulation involving airfoils, the most critical region is the leading edge, not only due to the high variations of the curvature of the airfoil but also because under-resolved flow features are convected contaminating the solution around the whole profile.

The next example involves the subsonic flow over a bump at free stream Mach number $M_\infty = 0.5$ and it is used to demonstrate the possibilities of NEFEM using ultra coarse meshes and high-order approximations. Figure 57 (a) shows the computational mesh, with only two curved elements and 22

Preprint of
R. Sevilla, S. Fernández-Méndez and A. Huerta
NURBS-Enhanced Finite Element Method (NEFEM): A seamless bridge between CAD and FEM
Archives of Computational Methods in Engineering, 18 (4); 441-484, 2011

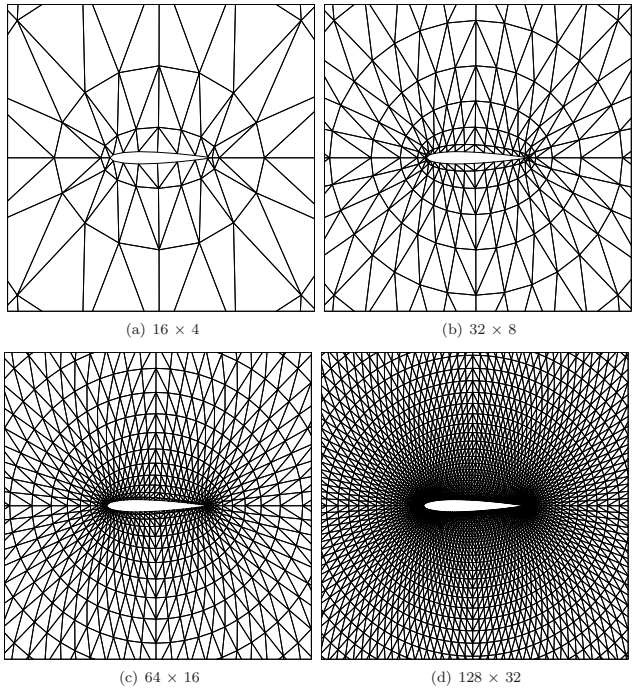

(a) 16 × 4 (b) 32 × 8

(c) 64 × 16 (d) 128 × 32

Figure 53: Inviscid subsonic flow around a NACA0012 airfoil: detail of O-meshes for low-order computations

Preprint of
R. Sevilla, S. Fernández-Méndez and A. Huerta
NURBS-Enhanced Finite Element Method (NEFEM): A seamless bridge between CAD and FEM
Archives of Computational Methods in Engineering, 18 (4); 441-484, 2011

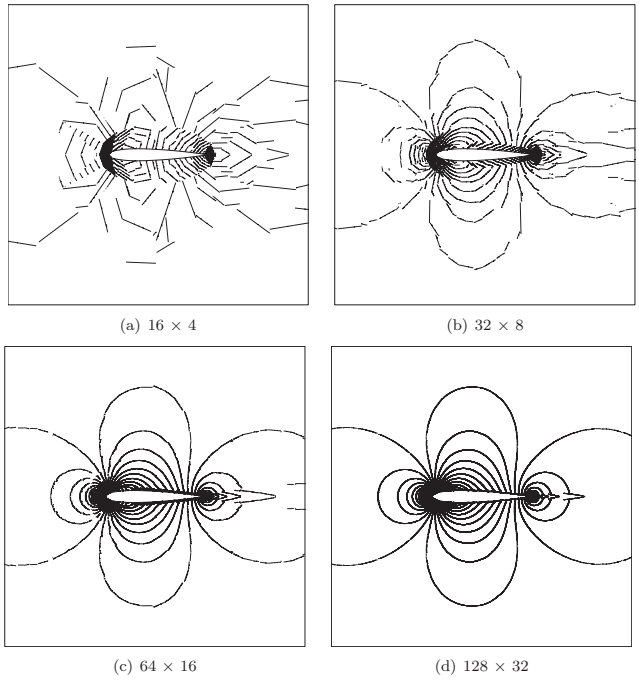

(a) 16 × 4 (b) 32 × 8

(c) 64 × 16 (d) 128 × 32

Figure 54: Inviscid subsonic flow around a NACA0012 airfoil: Mach number isolines with isoparametric FE and p=1

Preprint of
R. Sevilla, S. Fernández-Méndez and A. Huerta
NURBS-Enhanced Finite Element Method (NEFEM): A seamless bridge between CAD and FEM
Archives of Computational Methods in Engineering, 18 (4); 441-484, 2011

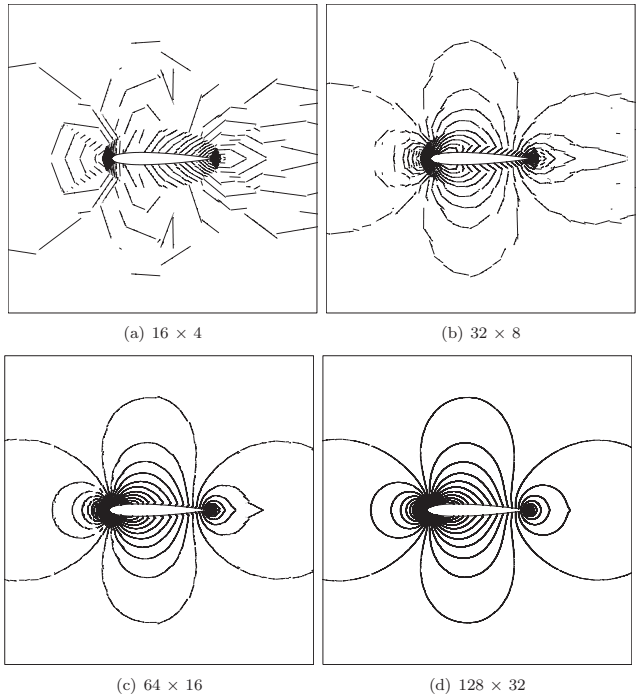

(a) 16 × 4 (b) 32 × 8

(c) 64 × 16 (d) 128 × 32

Figure 55: Inviscid subsonic flow around a NACA0012 airfoil: Mach number isolines with NEFEM and p=1

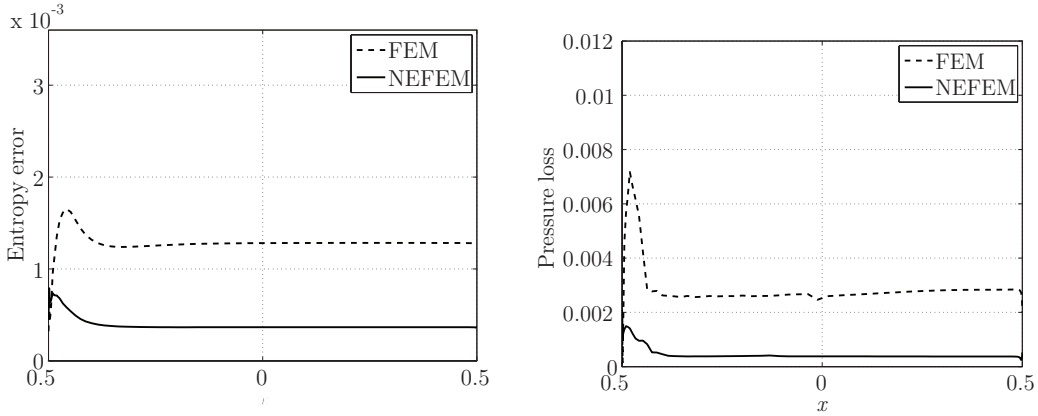

(a) Entropy error (b) Pressure loss

Figure 56: Inviscid subsonic flow around a NACA0012 airfoil: (a) entropy error and (b) pressure loss in the upper part of the airfoil

Preprint of
R. Sevilla, S. Fernández-Méndez and A. Huerta
NURBS-Enhanced Finite Element Method (NEFEM): A seamless bridge between CAD and FEM
Archives of Computational Methods in Engineering, 18 (4); 441-484, 2011

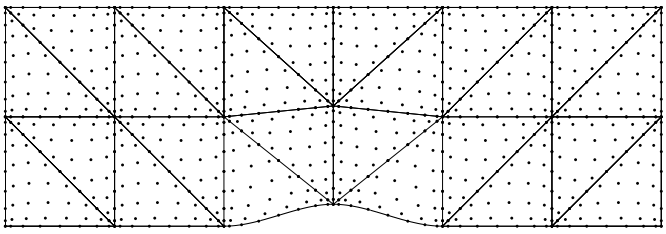

(a) Mesh and Fekette nodal distribution

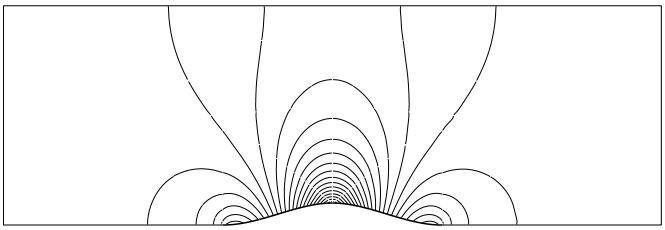

(b) Mach number

Figure 57: Inviscid subsonic flow over a bump: (a) Coarse mesh and (b) NEFEM solution with $p = 8$

straight-sided elements. Fekette nodal distributions are represented corresponding to a degree of approximation $p = 8$ and the Mach number isolines are depicted in Figure 57 (b). Figure 58 shows the convergence of the entropy error as p is uniformly increased starting with $p = 2$ up to $p = 9$, in the discretization shown in Figure 57 (a). As expected for a problem with a smooth solution, optimal (exponential) convergence is achieved, see Theorem 2 in Section 4.5. It is worth remarking that using a degree of approximation $p = 4$ the entropy error is less than 10^{-4}, with 360 degrees of freedom. For very high-order approximations, let say $p = 8$, the entropy error is less than 10^{-5} and a perfect symmetric Mach distribution pattern is obtained, see Figure 57 (b), with 1 080 degrees of freedom.

The flow around a circle is considered next, but now a very coarse mesh is used and high-order approximations are introduced in order to explore the necessity of exact boundary representations in this context.

This problem has been extensively studied in the past and many authors have advocated the use of isoparametric FEs to reduce the entropy production near curved walls. A comparison between isoparametric curved FEs and subparametric FEs with linear approximation for the geometry is often presented in order to illustrate the necessity of using curved elements. That

Preprint of
R. Sevilla, S. Fernández-Méndez and A. Huerta
NURBS-Enhanced Finite Element Method (NEFEM): A seamless bridge between CAD and FEM
Archives of Computational Methods in Engineering, 18 (4); 441-484, 2011

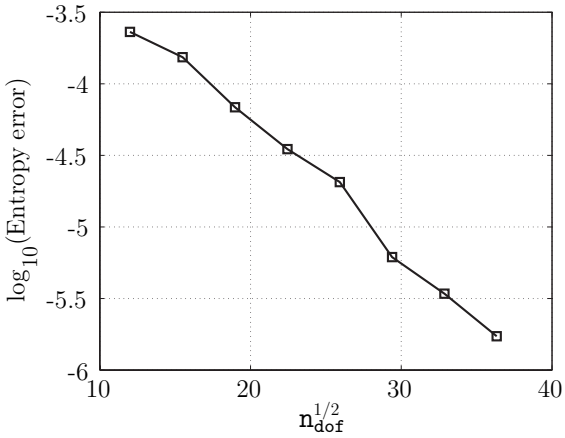

Figure 58: Inviscid subsonic flow over a bump: p-convergence of the entropy error with NEFEM

is, the polygonal approximation is maintained but the degree of the approximation is increased, see [9, 34, 57] to name a few. The main problem of considering subparametric formulations with only a linear approximation of the geometry is that the solution of a different problem is considered, that is the flow around a polygon rather than the flow around a circle. In addition the corners of the approximated boundary produce rarefaction waves that are better resolved when the polynomial degree of the approximation is increased, as pointed out in [55]. In order to illustrate that issue, Figure 59 shows the Mach number isolines computed with a subparametric formulation. A mesh with 16 straight-sided elements around the circle is considered and the degree of the approximation is $p = 4$. The rarefaction waves can be observed in the detailed view near corners of the polygonal boundary.

This experiment shows that subparametric formulations with a linear approximation of the geometry are not well suited in this context but this does not imply that isoparametric FEs are the best alternative in the presence of curved walls. In fact, it is worth remarking that when isoparametric FEs are considered, the boundary of the computational domain is only a $\mathcal{C}^0$ approximation of the true boundary. Therefore, a small discontinuity of the outward unit normal is introduced and some inaccuracies near curved walls can still be observed.

In order to show the benefits of NEFEM, the coarse mesh represented in Figure 60 is considered and high-order isoparametric FE and NEFEM

Preprint of
R. Sevilla, S. Fernández-Méndez and A. Huerta
NURBS-Enhanced Finite Element Method (NEFEM): A seamless bridge between CAD and FEM
Archives of Computational Methods in Engineering, 18 (4); 441-484, 2011

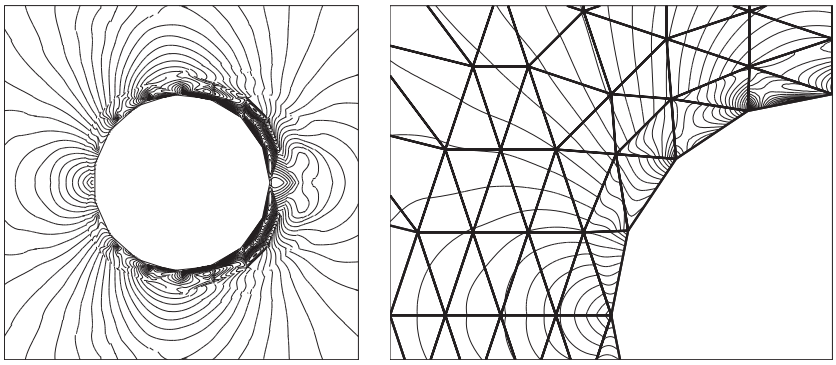

Figure 59: Inviscid subsonic flow around a circle: subparametric FE solution using straight-sided elements and high-order approximation of the solution ($p = 4$)

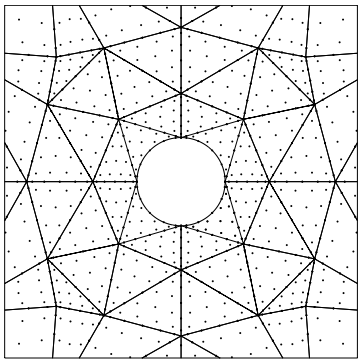

Figure 60: Inviscid subsonic flow around a circle: coarse mesh and Fekkete nodal distribution for $p = 6$

are compared. It is worth emphasizing that only four curved elements are considered to describe the circle, corresponding to 24 nodes over the curved boundary for a degree of approximation $p = 6$. Figure 60 shows the Mach number isolines for isoparametric FEs and NEFEM with a degree of approximation $p = 6$ and $p = 7$. The solution with very high-order isoparametric FEs is not completely symmetric with respect to the y axis, reflecting a small entropy production behind the circle. It is worth remarking that for $p = 6$ the maximum difference between the approximated boundary and the true circle is less than 10^{-4} and the asymmetry in the Mach number distribution is remarkable. For $p = 7$ the maximum difference between the approximated boundary and the true circle is almost 10^{-5} and a visually symmetric Mach number distribution is still not obtained. The discontinuity in the outward

Preprint of
R. Sevilla, S. Fernández-Méndez and A. Huerta
NURBS-Enhanced Finite Element Method (NEFEM): A seamless bridge between CAD and FEM
Archives of Computational Methods in Engineering, 18 (4); 441-484, 2011

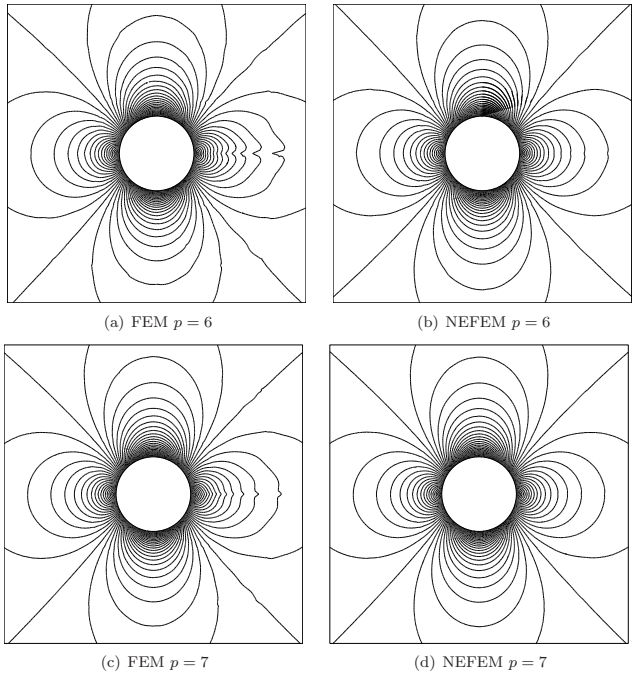

(a) FEM $p = 6$ (b) NEFEM $p = 6$

(c) FEM $p = 7$ (d) NEFEM $p = 7$

Figure 61: Inviscid subsonic flow around a circle: Mach number distribution in the coarse mesh shown in Figure 60 with isoparametric FE and NEFEM and high-order approximations

unite normal in the stagnation point behind the circle, due to the piecewise $\mathcal{C}^0$ approximation of the circle with isoparametric FEs, has a big impact in the entropy production, even with very high-order isoparametric approximations. In contrast, it is worth remarking the quality of the solution obtained with NEFEM with a degree of approximation $p = 6$. The solution is perfectly symmetric with respect to the y axis showing that the inaccuracies observed with isoparametric FEs are not due to the coarse mesh considered in this example, but to geometric inaccuracies.

The last example in this section involves the simulation of the flow around a (non-symmetric) RAE2822 airfoil at free-stream Mach number $M_\infty = 0.5$ and angle of attack $\alpha = 0^o$. Figure 62 shows the computational mesh and the Mach number distribution for $p = 8$. Despite the ultra coarse mesh considered, with NEFEM and high-order approximations the complex flow features are well resolved. To quantify the accuracy of high-order NEFEM computations, Figure 63 shows the convergence of the lift coefficient (C_L) as the degree of the approximation is uniformly increased starting with $p = 2$

Preprint of
R. Sevilla, S. Fernández-Méndez and A. Huerta
NURBS-Enhanced Finite Element Method (NEFEM): A seamless bridge between CAD and FEM
Archives of Computational Methods in Engineering, 18 (4); 441-484, 2011

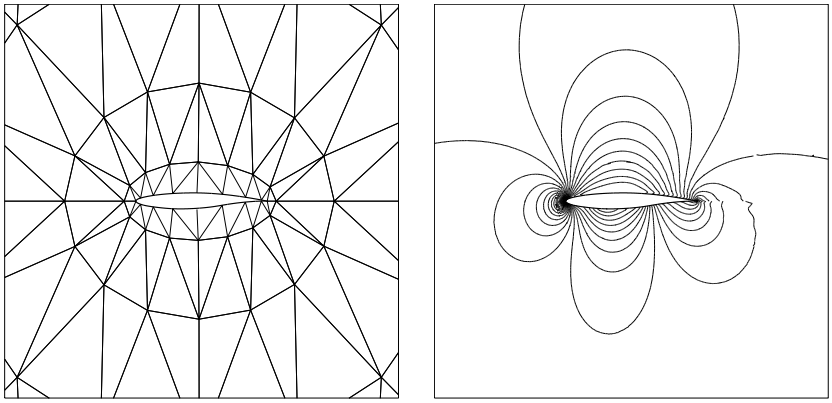

(a) Mesh (b) Mach number

Figure 62: Inviscid subsonic flow around a RAE2822 airfoil: coarse mesh and Mach number isolines for NEFEM and $p = 8$

in the coarse mesh shown in Figure 62 (a). Recall that the lift coefficient is defined as

$$C_L = \frac{1}{0.5\rho_\infty v_\infty^2 L} \int_\Gamma \mathrm{p}(n_2 \cos\alpha - n_1 \sin\alpha) d\Gamma,$$

where L is the chord length of the airfoil and Γ is the curve describing the airfoil.

It is worth noting that with $p = 7$ the estimated lift coefficient is $C_L = 0.2764$ and with $p = 8$ is $C_L = 0.2769$, showing mesh convergence of this aerodynamic force to the required engineering accuracy, that is less than one lift count difference between the solution with $p = 7$ and $p = 8$, with less than 12 000 degrees of freedom.

6.3. Electromagnetic scattering

In this section a DG formulation is considered for the simulation of the scattering of a single plane electromagnetic wave by *Perfect Electric Conductor* (PEC) obstacles.

The governing equations are the transient Maxwell's equations. For a linear isotropic material of relative permittivity ε and relative permeability μ, and assuming that there are no current sources in the material, the time dependent Maxwell's equations can be written in the conservative form of Equation (21) with a source term. In 3D the vector of conserved quantities

Preprint of
R. Sevilla, S. Fernández-Méndez and A. Huerta
NURBS-Enhanced Finite Element Method (NEFEM): A seamless bridge between CAD and FEM
Archives of Computational Methods in Engineering, 18 (4); 441-484, 2011

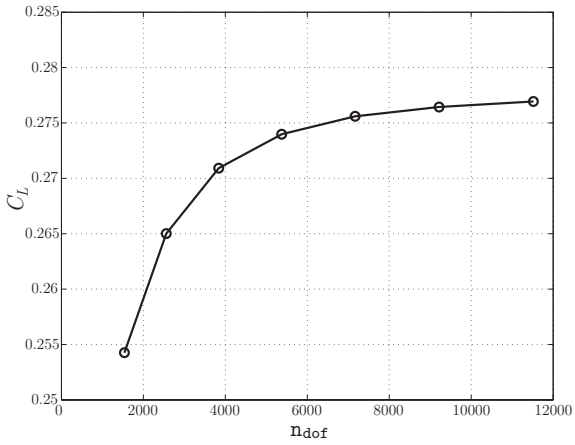

Figure 63: Inviscid subsonic flow around a RAE2822 airfoil: lift coefficient convergence for increasing p in the mesh of Figure 62 (a)

$\boldsymbol{U}$ and the fluxes $\boldsymbol{F}_k$ are

$$\boldsymbol{U} = \begin{pmatrix} \varepsilon \boldsymbol{E} \\ \mu \boldsymbol{H}^t \end{pmatrix} = \begin{pmatrix} \varepsilon E_1 \\ \varepsilon E_2 \\ \varepsilon E_3 \\ \mu H_1 \\ \mu H_2 \\ \mu H_3 \end{pmatrix}, \quad \boldsymbol{F}_1 = \begin{pmatrix} 0 \\ H_3 \\ -H_2 \\ 0 \\ -E_3 \\ E_2 \end{pmatrix}, \quad \boldsymbol{F}_2 = \begin{pmatrix} -H_3 \\ 0 \\ H_1 \\ E_3 \\ 0 \\ -E_1 \end{pmatrix}, \quad \boldsymbol{F}_3 = \begin{pmatrix} H_2 \\ -H_1 \\ 0 \\ -E_2 \\ E_1 \\ 0 \end{pmatrix},$$

and the source term is given by

$$\boldsymbol{S} = \begin{pmatrix} (1-\varepsilon)\dfrac{\partial \boldsymbol{E}^i}{\partial t} \\ (1-\mu)\dfrac{\partial \boldsymbol{H}^i}{\partial t} \end{pmatrix},$$

where $\boldsymbol{E} = (E_1, E_2, E_3)$ and $\boldsymbol{H} = (H_1, H_2, H_3)$ denote the scattered electric and magnetic fields respectively, and $\boldsymbol{E}^i$ and $\boldsymbol{H}^i$ are the electric and magnetic incident fields respectively.

In 2D, the hyperbolic system (21) decouples into the *Transverse Electric* (TE) and *Transverse Magnetic* (TM) modes. The vector of conserved

Preprint of
R. Sevilla, S. Fernández-Méndez and A. Huerta
NURBS-Enhanced Finite Element Method (NEFEM): A seamless bridge between CAD and FEM
Archives of Computational Methods in Engineering, 18 (4); 441-484, 2011

quantities, the fluxes and the source are given by

$$\boldsymbol{U} = \begin{pmatrix} \varepsilon E_1 \\ \varepsilon E_2 \\ \mu H_3 \end{pmatrix}, \ \boldsymbol{F}_1 = \begin{pmatrix} 0 \\ H_3 \\ E_2 \end{pmatrix}, \ \boldsymbol{F}_2 = \begin{pmatrix} -H_3 \\ 0 \\ -E_1 \end{pmatrix}, \ \boldsymbol{S} = \begin{pmatrix} (1-\varepsilon)\dfrac{\partial E_1^i}{\partial t} \\ (1-\varepsilon)\dfrac{\partial E_2^i}{\partial t} \\ (1-\mu)\dfrac{\partial H_3^i}{\partial t} \end{pmatrix},$$

for the TE mode, and

$$\boldsymbol{U} = \begin{pmatrix} \mu H_1 \\ \mu H_2 \\ \varepsilon E_3 \end{pmatrix}, \ \boldsymbol{F}_1 = \begin{pmatrix} 0 \\ -E_3 \\ -H_2 \end{pmatrix}, \ \boldsymbol{F}_2 = \begin{pmatrix} E_3 \\ 0 \\ H_1 \end{pmatrix}, \ \boldsymbol{S} = \begin{pmatrix} (1-\mu)\dfrac{\partial H_1^i}{\partial t} \\ (1-\mu)\dfrac{\partial H_2^i}{\partial t} \\ (1-\varepsilon)\dfrac{\partial E_3^i}{\partial t} \end{pmatrix}, \quad (22)$$

for the TM mode.

The numerical simulation of electromagnetic scattering problems involves approximating the interaction between a known incident field and a scatterer. The scattered field produced by this interaction is a wave that propagates outwards towards infinity. It is crucial to use a mechanism to perform the absorption of outgoing waves. The numerical examples presented in this chapter consider a *Perfectly Matched Layer* (PML) surrounding the computational in order to absorb the outgoing waves, see for instance [11, 1, 91]. The setup of the problem is illustrated in Figure 64, showing a PML surrounding the computational domain Ω.

The radar cross section (RCS) is one of the most important quantities of interest in electromagnetic scattering problems. It provides a description of how an object reflects an incident electromagnetic wave, see [43, 5]. For example, the *scattering width* is defined as

$$\chi = \lim_{r\to\infty} (2r)^{\mathtt{n_{sd}}} \pi \frac{|E_3|^2}{|E_3^i|^2} = \lim_{r\to\infty} (2r)^{\mathtt{n_{sd}}} \pi \frac{|H_3|^2}{|H_3^i|^2}.$$

Typically, the RCS (per unit area/length) is measured in Decibels, this conversion is achieved by computing

$$RCS = 10 \log_{10}(\chi). \quad (23)$$

Preprint of
R. Sevilla, S. Fernández-Méndez and A. Huerta
NURBS-Enhanced Finite Element Method (NEFEM): A seamless bridge between CAD and FEM
Archives of Computational Methods in Engineering, 18 (4); 441-484, 2011

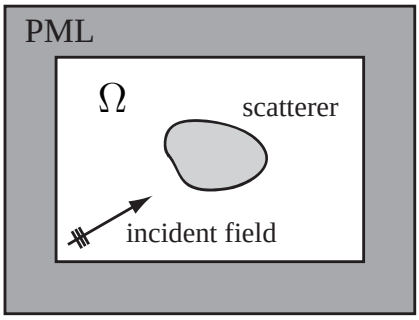

Figure 64: Schematic of an electromagnetic scattering problem with a PML surrounding the computational domain

When only near field data is available, the RCS can be evaluated by performing a near-to-far field transformation, for further details see [88, 43, 5].

In this section, several numerical examples are shown in 2D and 3D to illustrate the possibilities and benefits of NEFEM. The results are often compared to the curved FE techniques presented in Section 5 and to other techniques used by the CEM community. The behavior and benefits of NEFEM in the presence of complex scatterers with small geometric features are also explored and challenging problems including complex scatterers and higher frequencies are considered.

The first example consists on a planar wave traveling in the x^+ direction and scattered by a PEC circular cylinder of diameter 4λ, where λ denotes the wavelength of the incident field. A coarse mesh with only four elements for the discretization of the curved boundary is considered, and high-order approximations are used to properly capture the solution. Figure 65 shows the computational mesh, the transverse scattered field computed with NEFEM and $p = 10$, and the RCS. A 2λ thick PML is introduced in order to absorb outgoing waves.

The RCS error evolution for increasing p is depicted in Figure 66. For the same discretization (i.e. same degree of interpolation), NEFEM results are more accurate than isoparametric or Cartesian FE, with an approximate boundary description, and also more accurate than p-FEM, with an exact boundary representation. For instance, NEFEM with $p = 10$ produces a RCS error in $\mathcal{L}^2([-\pi, \pi])$ norm of about 10^{-2}, whereas isoparametric or Cartesian FE require $p = 12$ to achieve a comparable accuracy, and p-FEM requires

Preprint of
R. Sevilla, S. Fernández-Méndez and A. Huerta
NURBS-Enhanced Finite Element Method (NEFEM): A seamless bridge between CAD and FEM
Archives of Computational Methods in Engineering, 18 (4); 441-484, 2011

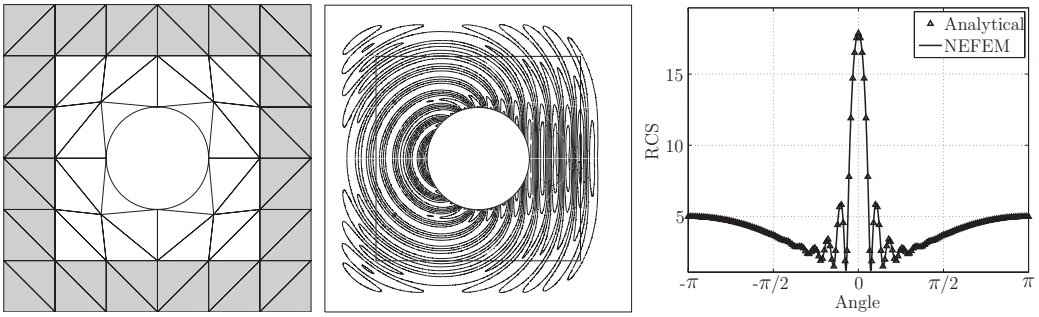

(a) Mesh (b) E_ϑ field (c) TM RCS

Figure 65: Scattering by a PEC cylinder of diameter 4λ

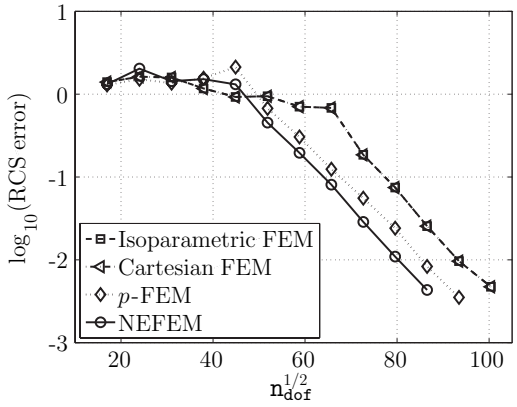

Figure 66: Scattering by a PEC cylinder of diameter 4λ: p-convergence comparison of several curved FEs

$p = 11$. Thus, NEFEM is able to reach the desired accuracy with a reduction of about 30% compared to isoparametric or Cartesian FEs, and of 15% compared to p-FEM (also with an exact boundary representation). This difference in $\mathtt{n}_{\mathtt{dof}}$implies important differences in computational cost. NEFEM computation requires 2 585 time steps to reach the time-harmonic steady state, whereas isoparametric and Cartesian FEs employ 3 692 time steps and p-FEM requires 3 114 time steps. In addition, each time step with NEFEM requires less computational cost due to the lower p needed to achieve the desired accuracy.

The difference between isoparametric FEs and Cartesian FEs are indistinguishable, showing that a Cartesian approximation of the solution does

Preprint of
R. Sevilla, S. Fernández-Méndez and A. Huerta
NURBS-Enhanced Finite Element Method (NEFEM): A seamless bridge between CAD and FEM
Archives of Computational Methods in Engineering, 18 (4); 441-484, 2011

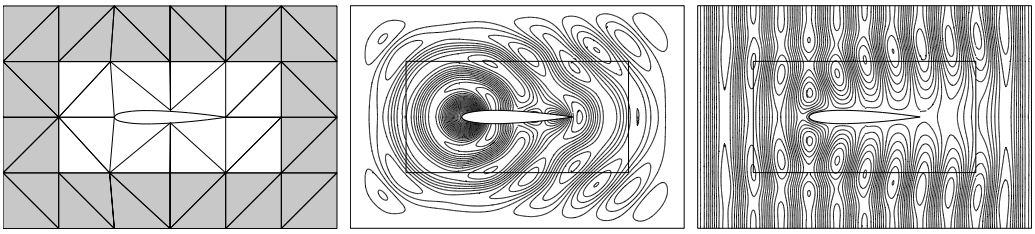

(a) Mesh (b) H_3 field (c) E_3^T field

Figure 67: Scattering by a PEC NACA0012 airfoil of chord length 2λ

not offer any advantage if an approximated boundary representation is considered. The difference between isoparametric FEs and p-FEM is only due to geometric errors, and relevant differences in accuracy are observed. Finally, NEFEM also considers the exact boundary representation and outperforms p-FEM, showing that the Cartesian approximation combined with an exact boundary representation, i.e. NEFEM, provides the maximum accuracy for a given spatial discretization. Finally, note that with an approximate boundary representation the exponential convergence is exhibited for $p > 8$ whereas with an exact boundary representation the exponential convergence is achieved for $p > 5$.

To conclude, it is worth remarking that only one element per two wavelengths is considered in this example and a RCS error of 10^{-2} is obtained with $p = 10$, that is, using less than 6 nodes per wavelength. Thus, the exact geometry considered in NEFEM combined with the Cartesian approximation allows to compute accurate solutions with the minimum $\mathtt{n_{dof}}$, compared to other curved FEs and other techniques used by the CEM community.

In the next example a planar wave traveling in the x^+ direction and scattered by the NACA0012 airfoil [56] of chord length 2λ is considered. Figure 67 shows an ultra coarse computational mesh with a λ thick PML, the scattered H_3 field and the total (scattered plus incident) E_3 field for a NEFEM solution with $p = 6$. Note that only two elements are considered in the upper part of the airfoil. Figure 68 illustrates the convergence of the solution for increasing p, with isoparametric FEs and NEFEM. As no analytical solution is available, a reference solution is computed in a fine mesh with high-order approximation and a thicker PML.

For isoparametric FEs, the RCS error in $\mathcal{L}^2([-\pi, \pi])$ norm decreases as p increases, but it is important to remark that the RCS error in the $\mathcal{L}^\infty([-\pi, \pi])$

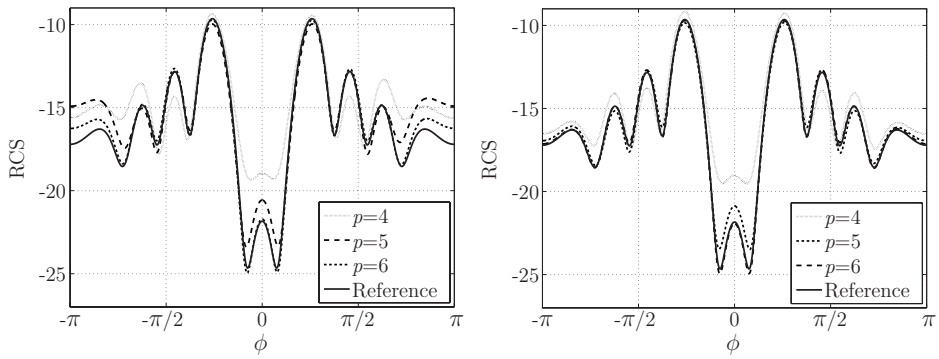

(a) FEM (b) NEFEM

Figure 68: Scattering by a PEC NACA0012 airfoil of chord length 2λ: TE RCS comparison as p increases

norm behaves different. In particular, the RCS error for angles near $-\pi$ or π is higher with $p = 5$ than using $p = 4$, showing important discrepancies with respect to the reference solution. Recall that, for isoparametric FEs, as p increases not only the solution is represented with higher degree, but also the geometry. Thus, slightly different profiles are considered for each p. Moreover, the approximated boundary is only $\mathcal{C}^0$ on the boundary nodes. In particular a discontinuity of the profile in the leading edge is clearly observable using coarse meshes and high-order isoparametric FEs, see Figures 69 (a), (b) and (c). With NEFEM, the exact boundary representation is considered with no dependence on the spatial discretization (i.e. the degree of the polynomial approximation), see Figures 69 (d), (e) and (f). Consequently, with NEFEM, the RCS error is uniformly reduced for all viewing angles as the degree of the approximation is increased, see Figure 68 (b).

Figure 70 compares the RCS error distribution with isoparametric FEs and NEFEM, for a degree of approximation $p = 5$ and $p = 6$. Note that the maximum error with isoparametric FEs is observed at viewing angles corresponding to the leading edge ($\phi = -\pi$ and $\phi = \pi$), whereas for NEFEM the maximum error is obtained near the singularity ($\phi = 0$).

This example illustrates the sensitivity of the RCS to poor geometric representations. Isoparametric approximations are not sufficient when coarse meshes and high-order approximations are considered. Geometric errors may lead to important discrepancies in the RCS. Thus, h-refinement is usually performed at the leading edge of airfoils to provide an accurate representation

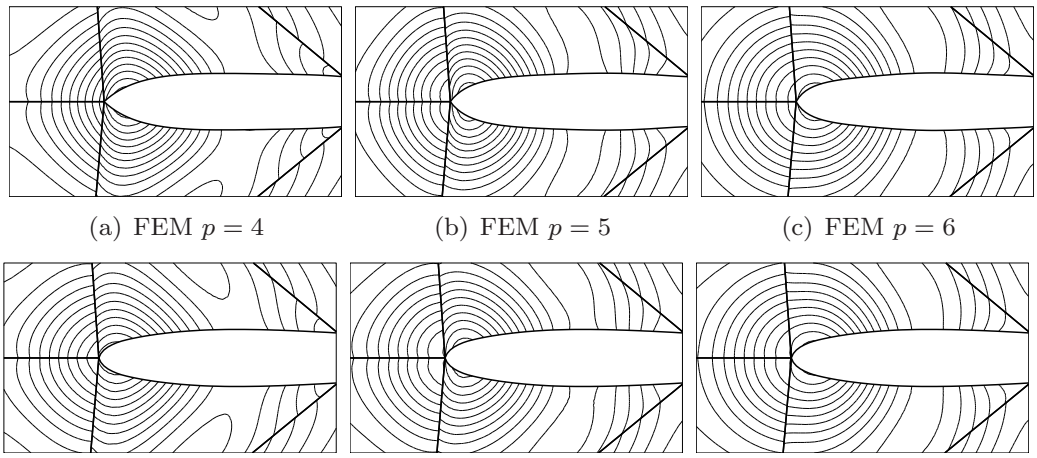

(a) FEM $p = 4$ (b) FEM $p = 5$ (c) FEM $p = 6$

(d) NEFEM $p = 4$ (e) NEFEM $p = 5$ (f) NEFEM $p = 6$

Figure 69: Scattering by a PEC NACA0012 airfoil of chord length 2λ: detailed view of the transverse scattered field near the leading edge for isoparametric FE and NEFEM increasing p

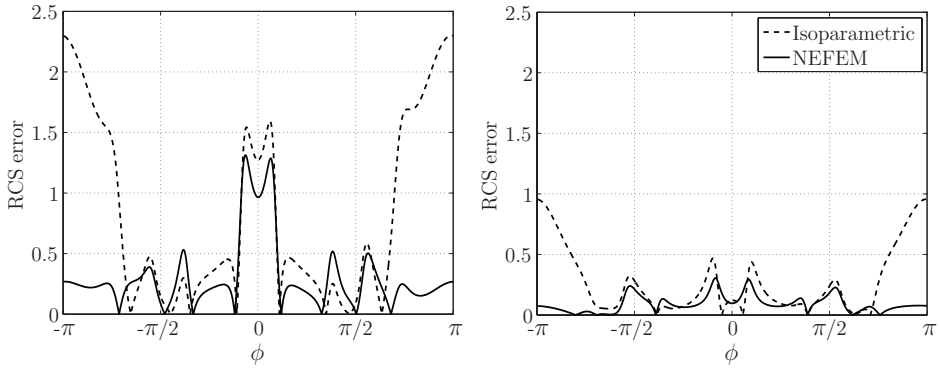

(a) $p = 5$ (b) $p = 6$

Figure 70: Scattering by a PEC NACA0012 airfoil of chord length 2λ: RCS error comparison for isoparametric FEM and NEFEM

Preprint of
R. Sevilla, S. Fernández-Méndez and A. Huerta
NURBS-Enhanced Finite Element Method (NEFEM): A seamless bridge between CAD and FEM
Archives of Computational Methods in Engineering, 18 (4); 441-484, 2011

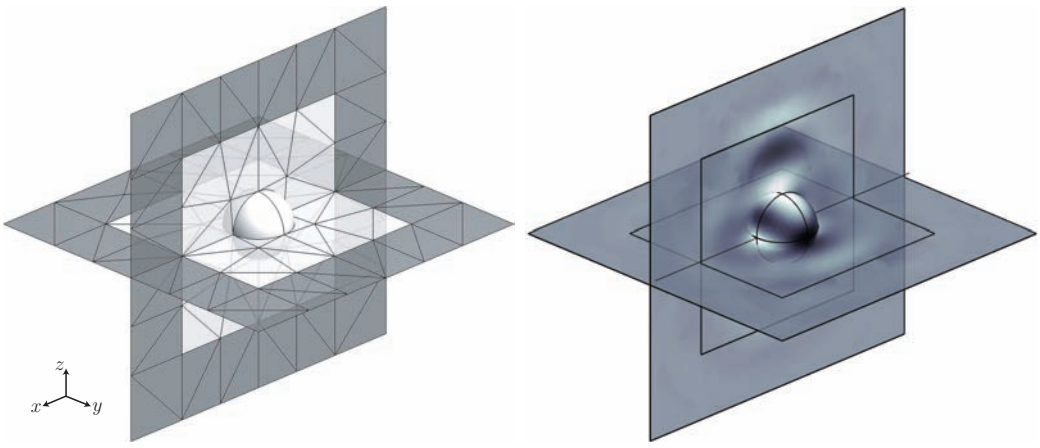

(a) Mesh (b) E_1 field

Figure 71: Scattering by a PEC sphere of diameter λ

of the geometry. With NEFEM, the exact boundary representation allows to mesh the domain with no dependence on the geometrical complexity. Using only one element per wavelength and $p = 5$, i.e. 6 nodes per wavelength, an accurate solution is obtained, without performing h-refinement. The maximum error in a NEFEM computations is observed where the solution is complex, not where the geometry is complex.

Next example considers an incident plane wave traveling in the z^+ direction and scattered by a PEC sphere of diameter λ. The sphere is exactly described with a quadratic singular NURBS surface, and a coarse mesh with only eight elements for the discretization of the curved boundary is considered, see two cuts of the volume mesh and the surface mesh of the sphere in Figure 71 (a). The mesh has 1 271 elements with planar faces and 32 curved elements (8 elements with a face on the NURBS boundary and 24 elements with an edge on the NURBS boundary). Scattered E_1 field computed with NEFEM and a polynomial approximation of degree $p = 5$ is represented in Figure 71 (b), showing the field intensity on the sphere surface and illustrating the absorption of outgoing waves in the PML.

Figures 72 and 73 compare the RCS computed with degree $p = 3$ and $p = 4$ with the analytical solution, for vertical and horizontal polarization respectively. For Cartesian FEs, the RCS error is not reduced for all viewing angles as p increases. In particular, the RCS near viewing angles $-\pi$ and π is more accurate with $p = 3$ than using $p = 4$, see Figures 72 (a)

Preprint of
R. Sevilla, S. Fernández-Méndez and A. Huerta
NURBS-Enhanced Finite Element Method (NEFEM): A seamless bridge between CAD and FEM
Archives of Computational Methods in Engineering, 18 (4); 441-484, 2011

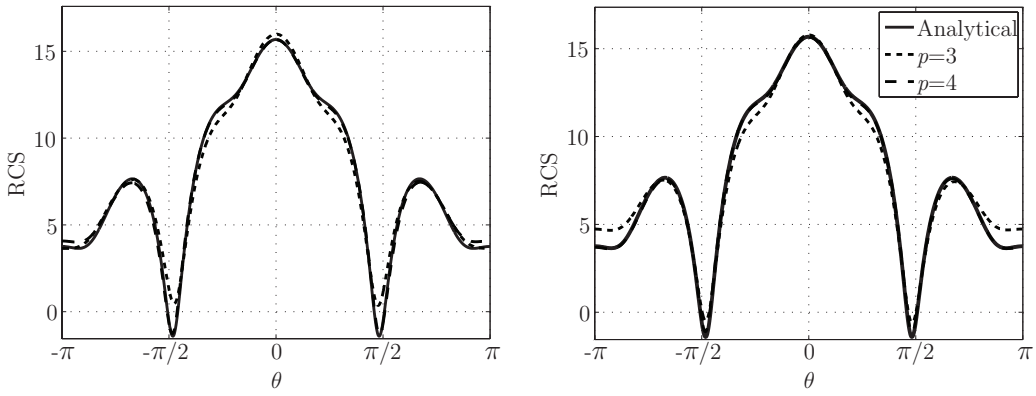

(a) Cartesian FEM (b) NEFEM

Figure 72: Scattering by a PEC sphere of diameter λ: RCS comparison for increasing p and for the vertical polarization

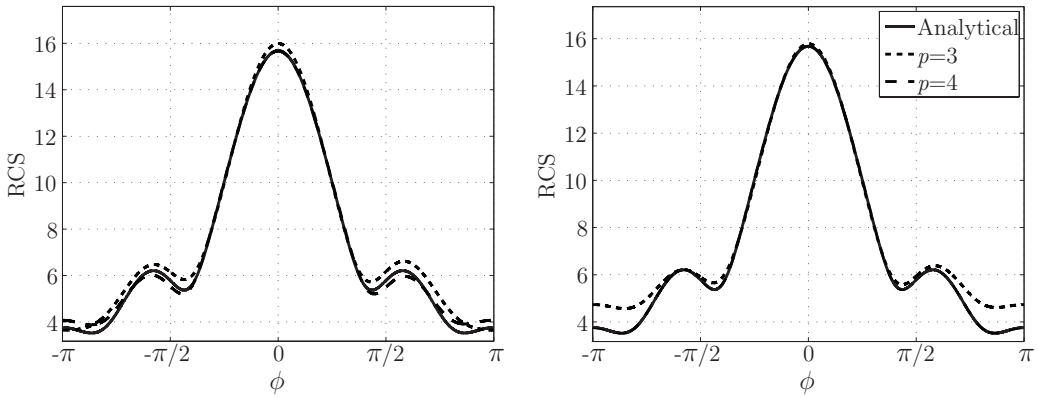

(a) Cartesian FEM (b) NEFEM

Figure 73: Scattering by a PEC sphere of diameter λ: RCS comparison for increasing p and for the horizontal polarization

Preprint of
R. Sevilla, S. Fernández-Méndez and A. Huerta
NURBS-Enhanced Finite Element Method (NEFEM): A seamless bridge between CAD and FEM
Archives of Computational Methods in Engineering, 18 (4); 441-484, 2011

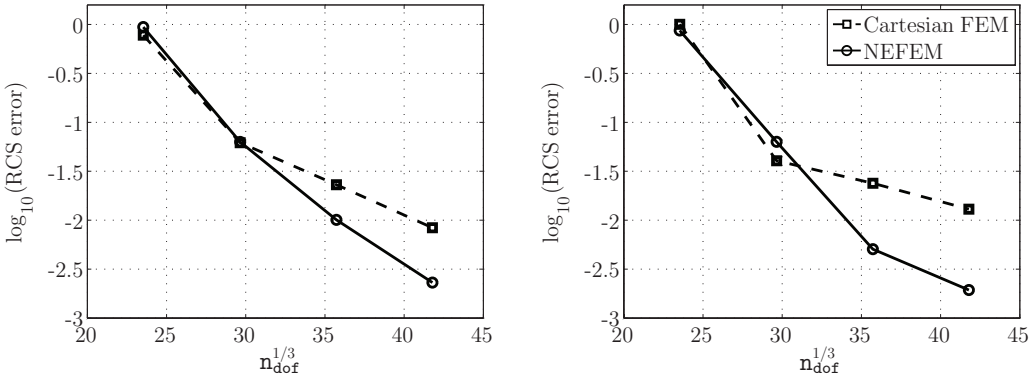

(a) Vertical polarization (b) Horizontal polarization

Figure 74: Scattering by a PEC sphere of diameter λ: p-convergence comparison of the RCS error

and 73 (a). Again, the approximate boundary representation has a critical influence in the RCS. NEFEM exhibits the same robustness than in the previous examples. The error is decreased for all viewing angles as the degree of the approximation is increased. A perfect match between analytical and computed solution is observed with $p = 4$, see Figures 72 (b) and 73 (b).

Note that Cartesian FEs offer a slightly different performance for vertical and horizontal polarizations. In fact, higher errors are observed for the horizontal polarization, whereas for NEFEM, almost identical performance is observed for both polarizations. To compare accuracy, Figure 74 represents the RCS error in the $\mathcal{L}^2(-\pi, \pi)$ norm for increasing p, starting with $p = 2$, showing the superiority of NEFEM compared to Cartesian FEs. The most critical difference is observed in the horizontal polarization for $p = 5$. NEFEM is almost one order of magnitude more precise than the corresponding Cartesian FEs. It is worth remarking that the RCS error for Cartesian FEs is controlled by the geometric error for $p > 3$. In fact, the isoparametric approximation of the sphere with 8 curved elements is considered in Section 6.1, and a similar performance is observed in a second-order elliptic problem.

Compared to other techniques, NEFEM is also more accurate and efficient. For instance, to achieve an accuracy of 10^{-2} measuring the maximum norm of the scattering width, more than 100 000 degrees of freedom are required using high-order edge elements [60]. With NEFEM, a degree of approximation $p = 4$ provides an error of 4.7×10^{-3}, using 45 605 degrees of freedom, that is, NEFEM is two times more accurate by using 50% of

Preprint of
R. Sevilla, S. Fernández-Méndez and A. Huerta
NURBS-Enhanced Finite Element Method (NEFEM): A seamless bridge between CAD and FEM
Archives of Computational Methods in Engineering, 18 (4); 441-484, 2011

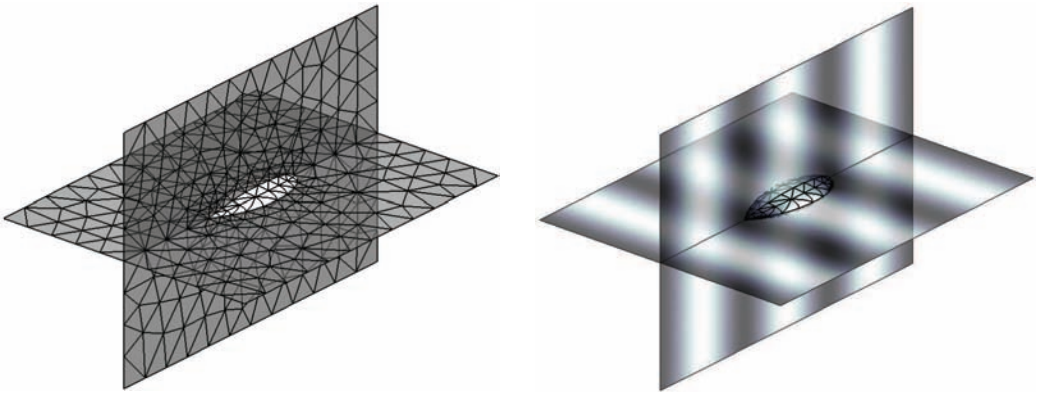

(a) Mesh (b) E_3^T field

Figure 75: Scattering by a PEC NASA almond of characteristic length λ: computational mesh and NEFEM solution with $p = 4$

the $\mathtt{n}_{\mathtt{dof}}$, showing that NEFEM is also competitive in 3D compared to other techniques used by the CEM community.

The following example considers a popular benchmark for 3D RCS computations, the scattering by a PEC NASA almond, see [30, 101]. One of the challenges of this example is the singularity exhibited by the solution on the tip of the almond. Moreover, the high variation on the surface curvature introduces extra complexity in the scattered field distribution.

The monostatic RCS computation of an almond of characteristic length λ is considered. The mesh employed for the computation has 10 805 elements with planar faces and 336 curved elements (120 with a face on the NURBS boundary, and 216 with an edge on the NURBS boundary). Figure 75 (a) shows two cuts of the volume mesh, corresponding to the free-space, and the surface mesh on the almond. The total component of the E_3 field for a NEFEM solution with $p = 4$ is represented in Figure 75 (b), for a wave incident onto the tip of the almond.

The monostatic RCS evaluation is performed by computing $N^i = 18$ solutions corresponding to a series of incident angles $\phi_j^i = j\pi/N^i$, with $j = 0, \ldots, N^i$. The monostatic pattern for the vertical polarization is represented in Figure 76, and compared with a reference solution, showing excellent agreement. The difference between both solutions is 1.5×10^{-2} in the $\mathcal{L}^2(-\pi, \pi)$ norm. The reference data corresponds to a computation using high-order edge elements, see [59]. In the NEFEM computation, the markers

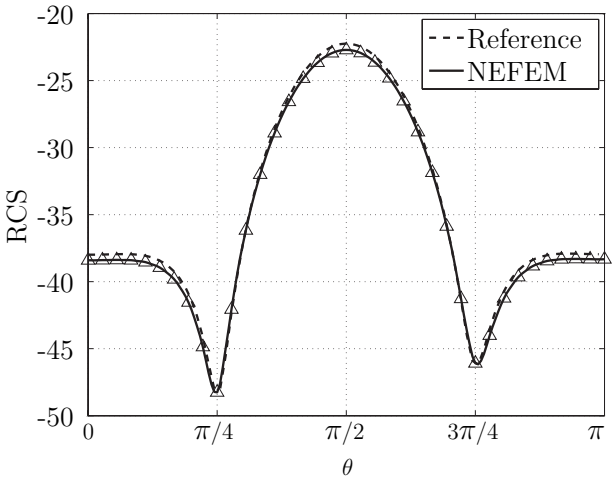

Figure 76: Scattering by a PEC NASA almond of characteristic length λ: monostatic RCS for a NEFEM solution with $p = 4$, compared with high-order edge elements of [59]

correspond to the 18 computations, and the continuous line corresponds to a postprocess of the monostatic data, as described in [76].

Previous examples show the potential of NEFEM in front of several FE methodologies for the numerical solution of classical test cases, but the challenges of solving Maxwell's equations are not typically found in the equations, but in the geometrical complexity of the scatterer and/or in the wavelength of the incident field (with respect to the characteristic length of the scatterer).

The following example considers the scattering of an incident wave traveling in the z^+ direction by a PEC sphere of diameter 20λ. The mesh used in the computations has 124 135 elements with planar faces and 17 856 curved elements (11 176 elements with a face on the NURBS boundary and 6 680 elements with an edge on the NURBS boundary). The surface mesh on the sphere is represented in Figure 77 (a), and the first component of scattered electric field over the sphere for a NEFEM solution with $p = 5$ is represented in Figure 77 (b). A comparison of the computed RCS with the analytical solution is depicted in Figure 78, showing good agreement with the analytical solution. In fact, the RCS distributions overlap for a viewing angle in $[-\pi/4, \pi/4]$, see Figure 79, and some differences are observed in the other viewing angles. Note that the spatial discretization is relatively coarse for this frequency and a reasonable accuracy for engineering purposes is obtained. The relative RCS in the $\mathcal{L}^2(-\pi, \pi)$ norm is 4.7×10^{-2} for the vertical

Preprint of
R. Sevilla, S. Fernández-Méndez and A. Huerta
NURBS-Enhanced Finite Element Method (NEFEM): A seamless bridge between CAD and FEM
Archives of Computational Methods in Engineering, 18 (4); 441-484, 2011

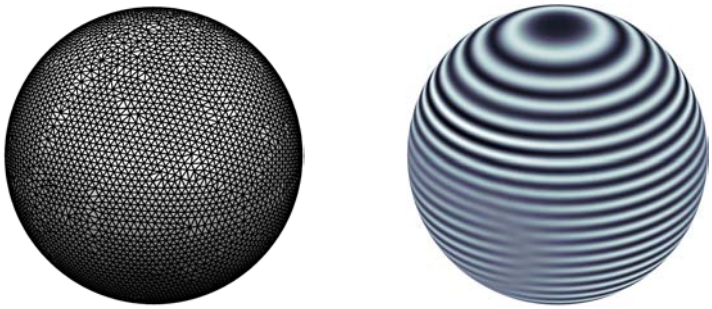

(a) Surface mesh (b) E_1

Figure 77: Scattering by a PEC sphere of diameter 20λ

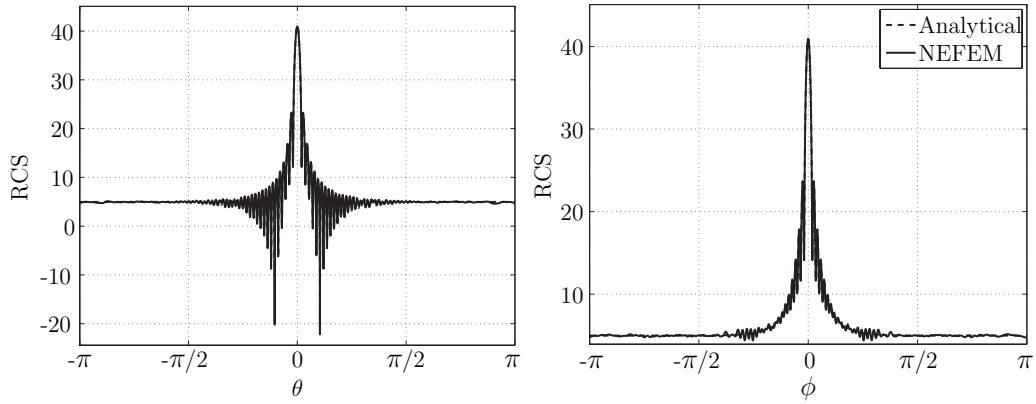

(a) Vertical polarization (b) Horizontal polarization

Figure 78: Scattering by a PEC sphere of diameter 20λ: RCS for a NEFEM solution with $p = 4$

Preprint of
R. Sevilla, S. Fernández-Méndez and A. Huerta
NURBS-Enhanced Finite Element Method (NEFEM): A seamless bridge between CAD and FEM
Archives of Computational Methods in Engineering, 18 (4); 441-484, 2011

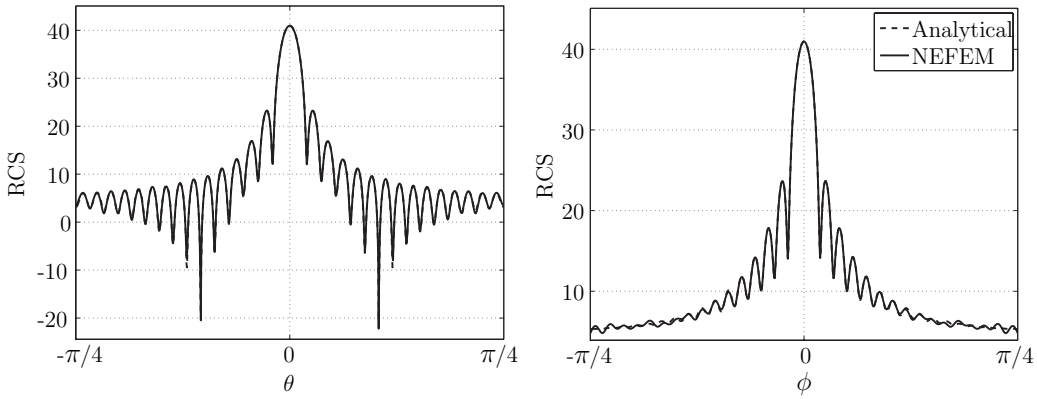

(a) Vertical polarization (b) Horizontal polarization

Figure 79: Scattering by a PEC sphere of diameter 20λ: RCS for a NEFEM solution with $p = 4$ in the range $[-\pi/4, \pi/4]$

polarization and 6.3×10^{-2} for the horizontal polarization. Again, the error in the RCS is higher for the horizontal polarization due to the singularity induced by the logarithmic scale. If the error is measured in the scattering width, an error of 1.2×10^{-2} is obtained for both polarizations. If lower errors are required, further p-refinement can be performed on the same mesh.

NEFEM is also a competent approach to 3D challenging simulations compared to other techniques. For instance, the method proposed by [50] is applied to compute the scattering by a conducting sphere in the frequency domain. To achieve a relative error of about 10^{-2} for a sphere of diameter 15λ, almost 4 million of degrees of freedom are needed. In this section, same accuracy is obtained with NEFEM for a higher frequency problem (sphere of diameter 20λ) using 4 344 725 degrees of freedom. It is worth mentioning that an improved PML is applied in [50] in the frequency domain, that allows a 0.2λ thick PML, whereas the NEFEM computation uses a λ thick PML, demonstrating, once more, the benefits of NEFEM.

It is also worth remarking that even if the surface mesh of the obstacle is refined for high frequency applications, an accurate geometric model is still important. As noted in [50], as the frequency is increased, geometric errors are more influential in the scattered field. For instance, with isoparametric FEs, the geometric singularities introduced at boundary edges may produce non physical diffraction.

Next example considers the scattering of a plane electromagnetic wave

Preprint of
R. Sevilla, S. Fernández-Méndez and A. Huerta
NURBS-Enhanced Finite Element Method (NEFEM): A seamless bridge between CAD and FEM
Archives of Computational Methods in Engineering, 18 (4); 441-484, 2011

(a) Surface mesh (b) E_3 (c) H_3

Figure 80: Scattering by a PEC NASA almond of characteristic length 8λ: surface mesh and two components of the scattered field for a NEFEM solution with $p = 5$

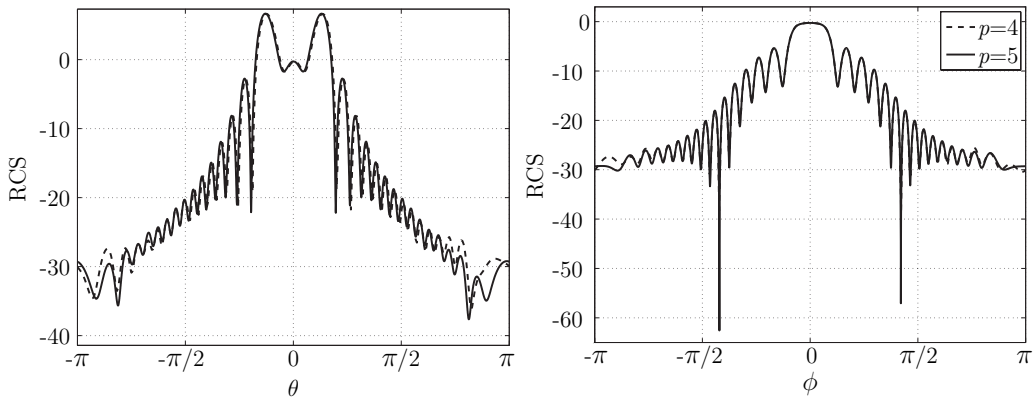

(a) Vertical polarization (b) Horizontal polarization

Figure 81: Scattering by a PEC NASA almond of characteristic length 8λ: RCS for a NEFEM solution with $p = 5$

by a PEC NASA almond of characteristic length 8λ. The mesh has 9 348 elements with planar faces and 1 200 curved elements. The surface mesh on the almond is represented in Figure 80 (a), and a detailed view of two components of the scattered field are represented over the almond surface in Figures 80 (b) and (c), corresponding to a wave incident onto the tip of the almond.

Figure 81 shows the RCS for vertical and horizontal polarizations. Two RCS patterns are displayed, for a NEFEM solution with $p = 4$ and $p = 5$ respectively. Results show a perfect agreement with published results [42], which are obtained with linear FEs in a tetrahedral mesh with 1 121 431 mesh nodes. Thus, this example shows the competitiveness of NEFEM compared to other formulations for more challenging applications. Even if a DG formulation is considered, i.e. duplicating nodes at inter-element faces,

Preprint of
R. Sevilla, S. Fernández-Méndez and A. Huerta
NURBS-Enhanced Finite Element Method (NEFEM): A seamless bridge between CAD and FEM
Archives of Computational Methods in Engineering, 18 (4); 441-484, 2011

(a) Surface mesh (b) E_3 (c) H_3

Figure 82: Scattering by a PEC NASA almond of characteristic length 21λ: surface mesh on the almond and two components of the scattered field for a NEFEM solution with $p = 3$

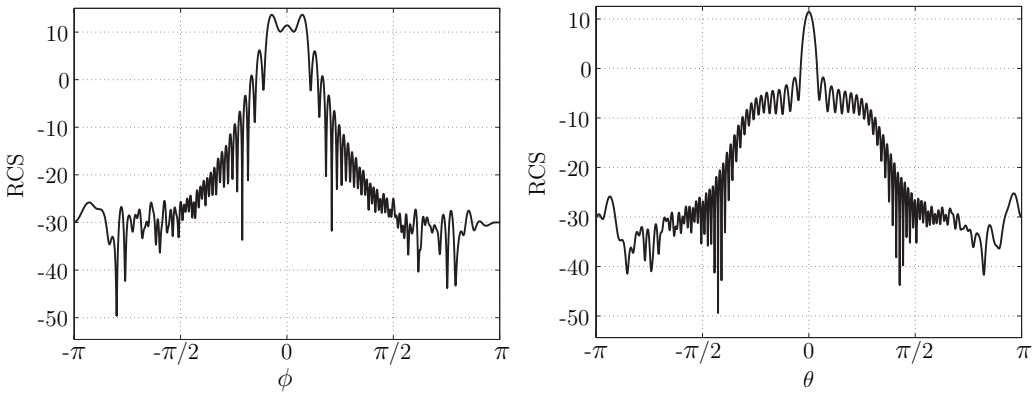

(a) Vertical polarization (b) Horizontal polarization

Figure 83: Scattering by a PEC NASA almond of characteristic length 21λ: RCS for a NEFEM solution with $p = 4$

the computation requires less degrees of freedom to obtain similar accuracy, due to the good performance of NEFEM with coarse meshes and high-order approximations.

Next, the scattering by a PEC NASA almond of characteristic length 21λ is considered. The mesh has 48 699 elements with planar faces and 6 008 curved elements. Figure 82 shows the surface mesh on the almond and two components of the scattered field computed with NEFEM and $p = 3$, corresponding to a wave incident onto the tip of the almond. RCS distribution for vertical and horizontal polarization are represented in Figure 83. Results compare well with published results [42], and again show the competitiveness of NEFEM for higher frequency problems. The tetrahedral mesh used in [42] has 51 342 008 linear elements, and approximately 8 million of nodes. With NEFEM and $p = 4$ the mesh has 2 million of nodes (including

Preprint of
R. Sevilla, S. Fernández-Méndez and A. Huerta
NURBS-Enhanced Finite Element Method (NEFEM): A seamless bridge between CAD and FEM
Archives of Computational Methods in Engineering, 18 (4); 441-484, 2011

the duplication due to the DG formulation), requiring four times less degrees of freedom than using standard linear FEs.

The results presented in this section has shown the benefits of NEFEM using standard FE meshes. However, the possibilities of NEFEM still go beyond.

It is well known that, in the context of FEs, the size of the model is sometimes subsidiary of the geometrical complexity and not only on solution itself. In particular, FE simulation of the scattering by complex objects with small geometric details requires drastic h-refinement to capture the geometry. Moreover, for scattering applications, small geometric details are influential in the solution, specially for high frequency problems, and a simplification of the geometry may lead to important discrepancies in the computed scattered field. Nevertheless, as it will be shown next, in the NEFEM context, when small is influential it does not imply small elements.

Two numerical examples that show the possibilities of NEFEM when the scatterer contains small geometric features are shown. As noted earlier, in Section 4.1, it is important to remark that the only restriction for a NEFEM element is that the edges and/or faces on the boundary belong to one NURBS. It is neither necessary to locate nodes at boundary corners or edges (entities with $\mathcal{C}^0$ continuity) nor to refine the mesh near the boundary to capture the geometry. It is exactly represented in NEFEM independently on the spacial discretization. The computational meshes in this section are chosen to emphasize the possibilities of NEFEM.

The scattering by a PEC *irregular* circular cylinder of diameter 4λ is considered. Two computational meshes are employed for the analysis, see a detail near the scatterer in Figure 84. The first mesh is a standard FE mesh in which h-refinement is performed in order to provide an accurate description of the small geometric features, see Figure 84 (a). The resulting mesh has 130 curved elements. The second mesh, represented in Figure 84 (b), is a coarse *NEFEM mesh* with only 16 curved elements, some of them (represented in red) containing small geometric details and corner singularities inside an edge.

Figure 85 shows the transverse field H_3 computed in the refined mesh with a degree of interpolation $p = 5$, and in the coarse NEFEM mesh with a degree of interpolation $p = 12$. The scattered fields are indistinguishable, even near the most critical zone. Nevertheless, a slight difference near the corner singularity can be appreciated, see a detailed view of the solution in Figure 86. Obviously, the discrepancy is originated by the limitations

Preprint of
R. Sevilla, S. Fernández-Méndez and A. Huerta
NURBS-Enhanced Finite Element Method (NEFEM): A seamless bridge between CAD and FEM
Archives of Computational Methods in Engineering, 18 (4); 441-484, 2011

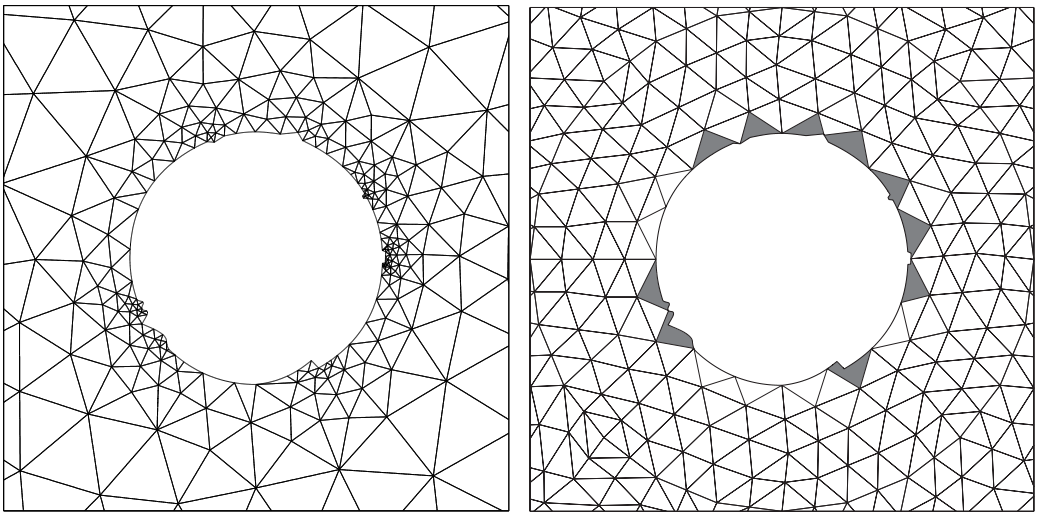

(a) Refined FEM mesh (b) Coarse NEFEM mesh

Figure 84: Scattering by an irregular circular cylinder of diameter 4λ: detail of a standard FE mesh refined towards the small geometric details, and a coarse NEFEM mesh with elements containing corner geometric singularities

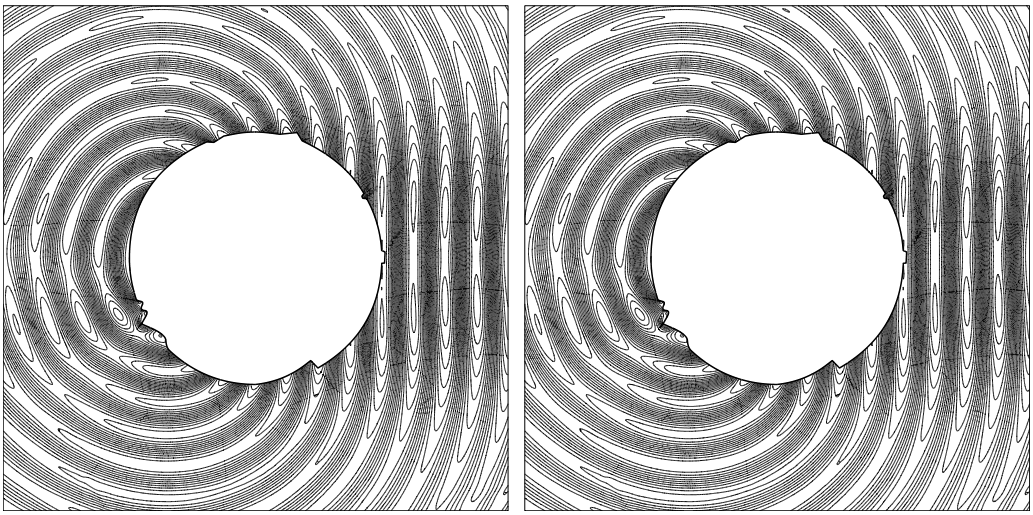

(a) Refined FEM mesh (b) Coarse NEFEM mesh

Figure 85: Scattering by an irregular circular cylinder of diameter 4λ: H_3 field computed in the discretizations shown in Figure 84

Preprint of
R. Sevilla, S. Fernández-Méndez and A. Huerta
NURBS-Enhanced Finite Element Method (NEFEM): A seamless bridge between CAD and FEM
Archives of Computational Methods in Engineering, 18 (4); 441-484, 2011

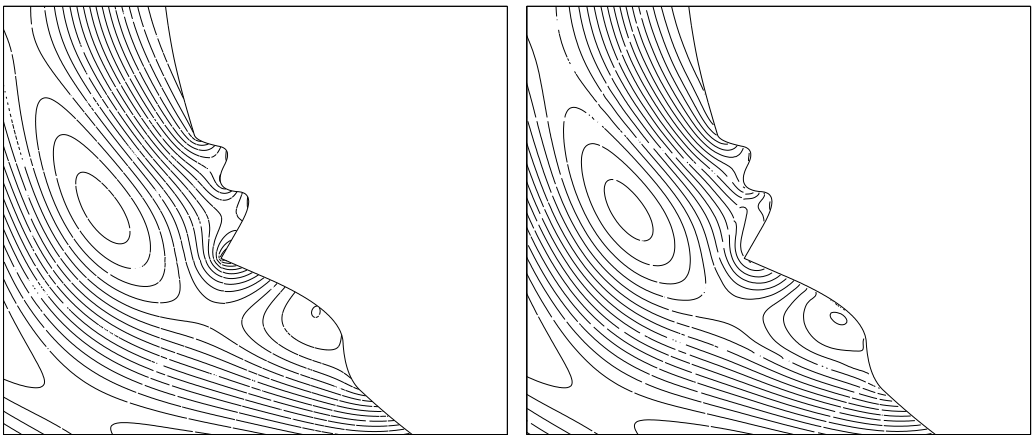

(a) Refined FEM mesh (b) Coarse NEFEM mesh

Figure 86: Scattering by an irregular circular cylinder of diameter 4λ: detail of the H_3 field

of the standard FE nodal interpolation for the approximation of a singular solution, see [85] and following examples in this section. Despite of this known limitation, it is important to remark that the quantity of interest, the RCS, shows very good agreement when it is compared with the RCS computed with the refined mesh, see Figure 87. In fact, two NEFEM computations are performed in the coarse mesh of Figure 84 (b), with $p = 6$ and $p = 12$, illustrating the convergence as the degree of approximation is increased. For $p = 12$ the relative RCS error in the $\mathcal{L}^2(-\pi, \pi)$ norm is 4.1×10^{-2}.

Finally, it is worth mentioning that the drastic difference between minimum mesh sizes, in the discretizations shown in Figure 84, induces important differences in the time-step size when explicit time integrators are used and, therefore, adds another advantage of NEFEM. In the refined mesh with $p = 5$ the minimum distance between two mesh nodes is 1.4×10^{-5}, whereas in the NEFEM coarse mesh with $p = 12$ the minimum distance is 1.2×10^{-3}. The computation with the refined mesh requires 527 459 time steps, whereas the computation in the coarse NEFEM mesh requires 6 620 time steps.

The aim of the last example is to show the possibilities of *NEFEM elements*, containing edge singularities, in 3D domains. In large scale 3D computations, very small geometric details may lead to unaffordable computational times with explicit time-marching algorithms, due to the excessive h-refinement needed to accurately capture the geometry.

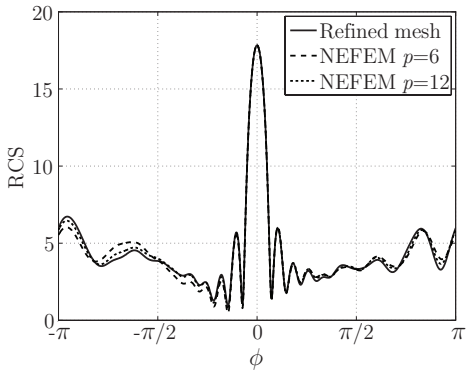

Figure 87: Scattering by an irregular circular cylinder of diameter 4λ: RCS comparison

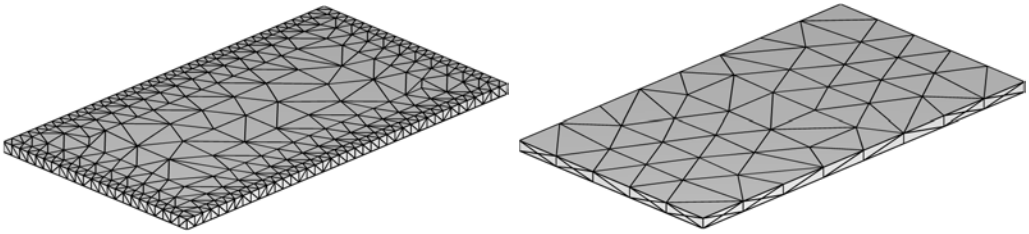

(a) Reference FEM mesh (b) FEM mesh

Figure 88: Scattering by a PEC thin plate: standard FE meshes

To show the capabilities of NEFEM in this scenario, the scattering by a PEC *thin* plate of dimensions $\lambda \times 4\lambda/7 \times \lambda/22$ is considered. The small thickness of the plate, with respect to the wave length λ, implies that h-refinement in standard FE meshes is controlled by the thickness of the plate, not by the desired number of nodes per wavelength.

Two standard FEM computational meshes are considered to compare the accuracy of NEFEM computations. Figure 88 (a) shows a standard FE mesh with refinement towards the singularities of the plate. The second mesh, in Figure 88 (b), is a FEM mesh with a desired mesh size of about $\lambda/8$. As usual, a standard mesh generator needs to perform extra h-refinement to offer an accurate description of the geometrical model. Therefore, the minimum mesh size in a standard FE mesh is, at least, $\lambda/22$.

Nevertheless, the mesh size for NEFEM is not controlled by small geometric features, and the desired mesh size is maintained, even in the presence of singularities in the boundary of the domain. The plate is exactly represented

Preprint of
R. Sevilla, S. Fernández-Méndez and A. Huerta
NURBS-Enhanced Finite Element Method (NEFEM): A seamless bridge between CAD and FEM
Archives of Computational Methods in Engineering, 18 (4); 441-484, 2011

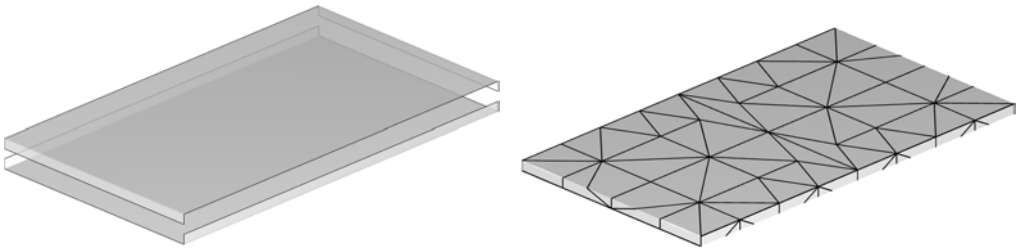

(a) NURBS surfaces (b) NEFEM mesh

Figure 89: Scattering by a PEC thin plate: NURBS surfaces (separated for visualization) and NEFEM coarse mesh with elements containing edge singularities

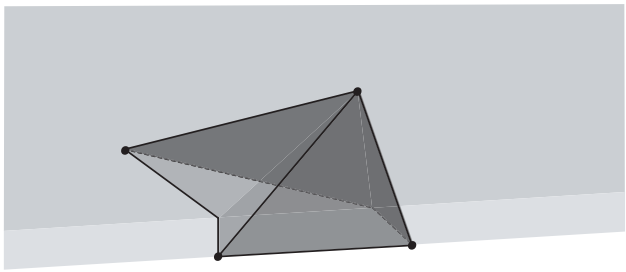

Figure 90: Detailed view of a NEFEM element containing an edge singularity in its boundary face

by two NURBS surfaces with $\mathcal{C}^0$ continuity at the edges of the plate, as illustrated in Figure 89 (a). A NEFEM coarse mesh is represented in Figure 89 (b). Note that, to obtain the desired mesh size, some elements contain an edge singularity inside one NURBS face, see a detailed view of a NEFEM element in Figure 90.

Figure 91 compares the RCS distribution for vertical and horizontal polarizations. An excellent agreement is observed between the three computations, showing the potential of NEFEM coarse meshes with elements containing singularities. Again, the maximum disagreement is obtained at singularities of the RCS due to its logarithmic scale. The error of the scattering width and in the $\mathcal{L}^2(-\pi,\pi)$ norm for NEFEM is 3.2×10^{-2} and 4.7×10^{-2} for the vertical and horizontal polarizations respectively. Despite the known limitation of polynomial approximation for the approximation of singular solutions it

Preprint of
R. Sevilla, S. Fernández-Méndez and A. Huerta
NURBS-Enhanced Finite Element Method (NEFEM): A seamless bridge between CAD and FEM
Archives of Computational Methods in Engineering, 18 (4); 441-484, 2011

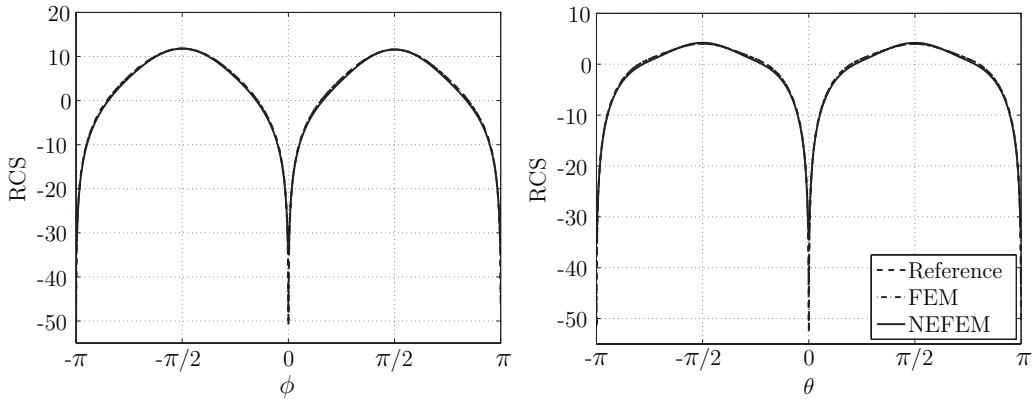

(a) Vertical polarization (b) Horizontal polarization

Figure 91: Scattering by a PEC thin plate: comparison of the RCS computed in the discretizations shown in Figures 88 (a), 88 (b) and 89 (a)

is remarkable the quality obtained in the RCS patterns by using NEFEM meshes.

7. Closing remarks

This papers presents a complete overview of recently proposed NURBS-enhanced finite element method (NEFEM). This methodology is an improvement of the standard FEM where the exact CAD description of the geometrical model is considered, but only for the boundary of the computational domain. At elements intersecting the NURBS boundary specific strategies to perform the interpolation and the numerical integration are proposed. NEFEM defines the approximation directly with Cartesian coordinates, ensuring reproducibility of polynomials in the physical space. The key idea of the numerical integration technique is to use specifically designed mappings for curved elements in order to decouple complexity of the NURBS boundary description, allowing a seamless treatment of trimmed and singular NURBS surfaces in 3D. It is worth recalling that at elements not intersecting the boundary classical FE are used, preserving the efficiency of the FEM.

The application and superiority of NEFEM with respect to other curved FE techniques has been presented. Ranging from second-order elliptic problems solved with a standard continuous Galerkin formulation to more complex applications such as the numerical solution of Euler and Maxwell's equa-

Preprint of
R. Sevilla, S. Fernández-Méndez and A. Huerta
NURBS-Enhanced Finite Element Method (NEFEM): A seamless bridge between CAD and FEM
Archives of Computational Methods in Engineering, 18 (4); 441-484, 2011

tions solved with a discontinuous Galerkin formulation, the benefits of NEFEM have been well established. NEFEM is not only more accurate than classical isoparametric FEM or Cartesian FEM that use an approximated boundary representation of the computation domain, but also outperforms p-FEM with an exact boundary representation, showing the importance of both the Cartesian approximation of the solution and the exact boundary representation.

In addition, the use of NEFEM implies that the spatial discretization is no longer subsidiary to the geometrical complexity. The behavior and potential of *NEFEM elements* have been shown as a powerful way of avoiding excessive mesh refinement to capture geometric details. With NEFEM, the mesh is refined where the solution is complex not where the geometry is complex.

8. Areas of further research

The potential and benefits of NEFEM for the treatment of curved boundaries have been demonstrated during the last years. However NEFEM is still a relative new approach and several research lines are still open. Some interesting topics are discussed next.

NEFEM has not been applied in practical FE adaptive process, see for instance [48], and the potential benefits in this context are clear. In this scenario the computational mesh is locally refined (or the polynomial order of the approximation increased) to properly approximate both the solution and the geometry. As NEFEM does not require mesh refinement to capture geometric features, the adaptive process is only controlled by the complexity of the solution, reducing therefore the necessary number of degrees of freedom to achieve a desired accuracy. Thus, the study of h and p adaptive processes in a NEFEM framework is worth to be investigated and compared with other FE techniques.

The potential of NEFEM for high-order computations in coarse meshes has been shown in this paper. NEFEM meshes offer a drastically reduction of the number of degrees of freedom compared to standard FE meshes. In addition, when combined with explicit time marching algorithms, the affordable time step due to the use of coarse meshes makes that approach highly competitive. Nevertheless, one of the topics that deserves attention is the improvement of the quality of the polynomial approximation in the presence of singular solutions inside NEFEM elements. The enrichment of the polynomial basis, well known for standard FEM meshes, see for instance [24], is

Preprint of
R. Sevilla, S. Fernández-Méndez and A. Huerta
NURBS-Enhanced Finite Element Method (NEFEM): A seamless bridge between CAD and FEM
Archives of Computational Methods in Engineering, 18 (4); 441-484, 2011

worth to be investigated in the NEFEM context.

The generation of coarse meshes of complex geometric objects for NEFEM computations is not a trivial task. Although strictly speaking, NEFEM does not need a high-order mesh generator, the use of a linear mesh generator may lead to non-valid NEFEM meshes. Moreover, tools for meshing complex objects without refinement near geometric singularities in the boundary are not provided by any mesh generator. Thus, automatic mesh generation technology for NEFEM is a new challenge by itself.

References

[1] Abarbanel, S., Gottlieb, D.: On the construction of absorbing layers in CEM. Appl. Numer. Math. **27**(4), 331–340 (1998)

[2] Anderson, J.D.: Modern Compressible Flow: with Historical Perspective. McGraw-Hill, New York (1982)

[3] Babuška, I., Suri, M.: The optimal convergence rate of the p-version of the finite element method. SIAM J. Numer. Anal. **24**(4), 750–776 (1987)

[4] Babuška, I., Szabó, B.A., Katz, I.N.: The p-version of the finite element method. SIAM J. Numer. Anal. **18**(3), 515–545 (1981)

[5] Balanis, C.A.: Advanced Engineering Electromagnetics. John Wiley & Sons, New York (1989)

[6] Banerjee, U., Suri, M.: The effect of numerical quadrature in the p-version of the finite element method. Math.Comp. **59**(199), 1–20 (1992)

[7] Barth, T., Ohlberger, M.: Finite Volume Methods: Foundation and Analysis, in: E. Stein, R. de Borst, T.J.R. Hughes (Eds.), Fundamentals, Encyclopedia of Computational Mechanics, vol. 1. Wiley, New York (2004). Chapter 4

[8] Barth, T.J.: Simplified numerical methods for gas dynamics systems on triangulated domains. Ph.D. thesis, Stanford University (1998)

[9] Bassi, F., Rebay, S.: High-order accurate discontinuous finite element solution of the 2D Euler equations. J. Comput. Phys. **138**(2), 251–285 (1997)

Preprint of
R. Sevilla, S. Fernández-Méndez and A. Huerta
NURBS-Enhanced Finite Element Method (NEFEM): A seamless bridge between CAD and FEM
Archives of Computational Methods in Engineering, 18 (4); 441-484, 2011

[10] Bazilevs, Y., Hughes, T.J.R.: Weak imposition of Dirichlet boundary conditions in fluid mechanics. Comp. Fluids. **36**(1), 12–26 (2007)

[11] Berenger, J.P.: A perfectly matched layer for the absorption of electromagnetic waves. J. Comp. Phys **114**(2), 185–200 (1994)

[12] Bernardi, C.: Optimal finite-element interpolation on curved domains. SIAM J. Numer. Anal. **26**(5), 1212–1240 (1989)

[13] Brenner, S.C., Scott, L.R.: The Mathematical Theory of Finite Element Methods. Springer (1994)

[14] Cavendish, J.C., Gordon, W.J., Hall, C.A.: Ritz-Galerkin approximations in blending function spaces. Numer. Math. **26**(2), 155–178 (1976)

[15] Chen, Q., Babuška, I.: Approximate optimal points for polynomial interpolation of real functions in an interval and in a triangle. Comput. Methods Appl. Mech. Engrg. **128**(3–4), 405–417 (1995)

[16] Chen, Q., Babuška, I.: The optimal symmetrical points for polynomial interpolation of real functions in the tetrahedron. Comput. Methods Appl. Mech. Engrg. **137**(1), 89–94 (1996)

[17] Ciarlet, P.G., Raviart, P.A.: Interpolation theory over curved elements, with applications to finite element methods. Comput. Methods Appl. Mech. Engrg. **1**(1), 217–249 (1972)

[18] Cirak, F., Ortiz, M., Schröder, P.: Subdivision surfaces: a new paradigm for thin-shell finite-element analysis. Internat. J. Numer. Methods Engng. **47**(12), 2039–2072 (2000)

[19] Clough, R.W.: Early history of the finite element method from the view point of a pioneer. Internat. J. Numer. Methods Engng. **60**(1), 283–287 (2004)

[20] Cockburn, B.: Discontinuous Galerkin methods for Computational Fluid Dynamics, in: E. Stein, R. de Borst, T.J.R. Hughes (Eds.), Fluids, Encyclopedia of Computational Mechanics, vol. 3. Wiley, New York (2004). Chapter 4

[21] Cockburn, B., G. E. Karniadakis, C. W. Shu: The development of Discontinuous Galerkin methods. In: B. Cockburn, G.E. Karniadakis, C.W. Shu (eds.) Discontinuous Galerkin Methods, *Lecture Notes in Computational Science and Engineering*, vol. 11, pp. 3–50. Springer-Verlag, Berlin (2000)

[22] Cockburn, B., Karniadakis, G.E., Shu, C.W.: Discontinuous Galerkin methods, chap. The development of discontinuous Galerkin methods. In: B. Cockburn, G.E. Karniadakis and C.W. Shu, Editors. Springer, Berlin (2000)

[23] Cockburn, B., Shu, C.W.: TVB Runge-Kutta local projection discontinuous Galerkin finite element method for conservation-laws II. General framework. Math. Comp. **52**(186), 411–435 (1989)

[24] Costabel, M., Dauge, M.: Singularities of electromagnetic fields in polyhedral domains. Arch. Ration. Mech. Anal. **151**(3), 221–276 (1997)

[25] Cottrell, J.A., Hughes, T.J.R., Bazilevs, Y.: Isogeometric Analysis: Toward Integration of CAD and FEA. Wiley (2009)

[26] Coyle, J., Ledger, P.D.: Evidence of exponential convergence in the computation of Maxwell eigenvalues. Comput. Methods Appl. Mech. Engrg. **194**(2-5), 587 – 604 (2005)

[27] Dadone, A., Grossman, B.: Surface boundary conditions for the numerical solution of the Euler equations. AIAA Journal **32**(2), 285–293 (1994)

[28] Davis, P., Rabinowitz, P.: Methods of Numerical Integration, second edn. Academic Press (1984)

[29] Dey, S., Shephard, M.S., Flaherty, J.E.: Geometry representation issues associated with p-version finite element computations. Comput. Methods Appl. Mech. Engrg. **150**(1-4), 39–55 (1997)

[30] Dominek, A.K., Shamanski, H.T.: The almond test body. The Ohio State University ElectroScience Laboratory, Department of Electrical Engineering, Report 721929-9, NASA Langley Research Center (1990)

[31] Donea, J., Huerta, A.: Finite Element Methods for Flow Problems. Wiley (2005)

[32] Dorr, M.R.: The approximation-theory for the p-version of the finite-element method. SIAM J. Numer. Anal. **21**(6), 1180–1207 (1984)

[33] Dubiner, M.: Spectral methods on triangles and other domains. J. Sci. Comput. **6**, 345–390 (1991)

[34] Dumbser, M., Munz, C.D.: On source terms and boundary conditions using high order arbitrary discontinuous Galerkin schemes. Int. J. Appl. Math. Comput. Sci. **17**(3), 297–310 (2007)

[35] Ergatoudis, J., Irons, B.M., Zienkiewicz, O.C.: Curved isoparametric "quadrilateral" elements for finite element analysis. Internat. J. Solids Struct. **4**(1), 31–42 (1968)

[36] Fernández-Méndez, S., Huerta, A.: Imposing essential boundary conditions in mesh-free methods. Comput. Methods Appl. Mech. Engrg. **192**(12-14), 1257–1275 (2004)

[37] Gao, H., Wang, Z.J., Liu, Y.: A study of curved boundary representations for 2D high order Euler solvers. J. Sci. Comput. **44**(3), 323–336 (2010)

[38] Gordon, W.J., Hall, C.A.: Construction of curvilinear co-ordinate systems and applications to mesh generation. Internat. J. Numer. Methods Engng. **7**(4), 461–477 (1973)

[39] Gordon, W.J., Hall, C.A.: Transfinite element methods: Blending-function interpolation over arbitrary curved element domains. Numer. Math. **21**(2), 109–129 (1973)

[40] Gottlieb, S., Shu, C.W.: Total variation diminishing Runge-Kutta schemes. Math. Comp. **67**(221), 73–85 (1998)

[41] Gui, W., Babuška, I.: The h-version, p-version and h-p-version of the finite-element method in 1-dimension. 1 The error analysis of the p-version. Numer. Math. **49**(6), 577–612 (1986)

Preprint of
R. Sevilla, S. Fernández-Méndez and A. Huerta
NURBS-Enhanced Finite Element Method (NEFEM): A seamless bridge between CAD and FEM
Archives of Computational Methods in Engineering, 18 (4); 441-484, 2011

[42] Hachemi, M.E., Hassan, O., Morgan, K., Rowse, D., Weatherill, N.: A low-order unstructured-mesh approach for computational electromagnetics in the time domain. Philos. Trans. R. Soc. Lond. Ser. A Math. Phys. Eng. Sci. **362**(1816), 445–469 (2004)

[43] Harrington, R.F.: Time-Harmonic Electromagnetic Fields. McGraw-Hill, New York (1961)

[44] Harris, R., Wang, Z.J., Liu, Y.: Efficient implementation of high-order spectral volume method for multidimensional conservation laws on unstructured grids. In: 45th AIAA Aerospace Sciences Meeting and Exhibit. AIAA, Nevada (2007)

[45] Hesthaven, J.S.: Stable spectral methods on tetrahedral elements. SIAM J. Numer. Anal. **21**(6), 2352–2380 (2000)

[46] Hesthaven, J.S., Warburton, T.: Nodal high-order methods on unstructured grids I. time-domain solution of Maxwell's equations. J. Comp. Phys **181**(1), 186–221 (2002)

[47] Hirsch, C.: Numerical Computation of Internal and External Flows. Volume 1: Fundamentals of Numerical Discretization. John Wiley & Sons (1988)

[48] Huerta, A., Rodríguez-Ferran, A., Díez, P., Sarrate, J.: Adaptive finite element strategies based on error assessment. Internat. J. Numer. Methods Engng. **46**, 1803–1818 (1999)

[49] Hughes, T.J.R., Cottrell, J.A., Bazilevs, Y.: Isogeometric analysis: CAD, finite elements, NURBS, exact geometry and mesh refinement. Comput. Methods Appl. Mech. Engrg. **194**(39–41), 4135–4195 (2005)

[50] Huttunen, T., Malinen, M., Monk, P.: Solving Maxwell's equations using the ultra weak variational formulation. J. Comp. Phys **223**(2), 731–758 (2007)

[51] Inoue, K., Kikuchi, Y., Masuyama, T.: A NURBS finite element method for product shape design. J. Engrg. Design **16**(2), 157–174 (2005)

Preprint of
R. Sevilla, S. Fernández-Méndez and A. Huerta
NURBS-Enhanced Finite Element Method (NEFEM): A seamless bridge between CAD and FEM
Archives of Computational Methods in Engineering, 18 (4); 441-484, 2011

[52] Johnson, C.: Numerical Solution of Partial Differential Equations by the Finite Element Method. Cambridge University Press, Cambridge (1987)

[53] Kagan, P., Fischer, A., Bar-Yoseph, P.Z.: New B-spline finite element approach for geometrical design and mechanical analysis. Internat. J. Numer. Methods Engng. **41**(3), 435–458 (1998)

[54] Karniadakis, G.E., Sherwin, S.J.: Spectral/*hp* Element methods for CFD (Numerical Mathematics and Scientific computation). Oxford University Press, Oxford (1999)

[55] Krivodonova, L., Berger, M.: High-order accurate implementation of solid wall boundary conditions in curved geometries. J. Comput. Phys. **211**(2), 492–512 (2006)

[56] Ladson, C.L., Brooks, C.W., Hill, A.S., Sproles, D.W.: Computer program to obtain ordinates for naca airfoils. Tech. Rep. NASA TM-4741, NASA Langley Research Center (1996). URL http://techreports.larc.nasa.gov/ltrs/PDF/NASA-96-tm4741.pdf

[57] Landmann, B., Kessler, M., Wagner, S., Krämer, E.: A parallel, high-order discontinuous Galerkin code for laminar and turbulent flows. Computers & Fluids **37**(4), 427–438 (2008)

[58] Laney, C.B.: Computational gasdynamics. Cambridge University Press, Cambridge (1998)

[59] Ledger, P.D., Morgan, K., Hassan, O.: Electromagnetic scattering simulation using an $\mathbf{H}(\mathrm{curl})$ conforming *hp* finite element method in three dimensions. Internat. J. Numer. Methods Fluids **53**(8), 1267–1296 (2007)

[60] Ledger, P.D., Morgan, K., Hassan, O., Weatherill, N.P.: Plane wave $\mathbf{H}(\mathrm{curl}, \Omega)$ conforming finite elements for Maxwell's equations. Computat. Mech. **31**(3-4), 272–283 (2003)

[61] Lenoir, M.: Optimal isoparametric finite elements and error estimates for domains involving curved boundaries. SIAM J. Numer. Anal. **23**(3), 562–580 (1986)

Preprint of
R. Sevilla, S. Fernández-Méndez and A. Huerta
NURBS-Enhanced Finite Element Method (NEFEM): A seamless bridge between CAD and FEM
Archives of Computational Methods in Engineering, 18 (4); 441-484, 2011

[62] Luhon, C., Wagner, S.: New Results in Numerical and Experimental Fluid Mechanics VI, chap. Three-Dimensional Discontinuous Galerkin Codes to Simulate Viscous Flow by Spatial Discretization of High Order and Curved Elements on Unstructured Grids, pp. 145–153. Springer-Verlag, Berlin (2007)

[63] Luo, H., Pozrikidis, C.: A lobatto interpolation grid in the tetrahedron. IMA J. Appl. Math. **71**(2), 298–313 (2006)

[64] Luo, X.J., Shephard, M.S., Remacle, J.F.: Influence of geometric approximation on the accuracy of higher order methods. Tech. Rep. 1, SCOREC (2001)

[65] Lyness, J.N., Jespersen, D.: Moderate degree symmetric quadrature rules for the triangle. IMA J. Appl. Math. **15**, 19–32 (1975)

[66] Ma, Y.L., Hewitt, W.T.: Point inversion and projection for NURBS curve and surface: control polygon approach. Comput. Aided Geom. Des. **20**, 79–99 (2003)

[67] Mäkipelto, J.: Geometry based rational enrichment functions for triangular plane elasticity element. In: Proceedings of the 21st International Congress of Theoretical and Applied Mechanics. Poland (2004)

[68] McLeod, R.: A piecewise parabolic $\mathcal{C}^1$ approximation technique for curved boundaries. Comput. Math. Appl. **5**, 277–284 (1979)

[69] Muñoz, J.J.: Modelling unilateral frictionless contact using the null-space method and cubic B-Spline interpolation. Comput. Methods Appl. Mech. Engrg. **197**(9-12), 979–993 (2008)

[70] Nitsche, J.A.: Über ein variations zur lösung von dirichlet-problemen bei verwendung von teilräumen die keinen randbedingungen unterworfen sind. Abh. Math. Se. Univ. **36**, 9–15 (1971)

[71] Pascal, J.F., George, P.L.: Maillages : applications aux éléments finis. Hermès Science Publications, Paris (1999)

[72] Piegl, L., Tiller, W.: The NURBS Book. Springer-Verlag, London (1995)

Preprint of
R. Sevilla, S. Fernández-Méndez and A. Huerta
NURBS-Enhanced Finite Element Method (NEFEM): A seamless bridge between CAD and FEM
Archives of Computational Methods in Engineering, 18 (4); 441-484, 2011

[73] Raviart, P.A., Thomas, J.M.: Introduction à l'analyse numérique des équations aux dérivées partielles. Dunod, Paris (1998)

[74] Rogers, D.F.: An introduction to NURBS with historical perspective. Academic Press, Inc., San Diego, CA (2001)

[75] Schramm, U., Pilkey, W.: The coupling of geometric descriptions and finite elements using NURBS: a study of shape optimization. Finite Elem. Anal. Des. **15**(1), 11–34 (1993)

[76] Schuh, M.J., Woo, A.C., Simon, M.P.: The monostatic/bistatic approximation. IEEE Trans. Antennas Propagat. Mag. **35**(4), 76–78 (1994)

[77] Scott, L.R.: Finite element techniques for curved boundaries. Ph.D. thesis, Massachusetts Institute of Technology, Dept. of Mathematics (1973)

[78] Scott, L.R.: Interpolated boundary conditions in the finite element method. SIAM J. Numer. Anal. **12**(3), 404–427 (1975)

[79] Sevilla, R., Fernández-Méndez, S., Huerta, A.: NURBS-enhanced finite element method (NEFEM). Internat. J. Numer. Methods Engrg. **76**(1), 56–83 (2008)

[80] Sevilla, R., Fernández-Méndez, S., Huerta, A.: NURBS-enhanced finite element method (NEFEM) for Euler equations. Internat. J. Numer. Methods Fluids **57**(9), 1051–1069 (2008)

[81] Sevilla, R., Fernández-Méndez, S., Huerta, A.: 3D-NURBS-enhanced finite element method (NEFEM). Internat. J. Numer. Methods Engrg. **88**(2), 103–125 (2011). Accepted for publication

[82] Sevilla, R., Fernández-Méndez, S., Huerta, A.: Comparison of high-order curved finite elements. Internat. J. Numer. Methods Engrg. **87**(8), 719–734 (2011)

[83] Sherwin, S.J., Karniadakis, G.: A new triangular and tetrahedral basis for high-order (*hp*) finite element methods. Internat. J. Numer. Methods Engng. **38**(22), 3775–3802 (1995)

Preprint of
R. Sevilla, S. Fernández-Méndez and A. Huerta
NURBS-Enhanced Finite Element Method (NEFEM): A seamless bridge between CAD and FEM
Archives of Computational Methods in Engineering, 18 (4); 441-484, 2011

[84] Solin, P., Segeth, K.: Higher-Order Finite Element Methods. Chapman & Hall (2003)

[85] Szabó, B., Babuška, I.: Finite Element Analysis. John Wiley & Sons, New York (1991)

[86] Szabó, B., Düster, A., Rank, E.: The p-version of the Finite Element Method, *Encyclopedia of Computational Mechanics*, vol. 1 (Fundamentals), chap. 5. Wiley, New York (2004)

[87] Szegö, G.: Orthogonal Polynomials (fourth edition). Americam Mathematical Society, Providence (1975)

[88] Taflove, A.: Computational Electrodynamics: The Finite-Difference Time-Domain Method. Artech House, Inc. (1995)

[89] Taylor, M.A., Wingate, B.A., Vincent, R.E.: An algorithm for computing fekete points in the triangle. SIAM J. Numer. Anal. **38**(5), 1707–1720 (2000)

[90] Toro, E.F.: Riemann solvers and numerical methods for fluid dynamics. Springer, Berlin (1997)

[91] Turkel, E., Yefet, A.: Absorbing PML boundary layers for wave-like equations. Appl. Numer. Math. **27**(4), 533–557 (1998)

[92] Van der Ven, H., Van der Vegt, J.J.W.: Space-time Discontinuous Galerkin finite element method with dynamic grid motion for inviscid compressible flows II. Efficient flux quadrature. Comput. Methods Appl. Mech. Engrg. **191**(41-42), 4747–4780 (2002)

[93] Wachspress, E.L.: A rational basis for function approximation. II Curved sides. J. Inst. Math. Appl. **11**(1), 83–104 (1973)

[94] Wachspress, E.L.: A rational finite element basis, vol. 114. Academic Press, New York (1975)

[95] Wachspress, E.L.: High-order curved finite elements. Internat. J. Numer. Methods Engng. **17**(5), 735–745 (1981)

[96] Wandzura, S., Xiao, H.: Symmetric quadrature rules on a triangle. Comput. Math. Appl. **45**(12), 1829–1840 (2003)

Preprint of
R. Sevilla, S. Fernández-Méndez and A. Huerta
NURBS-Enhanced Finite Element Method (NEFEM): A seamless bridge between CAD and FEM
Archives of Computational Methods in Engineering, 18 (4); 441-484, 2011

[97] Wang, Z.J., Liu, Y.: Extension of the spectral volume method to high-order boundary representation. J. Comput. Phys. **211**(1), 154–178 (2006)

[98] Wang, Z.J., Sun, Y.: A curvature-based wall boundary condition for the Euler equations on unstructured grids. In: Proceedings of the 40th AIAA Aerospace Sciences Meeting and Exhibit. AIAA, Nevada (2002)

[99] Wang, Z.J., Zhang, L., Liu, Y.: Spectral (finite) volume method for conservation laws on unstructured grids IV: extension to two-dimensional Euler equations. J. Comput. Phys. **194**(2), 716–741 (2004)

[100] Warburton, T.: An explicit construction of interpolation nodes on the simplex. J. Eng. Math. **56**(3), 247–262 (2006)

[101] Woo, A.C., Wang, H.T.G., Schub, M.J.: Benchmark radar targets for the validation of computational electromagnetics programs. IEEE Trans. Antennas Propagat. Mag. **35**(1), 84–89 (1993)

[102] Xue, D., Demkowicz, L.: Control of geometry induced error in *hp* finite element (FE) simulations. I. Evaluation of FE error for curvilinear geometries. Internat. J. Numer. Anal. Model. **2**(3), 283–300 (2005)

[103] Zienkiewicz, O.C.: The Finite Element Method in Engineering Science, second edn. McGraw-Hill, London (1971)

[104] Zienkiewicz, O.C.: Origins, milestones and directions of the finite element method - A personal view. Arch. Comput. Methods Engrg. **2**(1), 1–48 (1995)

[105] Zienkiewicz, O.C., Taylor, R.L.: The Finite Element Method, vol. 1. The basis, fifth edn. Butterwort-Heinemann (2000)

[106] Zlámal, M.: Curved elements in the finite element method. I. SIAM J. Numer. Anal. **10**(1), 229–240 (1973)

[107] Zlámal, M.: The finite element method in domains with curved boundaries. Internat. J. Numer. Methods Engng. **5**(3), 367–373 (1973)

[108] Zlámal, M.: Curved elements in the finite element method. II. SIAM J. Numer. Anal. **11**(2), 347–362 (1974)